ANALYSIS OF FRESHWATER LENS FORMATION IN SALINE AQUIFERS

BY

JOHN PATRICK GLASS

A DISSERTATION PRESENTED TO THE GRADUATE COUNCIL OF
THE UNIVERSITY OF FLORIDA
IN PARTIAL FULFILLMENT OF THE REQUIREMENTS FOR THE
DEGREE OF DOCTOR OF PHILOSOPHY

UNIVERSITY OF FLORIDA

1979

ACKNOWLEDGEMENTS

This research project was initiated by Dr. B. A. Christensen and Dr. Hillel Rubin. It was supported financially by the Office of Water Research and Technology of the U.S. Department of the Interior.

The author extends his gratitude to Dr. B. A. Christensen for his continued support and advice and for serving as Chairman of his Supervisory Committee.

Special thanks are due to Dr. Joel Melville whose day-to-day suggestions and assistance contributed substantially to the work.

Above all, I am thankful for the assistance of my wife, Claudette, who participated in the experimental work, helped with the preparation of the figures, typed the entire manuscript and supported me financially throughout my graduate study.

TABLE OF CONTENTS

TABLE OF CONTENTS—continued

LIST OF TABLES

LIST OF FIGURES

LIST OF FIGURES—continued

LIST OF FIGURES—continued

LIST OF FIGURES—continued

LIST OF SYMBOLS

The following symbols are employed in this dissertation. Dimensions, where applicable, are also given in terms of length L, mass M, time T in square brackets.

A = Area $[L^2]$

a = depth of the top of the confined aquifer below sea level, [L]

B = leakage coefficient, [L]

b = thickness of a confined aquifer [L]

b' = thickness of a leaky layer, [L]

b_x = body force in the x-direction, $[ML/T^2]$

b_y = body force in the y-direction, $[ML/T^2]$

b_z = body force in the z-direction, $[ML/T^2]$

c = fractional concentration of salinity

D = the dispersion tensor, $[L^2/T]$

D_ℓ = coefficient of longitudinal dispersion, $[L^2/T]$

D_m = coefficient of molecular diffusion, $[L^2/T]$

D_t = coefficient of transverse dispersion, $[L^2/T]$

d = spacing between plates of the Hele-Shaw model, [L]

F = an arbitrary function

f_j = the j^{th} term of the forcing matrix, $[L^3/T]$

g = acceleration due to gravity, $[L/T^2]$

h = vertical thickness of the flow region, [L]

I_0 = modified zeroth order Bessel function of the first kind

I_1 = modified first order Bessel function of the first kind

$\hat{i}$ = unit vector in the x-direction

$[J]$ = the Jacobian matrix

J_x = x-direction component of head gradient

J_y = y-direction component of head gradient

J_z = z-direction component of head gradient

$\hat{j}$ = unit vector in the y-direction

K = hydraulic conductivity for isotropic porous media, [L/T]

K' = hydraulic conductivity of a leaky layer, [L]

K_0 = modified zeroth order Bessel function of the second kind

K_0 = modified first order Bessel function of the second kind

K_{ij} = components of the hydraulic conductivity tensor for (i, j = x, y, z), [L/T]

K_{ij} = terms of the global stiffness matrix (in Chapter 6), [L^2/T]

k = intrinsic permeability, [L^2]

$\hat{k}$ = unit vector in the z-direction

K_{ij} = terms of the element stiffness matrix (in Chapter 6), [L^2/T]

L = a linear operator

N_i = the i^{th} shape function

n = porosity of the porous medium

P = pressure [$M/(LT^2)$]

P_f = pressure on the freshwater side of an interface, [$M/(LT^2)$]

P_s = pressure on the saltwater side of an interface, [$M/(LT^2)$]

Q = volumetric rate of injection into a well, [L^3/T]

Q' = dimensionless injection rate

Q_x = uniform horizontal flow per unit width of aquifer, [L^2/T]

$\vec{q}$ = discharge velocity vector, [L/T]

q_ℓ = longitudinal component of discharge velocity, [L/T]

q_x = x-direction component of discharge velocity, [L/T]

q_y = y-direction component of discharge velocity, [L/T]

q_z = z-direction component of discharge velocity, [L/T]

r = the radial coordinate of a cylindrical coordinate system, [L]

r_e = radius of a constant head boundary, [L]

r_t = radius of the toe of the interface, [L]

S = the boundary surface, [L^2]

S_s = specific storage, [1/L]

s = drawdown or pushup, [L]

t = time, [L]

t' = dimensionless time

u = x-direction component of flow velocity, [L/T]

V = volume, [L^3]

v = y-direction component of flow velocity, [L/T]

W_n = weighting factor for the n^{th} sample point

w = z-direction component of flow velocity, [L/T]

w_s = flow rate through the leaky layer, [L/T]

X = projection of the interface on the horizontal, [L]

X_i = x coordinate of node i, [L]

x = a horizontal coordinate of a cartesian coordinate system, [L]

x' = a dimensionless distance

x_t = distance to the toe of the interface, [L]

x_w = distance from the injection well to the sea coast, [L]

x'_w = dimensionless position of the injection well

Y_i = y coordinate of node i, [L]

y = a horizontal coordinate of a cartesian coordinate system, [L]

y' = a dimensionless distance

Z_i = z coordinate of node i, [L]

z = elevation above a datum, or the vertical coordinate, [L]

z_i = elevation of a point on the interface, [L]

α = coefficient of aquifer compressibility, [LT^2/M]

α = a coefficient (in Chapter 5 and 6)

α_ℓ = longitudinal dispersivity, [L]

α_t = transverse dispersivity, [L]

β = coefficient of fluid compressibility, [LT^2/M]

β = a constant (in Chapter 5), [L]

β^2 = a modified leakage coefficient (in Chapter 6) [T]

γ = unit weight of a fluid, [$M/(LT)^2$]

δ = the Ghyben-Herzberg coefficient

ζ = the third dimensionless coordinate in an oblique coordinate system

η = the second dimensionless coordinate in an oblique coordinate system

Θ = angular coordinate in a cylindrical coordinate system

μ = dynamic viscosity, [M/(LT)]

ν = kinematic viscosity, [L^2/T]

ξ = the first dimensionless coordinate in an oblique coordinate system

ρ = fluid density, [M/L^3]

$\bar{\rho}$ = average density, [M/L^3]

Φ = the Girinskii potential (in Chapter 5), [L^3/T]

Φ_n = nodal values of for n = 1 . . . 20, [L]

ϕ = piezometric head, [L]

$\hat{\phi}$ = an approximation to the piezometric head, [L]

ϕ_0 = undisturbed piezometric head in a static aquifer, [L]

ϕ_f = piezometric head of freshwater measured in terms of freshwater, [L]

ϕ_s = piezometric head of saltwater measured in terms of saltwater, [L]

Subscripts and Superscripts

f - freshwater or lighter fluid

i - on the interface

m - model

p - prototype

r - ratio

s - saltwater or heavier fluid

t - at the toe of the interface

x - x-direction

y - y-direction

z - z-direction

Abstract of Dissertation Presented to the Graduate Council
of the University of Florida in Partial Fulfillment
of the Requirements for the Degree of
Doctor of Philosophy

ANALYSIS OF FRESHWATER LENS FORMATION IN SALINE AQUIFERS

By

John Patrick Glass

June, 1979

Chairman: B. A. Christensen
Major Department: Civil Engineering

The injection of freshwater into a saline aquifer can, under favorable conditions, result in displacement of the saltwater and creation of a distinct body of freshwater called a freshwater lens. It may be desirable to do this either as a method of storing the freshwater for future use or in order to form a barrier against saltwater intrusion. In either case, it is important to know beforehand whether the lens will be stable or the injected water will be lost. The purpose of this study is to develop methods for analyzing the hydrodynamic factors involved in the formation and maintenance of such lenses.

A series of laboratory tests using vertical Hele-Shaw models was performed to determine the shape and rate of movement of the initially vertical interface between two fluids of different density. The results of these tests were compared with the predictions of two formulas

proposed by previous investigators. It was found that for relatively thick aquifers it is not correct to neglect the vertical components of flow as has formerly been done.

An analytical method is presented for the location of the boundary of a steady freshwater lens in a coastal aquifer. A vertically integrated potential function is used to superimpose the flow from the injected well on the pre-existing uniform seaward flow in the aquifer. This results in a quasi-three dimensional solution for the position of the coastal interface.

A pair of coupled ordinary differential equations is derived which describe the steady flow of freshwater injected into a leaky saline aquifer under the Dupuit assumption. The non-linear system of equations is solved numerically by isolating the unique integral curve which results in the only physically possible boundary conditions. A design chart is presented by which the maximum possible size of freshwater lens can be determined for various aquifer conditions.

A three dimensional finite element model is developed which can be used to locate the boundaries of a steady freshwater lens under a wide variety of conditions. The model uses isoparametric elements of the quadrilateral family having twenty nodes each. This permits very close approximation to the curved flow boundaries typical of freshwater lenses. Inhomogeneous and anisotropic aquifers can be treated.

A finite difference model developed for the U.S. Geological Survey is used to analyze the axisymmetric flow in transient freshwater lenses. Simulation of lens formation in a variety of saline aquifer configurations indicates that previously available methods of analysis which neglect vertical components of flow may be reliable in very thin

aquifers. For thicker aquifers, however, vertical flow can predominate resulting in a much more rapid rate of gravitational segregation of the fluids.

CHAPTER 1

INTRODUCTION

Groundwater flow is an important part of the hydrologic cycle which nature uses to even out the temporal and spatial variations inherent in rainfall. It has long been man's practice to take water from groundwater reservoirs with the assumption that the water removed will be replaced by natural processes. In many cases, this arrangement works well, with nature putting water into the ground and man taking it out. In some areas, though, the increased use of groundwater supplies coupled with decreased natural recharge due to man-made changes in the land surface is either draining the freshwater aquifers or opening them to saltwater intrusion. In recognition of this, efforts have been made to augment natural recharge by such means as spray irrigation, water spreading, seepage ponds and deep well injection. This signals a new conception of aquifers as a form of underground storage which can be used in much the same way as surface reservoirs. As an extension of this, it has been proposed to make use of the storage capacity available in saline aquifers by injecting freshwater into them in such a way that the resident saltwater is displaced and a lens of freshwater is created.

The variety of possible flow patterns that may result from the injection of freshwater into a saline aquifer can be viewed as a continuous spectrum bounded by three idealized extremes. One possibility is that the freshwater will disperse rapidly and lose its identity as a separate flow, merely serving to dilute the resident saltwater. In

another case, a flow pattern may develop which transports the freshwater away from the point of injection as a plume. A third alternative is that the freshwater will tend to remain near the point of injection creating an identifiable lens of freshwater which grows or diminishes accordingly as fluid is added to or removed from it. If the freshwater is injected in anticipation of its subsequent retrieval and re-use, the formation and maintenance of such a lens adjacent to the point of injection is essential.

The major factors influencing the formation of freshwater lenses are: (1) buoyancy, (2) mode of injection, (3) the properties of the porous medium, (4) dispersion, (5) flow of the resident saltwater. The relative intensities of these individual influences determine which of the previously described flow patterns will predominate. Favorable conditions for the development of freshwater lenses require that buoyancy, dispersion, and preexisting flow be relatively weak influences. In previous studies of freshwater lenses such ideal conditions have been assumed. In reality, these effects are never entirely absent. It is important, then, to determine at what point their effects become substantial and to have techniques for including their influences in the analysis of freshwater lenses.

CHAPTER 2

LITERATURE SURVEY

General

The analysis of freshwater lenses is one of a general class of problems involving the stratified flow of two miscible liquids through porous media. It is closely related to such other problems of that class as saltwater intrusion, interface upconing beneath wells, and deep well disposal of liquid wastes. A wealth of published information is available on each of these topics but much of it has no direct application to the study of freshwater lenses. Many of the methods developed for locating coastal interfaces, for instance, depend on conformal mapping techniques or otherwise on the theory of complex variables, which is limited to two dimensional problems. Likewise, much of the work done with deep well disposal deals with the movement and dispersion of plumes, emphasizing the rapid departure of the waste fluid from the scene of injection. Nonetheless, some of the work in each of these fields can be useful in lens analysis. It is only these studies and those which are directly concerned with fresh or hot water lenses that will be mentioned here.

Studies Dealing with Interface Location

The rotational movement of an initially vertical interface between two fluids of different density was studied by Gardner, Downie and Kendall (1962) because of its applicability to recovery processes in petroleum reservoirs. The initial motion of the interface and the

long term motion were found analytically using the assumption that the porous medium was thin and vertical flow could be neglected. These two solutions were then joined to give one equation which was assumed accurate for intermediate times as well. It was assumed in these derivations that the interface remained straight during its rotation toward the horizontal. Laboratory tests using models of square and circular cross-section packed with glass beads were performed which seemed to agree with the equation.

Dagan and Bear (1967) treated the upward movement of a freshwater-saltwater interface beneath a partially penetrating well using a perturbation expansion to linearize the interface boundary condition. They checked their results with a sand-packed model and found them to be reasonable when the disturbance of the interface was small. The range of applicability of this method, however, appears to be quite limited.

Shamir and Dagan (1971) developed a transient numerical model to predict the landward movement of a saltwater wedge in a coastal aquifer. The Dupuit assumption was used to formulate the governing equation which was then solved by an implicit finite difference method. Dispersion was neglected. The numerical results were checked against an analytical solution similar to that of Gardner, Downie and Kendall and with a Hele-Shaw model. The comparison with the analytical solution showed good agreement that the interface moved as a straight line. Comparison with the Hele-Shaw model, however, was not quite as good. The authors attributed this to the fact that vertical velocities were neglected in both the analytical and numerical solutions.

Strack (1976) studied the influence of inland production wells on the steady state shape of the saltwater wedge in coastal aquifers. His

analysis makes use of a vertically integrated potential function which can be defined so as to be single-valued, throughout the aquifer. Lines of constant potential can then be found in the horizontal plane which lead to a three-dimensional description of the interface based on the Ghyben-Herzberg principle.

A similar problem was studied by Kishi and Fukuo (1977). They considered the effect of inland pumping on the saltwater wedge in a fan shaped coastal aquifer. The Laplace equation in radial coordinates is integrated vertically to make it two dimensional. Using the Ghyben-Herzberg principle the dependent variable is transformed so that it will be single-valued in both the freshwater region and the interface region. The resulting equation is solved by the method of Green's functions to give a three-dimensional description of the interface.

Studies Dealing with Dispersion

Gardner, Downie and Wyllie (1962) considered the mixing across the interface between methane gas and nitrogen used as a cushion gas in a natural gas reservoir. A solution to the convective dispersion equation in radial coordinates was combined with the gravity segregation formula found by Gardner, Downie and Kendall.

Harleman and Rumer (1962) derived an equation for interface rotation which is the same as that found by Gardner, Downie and Kendall for the latter stages of movement. This equation also is based on the assumption of a straight interface. The same report also deals with longitudinal and lateral dispersion in both stationary and moving coastal interfaces. Laboratory tests using sand-packed models to simulate a coastal aquifer showed that in the absence of tidal fluctuations the mixing zone was quite thin, especially near the toe of the

interface. An equation was presented which predicted the thickness of the dispersion zone accurately in this region. When changing conditions in either the saltwater or the freshwater caused a shift in the equilibrium position of the interface the effects of longitudinal dispersion became pronounced. It was concluded that such shifts are responsible for most of the dispersion found in natural coastal aquifers.

Wooding (1963) obtained approximate solutions for the lateral dispersion across a stationary interface by transforming the governing equations into a natural coordinate system based on the shape of the interface. Using order of magnitude reasoning these equations were reduced to the form of Prandtl's boundary layer equations. For these, the usual similarity solution was obtained which relates the thickness of the mixing layer to the distance from the stagnation point and the slope of the interface.

Hoopes and Harleman (1965 and 1967) analyzed the dispersion of tracers injected into groundwater. Their work consisted of analytical and numerical solutions to the convective dispersion equation and laboratory experiments with a sand-packed model to verify these solutions. The relative effects of convection, lateral and longitudinal dispersion, and molecular diffusion were compared for the case of axisymmetric radial flow from an injection well and for the flow between an injection well and production well. It was shown that the effects of lateral dispersion on the steady flow between two wells was almost negligible except near the line joining the two wells.

Studies Concerned Directly with Freshwater Lenses

Glazunov (1967) proposed to use a cluster of three to five wells operated in various patterns of injection and production in order to

form freshwater lenses of the desired shape. His analysis neglects both dispersion and gravity segregation, treating the convection of an interface in two horizontal directions by a method introduced by Muskat (1946). In this method the interface is represented as a material surface which is transported along the streamlines by the flow while exerting no effect on it as a boundary.

Esmail and Kimbler (1967) studied the effects of radial flow geometry on gravity segregation and longitudinal dispersion in laboratory models composed of glued sand grains. The solution to the convective dispersion equation given by Gardner, Downie and Wyllie was verified for cyclic storage in freshwater lenses for several cycles of injection and production in the model. A dimensionless parameter analysis of the influence of radial geometry and interfacial mixing on the rate of gravity segregation was conducted resulting in an empirical equation for the rate of interface rotation. It was found that there is interaction between the processes of dispersion and interface rotation which retards gravity segregation. The authors concluded that the horizontal projection of the interface is proportional to the square root of the density gradient across it and that gravity segregation in their model had more effect on the recovery efficiency than did dispersion. Under these conditions, interface dispersion may actually improve the recovery efficiency by retarding gravity segregation.

Kumar and Kimbler (1970) continued the research with glued sand models, finding that the recovery efficiency improves after several cycles of injection and recovery.

Whitehead (1974) developed a computational method for predicting the recovery efficiency of a single well cyclic storage system in thin

horizontal saline aquifers. His method was based on the empirical equation of Esmail and Kimbler. Whitehead verified the results of his computational scheme using the glued sand grain model and found them to be accurate to within 10% for three storage cycles. The recovery efficiencies achieved in the laboratory tests were in the range of 70-100%. It was concluded that, given favorable subsurface conditions, the use of saline aquifers for freshwater storage could be economically feasible.

In a series of reports (Agrawal, 1975; D'Amico, 1975; Tate, 1976; Kimbler and Whitehead, 1977) the results of Whitehead were extended to include the effects of aquifer dip and viscosity difference between the resident and injected fluids. These studies also used glued sand models. The conclusions reached from these experiments were that the best conditions for cyclic storage occur when the saline aquifer is horizontal and the injected fluid has the same viscosity as the resident fluid.

It is widely recognized that a pre-existing uniform flow in the saline aquifer is detrimental to the recovery efficiency of a lens storage system. Langhtee (1974) proposed to surround the storage area with bounding wells which would be pumped in such a way that a stagnation zone would result inside the boundary. The required pumping rates for these wells were found by superimposing the streamline and equipotential pattern for the individual wells and solving for the pumping rates which would give the best least-squares fit to the desired piezometric head on the boundary.

Molz and Bell (1977) also considered the use of boundary wells for head gradient control. They used a linear programming technique to find

the optimum set of bounding wells which would give the desired stagnation in the storage area with the least expenditure of energy for pumping.

The shape and movement of naturally occurring freshwater lenses on Grand Cayman Island were studied by Childley and Lloyd (1977). They used a modified Ghyben-Herzberg ratio based on field measurements of salinity distribution in the mixing zone of the lens. The long term transient effects of seasonal variations in recharge rate were modeled numerically using the idea of a succession of steady states. Comparison of the numerical results with records of actual groundwater conditions on the island indicated that their model was useful in predicting long-term changes due to water supply wells and changes in recharge conditions. They concluded that, while it may take many years for a pumped lens to reach equilibrium, an overpumped lens can collapse locally in a matter of a few months.

Smith and Hanor (1975) report on a field test of the freshwater lens storage concept. A 10 centimeter fully penetrating well was drilled into a confined saline aquifer 36 meters thick to be used for injection and retrieval of freshwater. After the construction of this well it was discovered that a uniform flow of approximately 15 centimeters per day existed in the aquifer. Recognizing the unfavorable conditions, the investigators proceeded with two tests, each using about 757,000 liters of freshwater. In the first test, the water was stored for two hours and 41% was recovered. In the second test the storage period was six days and the recovery efficiency was 24.5%.

Werner and Kley (1977) conducted a field test of the storage of heated water in a water table aquifer 3.35 meters thick. A total of

430 cubic meters of water at a temperature of 45°C was injected and the movement of the heat was monitored with buried temperature sensors for a period of 64 days. The heated water remained close to the injection well throughout the test period but no attempt was made to recover it.

Molz, Warman and Jones (1978) reported a field test with a partially penetrating well in a confined aquifer 21 meters thick. A group of 14 observation wells were constructed to monitor the movement of the hot water injected. In this test, storage of 7570 cubic meters of hot water for 36 days resulted in an energy recovery factor of 0.69 which was considered promising.

Papadopulos and Larson (1978) applied a finite difference numerical model developed for the U.S. Geological Survey (INTERCOMP, 1976) to simulate the test results of Molz, Warman and Jones. The predicted recovery efficiency was 75% versus a value of 69% measured in the field. Considering the accuracy of the measured aquifer properties, this prediction was considered quite good.

CHAPTER 3

BASIC EQUATIONS AND FLUID PROPERTIES

Basic Equations

Darcy's Law

The groundwater flow to be dealt with in this report is limited to laminar flow in porous media with only primary porosity. The equation of motion for this flow is Darcy's law which can be expressed, in the cartesian coordinate system, as

$$q_x = K_{xx} J_x + K_{xy} J_y + K_{xz} J_z \tag{3.1a}$$

$$q_y = K_{yx} J_x + K_{yy} J_y + K_{yz} J_z \tag{3.1b}$$

$$q_z = K_{zx} J_x + K_{zy} J_y + K_{zz} J_z \tag{3.1c}$$

where

q_x, q_y, q_z = components of the discharge velocity in the x, y, and z directions, respectively

K_{ij} = components of the hydraulic conductivity tensor for ($i, j = x, y, z$)

$$J_x = -\frac{\partial \phi}{\partial x}$$

$$J_y = -\frac{\partial \phi}{\partial y}$$

$$J_z = -\frac{\partial \phi}{\partial z}$$

ϕ = piezometric head

If it is assumed that the coordinate axes are parallel to the principal directions of hydraulic conductivity then Darcy's law can be simplified to

$$\vec{q} = -K_{xx}\frac{\partial \phi}{\partial x}\hat{i} - K_{yy}\frac{\partial \phi}{\partial y}\hat{j} - K_{zz}\frac{\partial \phi}{\partial z}\hat{k} \qquad (3.2)$$

where $\hat{i}$, $\hat{j}$, and $\hat{k}$ are unit vectors in the x, y, and z directions, respectively. This assumption is not a major restriction to the use of equation (3.2) because in practice it is usually difficult to distinguish any directional hydraulic conductivities except the vertical and the horizontal. If the soil is isotropic or only one dimensional flow is being considered equation (3.2) reduces to

$$\vec{q} = -K \nabla \phi \qquad (3.3)$$

The value of the hydraulic conductivity, K, or of its directional components depends on the properties of both the soil and the fluid. Since the properties of saltwater and freshwater are somewhat different it may be necessary in the general case to consider the hydraulic conductivity as a function of the salt concentration. The flow resistance of the soil is then described in terms of its intrinsic permeability, k, which is related to hydraulic conductivity by

$$K = kg/\nu \qquad (3.4)$$

where ν is the kinematic viscosity of the fluid and g is the acceleration due to gravity.

The piezometric head, ϕ, appearing in equations (3.2) and (3.3) is defined as

$$\phi = z + P/\gamma \tag{3.5}$$

which depends on the unit weight, γ, of the fluid concerned. Since γ is also a function of salt concentration it is often more convenient to deal directly with pressure, P, in the equation of motion.

Continuity

The continuity equation for groundwater flow is

$$\nabla \cdot \vec{q} = -S_s \frac{\partial \phi}{\partial t} \tag{3.6}$$

in which S_s, the specific storage, is defined as

$$S_s = \rho g(\alpha + n\beta) \tag{3.7}$$

where

α = coefficient of soil compressibility

β = coefficient of compressibility for water

n = porosity

ρ = fluid density

The combination of equations (3.2) and (3.6) gives the governing equation for groundwater flow

$$\frac{\partial}{\partial x}\left[K_{xx}\frac{\partial \phi}{\partial x}\right] + \frac{\partial}{\partial y}\left[K_{yy}\frac{\partial \phi}{\partial y}\right] + \frac{\partial}{\partial z}\left[K_{zz}\frac{\partial \phi}{\partial z}\right] = S_s \frac{\partial \phi}{\partial t} \tag{3.8}$$

For steady flow in homogeneous and isotropic soil this reduces to the Laplace equation

$$\frac{\partial^2 \phi}{\partial x^2} + \frac{\partial^2 \phi}{\partial y^2} + \frac{\partial^2 \phi}{\partial z^2} = 0 \tag{3.9}$$

Well Flow in Leaky Aquifers

In dealing with flow to and from wells, it is customary to denote the head gradient in terms of drawdown, s, which is defined as

$$s = \phi - \phi_0 \tag{3.10}$$

where ϕ_0 is the head above the leaky layer (see Figure 3.1). The flow from an injection well causes an increase of head, in which case s will be called "push up" instead of drawdown. A leaky aquifer is one which is confined by a layer of material which has low hydraulic conductivity, but not so low that it can be considered impervious. The governing equation for flow in a leaky aquifer is

$$\nabla^2 s - s/B^2 = \frac{S_s}{Kb} \frac{\partial s}{\partial t} \tag{3.11}$$

The leakage coefficient, B, is given by

$$B^2 = Kbb'/K' \tag{3.12}$$

where

K' = hydraulic conductivity of the leaky layer

b' = thickness of the leaky layer

b = thickness of the aquifer

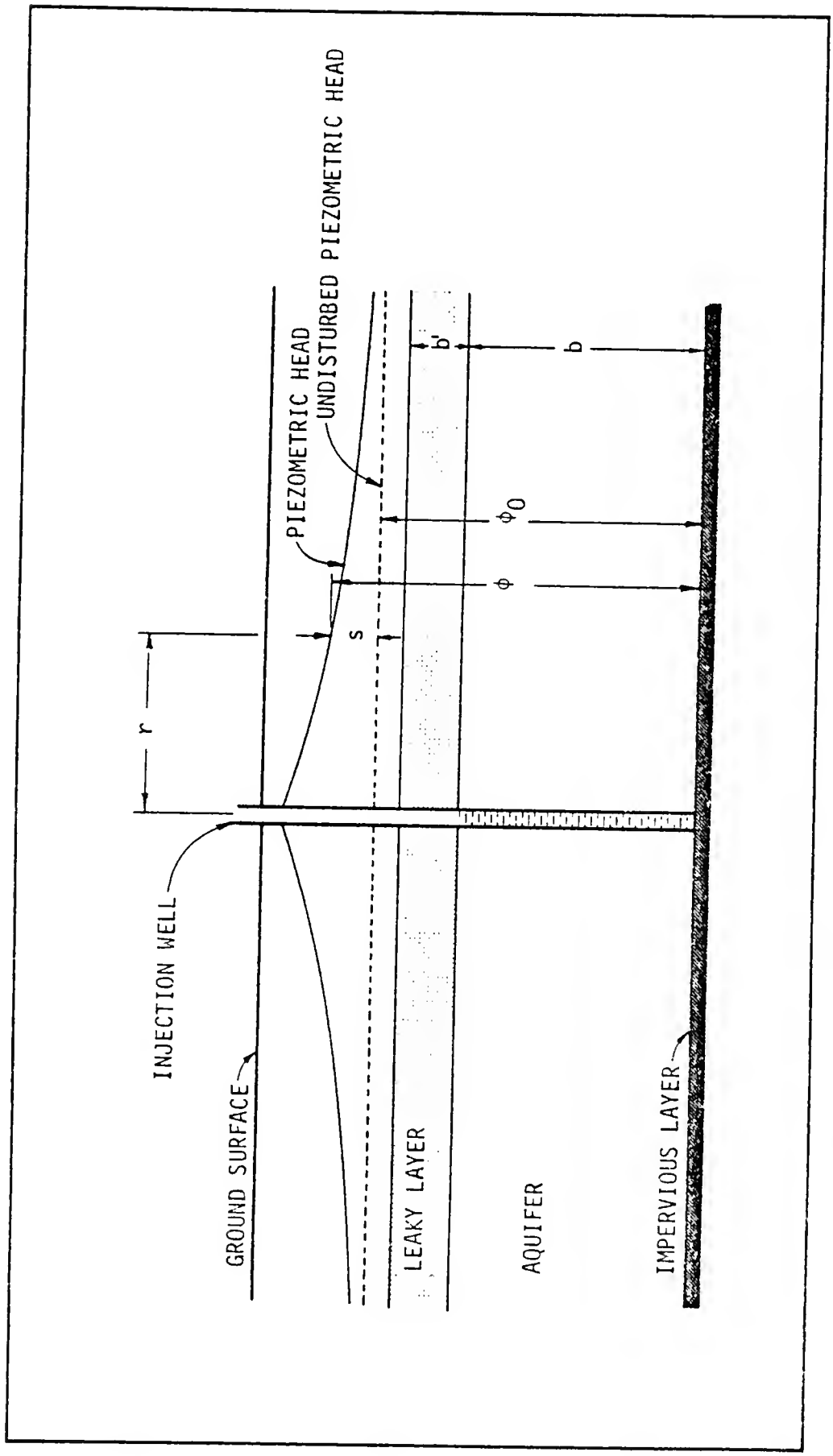

FIGURE 3.1. DEFINITION DIAGRAM FOR WELL FLOW IN A LEAKY AQUIFER

The Dispersion Equation

The mixing of saltwater with freshwater at the periphery of a freshwater lens is described by the convective dispersion equation

$$\frac{\partial c}{\partial t} + \frac{1}{n} \vec{q} \cdot \nabla c = \nabla \cdot D \cdot \nabla c \qquad (3.13)$$

in which c is the concentration of the fluid being followed and D is the dispersion tensor. For isotropic porous media this tensor has only two independent terms, D_ℓ and D_t, corresponding to longitudinal and transverse dispersion respectively, relative to the direction of the mean flow. The values of these coefficients depend not only on the properties of the porous medium but also on the flow velocity and the properties of the fluid involved. It is often assumed that these coefficients can be represented by

$$D_\ell = D_m + \alpha_\ell \, q_\ell / n \qquad (3.14a)$$

$$D_t = D_m + \alpha_t \, q_\ell / n \qquad (3.14b)$$

where

D_m = coefficient of molecular diffusion in the porous medium

α_ℓ = longitudinal dispersivity

α_t = transverse dispersivity

q_ℓ = discharge velocity in the direction of mean flow

The dispersivity coefficients α_ℓ and α_t are properties of the porous medium only. Their magnitudes are related to the intrinsic permeability and the pore size distribution, but the actual values must

be found experimentally. The longitudinal dispersion coefficient, D_ℓ, is usually 10 to 20 times greater than D_t but the ratio of the two depends on the flow velocity, being close to unity when the flow is very slow and the influence of molecular diffusion predominates.

For axisymmetric radial flow of a tracer-like substance from an injection well, equation (3.13) can be simplified to

$$\frac{\partial c}{\partial t} + \left(\frac{Q}{2\pi bnr}\right) \frac{\partial c}{\partial r} = \alpha_\ell \left(\frac{Q}{2\pi bnr}\right) \frac{\partial^2 c}{\partial r^2} \qquad (3.15)$$

because there are no components of either velocity or concentration gradient except in the radial direction. This equation has been solved numerically for the case of steady flow from the well and continuous tracer injection beginning instantanously (Hoopes and Harleman, 1965; and Shamir and Harleman, 1966).

Freshwater injected into a saline aquifer does not behave as a tracer because of the difference in density, so equation (3.15) does not apply even though the flow may be asixymmetric. Because vertical components of both velocity and concentration gradient are present, equation (3.13) must be used. The numerical solution of this equation will be the subject of Chapter 7 of this report.

Boundary Conditions at an Interface

When the mixing zone separating saltwater and freshwater is relatively thin, it is often convenient to neglect dispersion and assume that the two fluids are separated by a sharp interface. If such a boundary between the two fluids exists, a separate governing equation can be written for each zone and the two flows will be coupled by their common boundary condition at the interface.

The interface is a material surface which is always composed of the same fluid particles. The essential features of such a surface are that both pressure and the velocity component normal to the interface must be continuous across it. For a stationary interface the normal velocity component is zero so the boundary condition is concerned with pressure only. The pressure on the freshwater side of the interface is

$$P_f = \gamma_f \, (\phi_f - z_i) \tag{3.16a}$$

and on the saltwater side

$$P_s = \gamma_s \, (\phi_s - z_i) \tag{3.16b}$$

where z_i is the elevation of a point on the interface and the subscripts f and s stand for freshwater and saltwater, respectively. Requiring that these pressures be equal results in an expression for the boundary condition at a stationary interface

$$z_i = \frac{\gamma_s}{\Delta\gamma} \, \phi_s - \frac{\gamma_f}{\Delta\gamma} \, \phi_f \tag{3.17}$$

where

$$\Delta\gamma = \gamma_s - \gamma_f$$

For the special case where the saltwater is at rest and a hydrostatic pressure distribution prevails in the freshwater zone this reduces to the Ghyben-Herzberg relationship

$$\Delta z = - \frac{\gamma_f}{\Delta\gamma} \Delta\phi_f \tag{3.18a}$$

or

$$\Delta z = - \delta \Delta \phi_f \tag{3.18b}$$

where $\delta = \gamma_f / \Delta\gamma$ is the Ghyben-Herzberg ratio. This states that a change in the piezometric head of the freshwater causes a change in the elevation of the interface that is opposite in sign and greater in magnitude by a factor of δ.

If the interface is not stationary the condition of continuity of the normal velocity component must also be used. The interfacial surface can then be described by some function, F, such that

$$F(x, y, z, t) = 0 \tag{3.19}$$

This surface is convected by the flow so that

$$\frac{\partial F}{\partial t} + \frac{\vec{q}}{n} \cdot \nabla F = 0 \tag{3.20}$$

where

$\vec{q}$ = discharge velocity of interfacial particles

n = porosity of the aquifer

In terms of the velocities adjacent to the interface on both sides of it this becomes

$$n \frac{\partial F}{\partial t} + \vec{q}_f \cdot \nabla F = 0 \tag{3.21a}$$

for the freshwater, and

$$n \frac{\partial F}{\partial t} + \vec{q}_s \cdot \nabla F = 0 \tag{3.21b}$$

for the saltwater. In terms of the elevation of a point on the interface, z_i, the function, F, can be written as

$$F(x, y, z, t) = z - z_i\ (x, y, t) = 0 \tag{3.22}$$

Substituting this, together with Darcy's law, into equations (3.21) gives

$$-n \frac{\partial z_i}{\partial t} - K\nabla\phi_f \cdot \nabla(z - z_i) = 0 \tag{3.23a}$$

$$-n \frac{\partial z_i}{\partial t} - K\nabla\phi_s \cdot \nabla(z - z_i) = 0 \tag{3.23b}$$

Performing the vector operations indicated in these equations results in the boundary conditions for the freshwater zone and the saltwater zone. The interface boundary condition for the freshwater zone, then, is

$$n \frac{\gamma_f}{\Delta\gamma} \frac{\partial\phi_f}{\partial t} - n \frac{\gamma_s}{\Delta\gamma} \frac{\partial\phi_s}{\partial t} - K \frac{\gamma_f}{\Delta\gamma} (\nabla\phi_f)^2 + K \frac{\gamma_s}{\Delta\gamma} (\nabla\phi_f \cdot \nabla\phi_s)$$

$$- K \frac{\partial\phi_f}{\partial z} = 0 \tag{3.24a}$$

and for the saltwater zone,

$$n \frac{\gamma_f}{\Delta\gamma} \frac{\partial\phi_f}{\partial t} - n \frac{\gamma_s}{\Delta\gamma} \frac{\partial\phi_s}{\partial t} + K \frac{\gamma_s}{\Delta\gamma} (\nabla\phi_s)^2 + K \frac{\gamma_f}{\Delta\gamma} (\nabla\phi_f \cdot \nabla\phi_s)$$

$$- K \frac{\partial\phi_s}{\partial z} = 0 \tag{3.24b}$$

Fluid Properties

Density

Up to this point the fluids with which this report is concerned have been referred to simply as freshwater and saltwater. These convenient terms are used only in a relative sense and the actual properties of the fluids deserve some further elaboration. In the ensuing analysis the primary difference between the resident and injected fluids will be their density. In general, this is a property that depends on pressure, temperature and salt concentration. In this report, however, the change in density due to compressibility will be neglected because it is so small, and the thermal effects, while not necessarily small, will be eliminated by assuming that the temperature of the injected fluid is the same as that of the resident saltwater.

Figure 3.2 shows the relationship of density to temperature for water with several different salt concentrations. With the exception of the 3.5% concentration line, this figure is based on data for solutions of pure sodium chloride in water. The 3.5% concentration line shows the temperature versus density relation for seawater having a dissolved solids concentration of 3.5%. Saline groundwater is commonly associated with the intrusion of seawater into coastal aquifers. However, it is also found in many locations which have no apparent geological association with the oceans and where its concentration may be much greater or less than that of seawater.

Figure 3.3 shows the relationship of density to sodium chloride concentration. It is worthwhile to note that in this range the relationship is apparently linear.

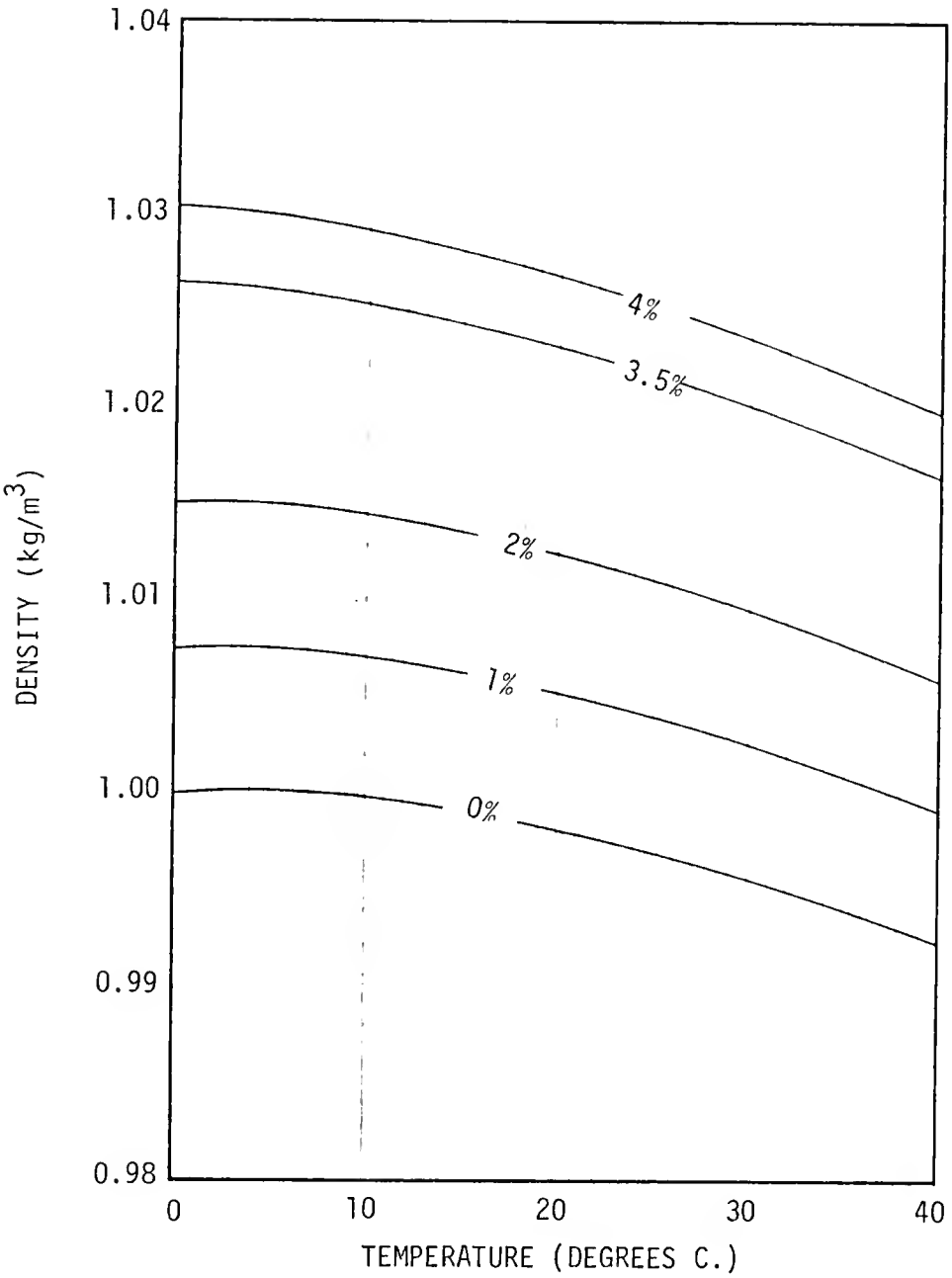

FIGURE 3.2. TEMPERATURE VS. DENSITY FOR WATER WITH VARIOUS SALT CONCENTRATIONS

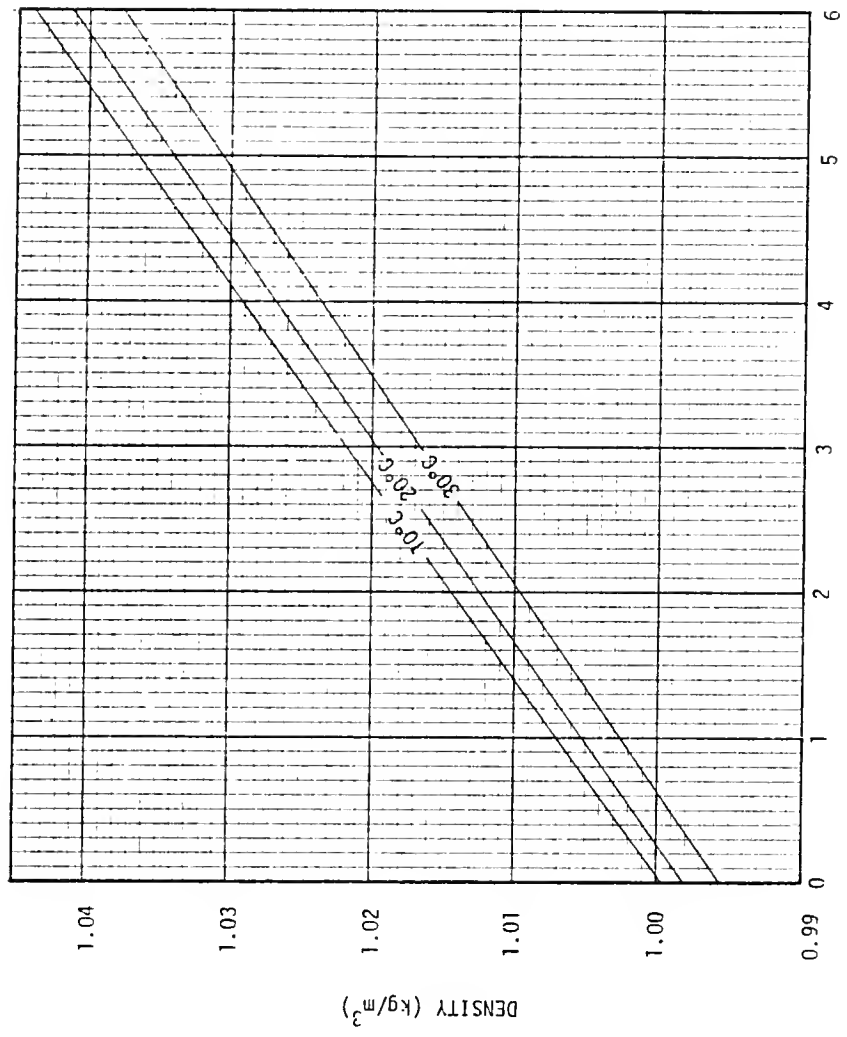

FIGURE 3.3. WATER DENSITY VS. SALT CONCENTRATION AT VARIOUS TEMPERATURES

Viscosity

It was shown in equation (3.4) that the hydraulic conductivity of an aquifer is partially determined by the kinematic viscosity of its water. Viscosity is a function of both temperature and salt concentration but within the range of present interest temperature is the more important factor of the two. The temperature dependence of kinematic viscosity for both pure water and seawater is shown in Figure 3.4. It is interesting to note that the kinematic viscosity of pure sodium chloride solutions, as given by Kaufmann (1960) for concentrations up to 4%, differ so little from the kinematic viscosity of pure water that they could not be distinguished from it if plotted at the scale of Figure 3.4. Since differences in temperature are not being considered in this study and the influence of salt concentration on viscosity is relatively weak, viscosity differences will be neglected also.

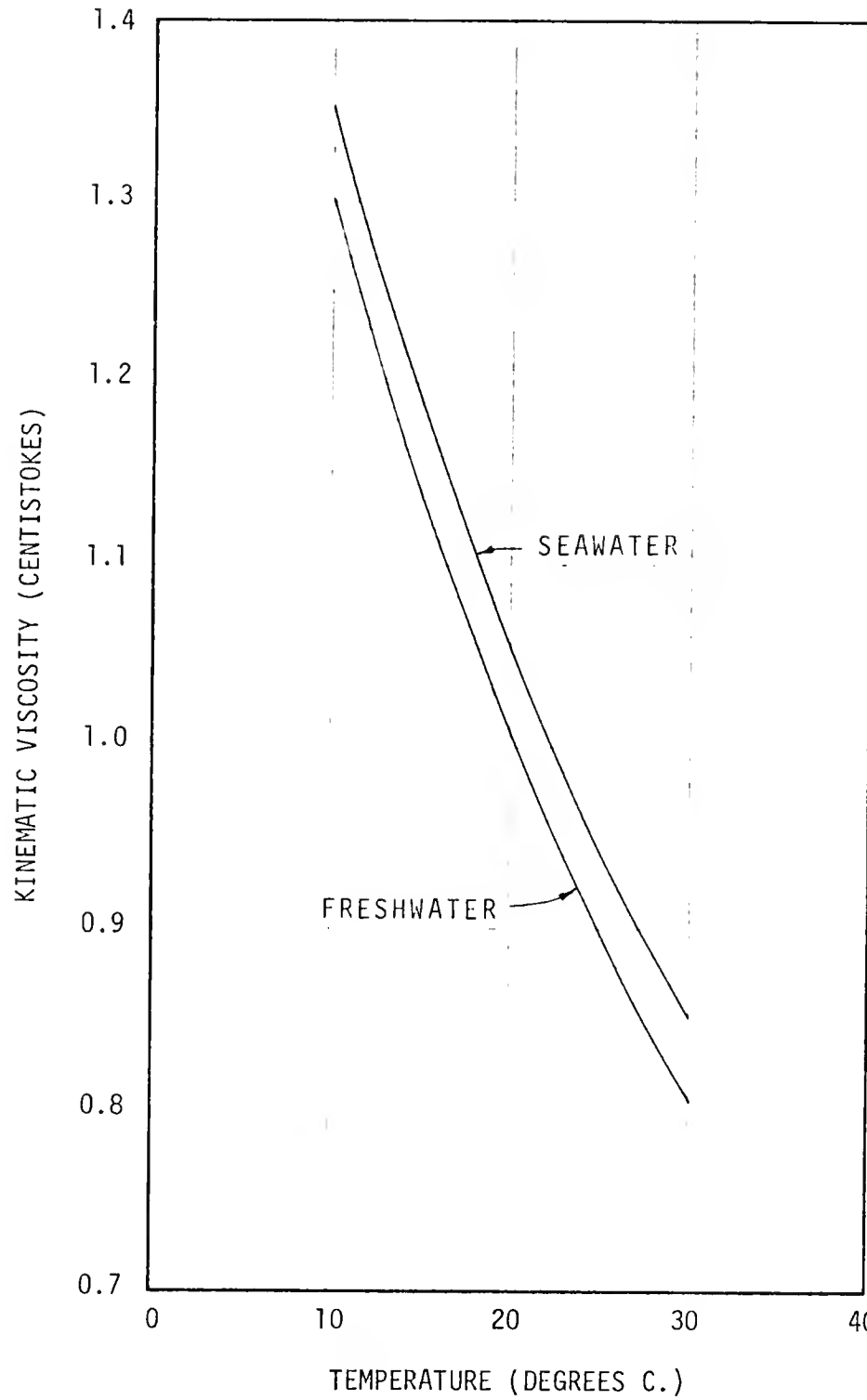

FIGURE 3.4. VISCOSITY VS. TEMPERATURE FOR FRESHWATER AND SALTWATER

CHAPTER 4

THE HELE-SHAW MODEL

General

Valuable insights into the flow phenomena associated with the injection of fresh water into saline groundwater can be obtained by studying certain simplified aspects of the problem. This chapter will describe the use of a physical model to analyze the movement of the interface between the two fluids in the absence of dispersion. The Hele-Shaw analog was chosen for this work because it is simple and inexpensive to construct and the test results are easily observable without elaborate instrumentation. The Hele-Shaw analog consists of one or more viscous liquids flowing in the gap between two closely spaced flat plates. Its usefulness in groundwater studies is based on the fact that the Navier-Stokes equations governing the viscous flow in this gap can be reduced to a form similar to Darcy's law in two dimensions.

The Viscous Flow Analogy

If u, v, and w are the velocity components in the x, y, and z directions, respectively then the Navier-Stokes equations for incompressible flow in a cartesian coordinate system are

$$\frac{\partial u}{\partial t} + u\frac{\partial u}{\partial x} + v\frac{\partial u}{\partial y} + w\frac{\partial u}{\partial z} = b_x - \frac{1}{\rho}\frac{\partial P}{\partial x} + \nu\nabla^2 u \qquad (4.1a)$$

$$\frac{\partial v}{\partial t} + u\frac{\partial v}{\partial x} + v\frac{\partial v}{\partial y} + w\frac{\partial v}{\partial z} = b_y - \frac{1}{\rho}\frac{\partial P}{\partial y} + \nu\nabla^2 v \qquad (4.1b)$$

$$\frac{\partial w}{\partial t} + u\frac{\partial w}{\partial x} + v\frac{\partial w}{\partial y} + w\frac{\partial w}{\partial z} = b_z - \frac{1}{\rho}\frac{\partial P}{\partial z} + \nu\nabla^2 w \qquad (4.1c)$$

where

b_x, b_y and b_z = components of acceleration due to body forces in the x, y, and z directions, respectively

ρ = density of the fluid

ν = kinematic viscosity of the fluid

P = pressure

Applying these equations to the flow between the plates shown in Figure 4.1, it can be assumed that because of the low Reynolds number (Re < 1 for this model) the flow is laminar and there is no velocity component, v, in the direction normal to the plates. Note also that, since the velocity at the surface of the plates is zero, the velocity gradients normal to the plates are very large compared to those in the x and z directions so that the latter can be neglected. Finally, the only body force acting on the fluid is gravity, so $b_z = -g$ and $b_x = b_y = 0$. Incorporating these observations into the Navier-Stokes equations and multiplying by ρ results in

$$\frac{\partial P}{\partial x} = \mu\frac{\partial^2 u}{\partial y^2} \qquad (4.2a)$$

$$\frac{\partial P}{\partial y} = 0 \qquad (4.2b)$$

$$\gamma + \frac{\partial P}{\partial z} = \mu\frac{\partial^2 u}{\partial y^2} \qquad (4.2c)$$

where $\gamma = \rho g$ is the unit weight of the fluid and $\mu = \rho\nu$ is its dynamic viscosity. Recalling that the piezometric head, ϕ, is defined as

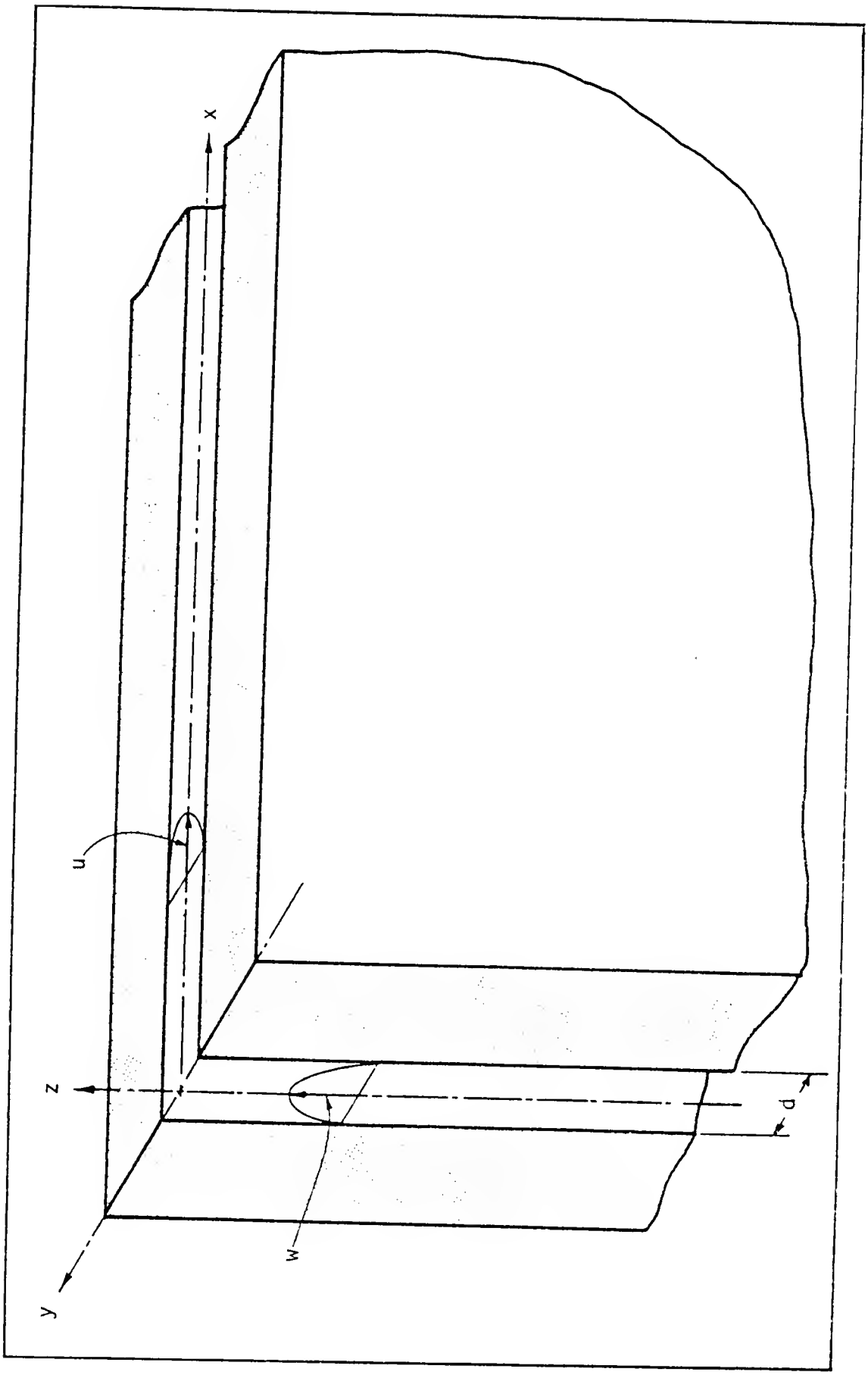

FIGURE 4.1. SCHEMATIC OF GAP BETWEEN PLATES

$$\phi = z + P/\gamma \tag{4.3}$$

it follows that equations (4.2) when expressed in terms of ϕ and divided by γ become

$$\frac{\partial \phi}{\partial x} = \frac{\mu}{\gamma} \frac{\partial^2 u}{\partial y^2} \tag{4.4a}$$

$$\frac{\partial \phi}{\partial y} = 0 \tag{4.4b}$$

$$\frac{\partial \phi}{\partial z} = \frac{\mu}{\gamma} \frac{\partial^2 u}{\partial y^2} \tag{4.4c}$$

From the second of these equations it is seen that at any point (x, z) in the plane of the model, the piezometric head is not a function of y. Therefore, the first and third of these equations can be integrated with respect to y giving

$$y \frac{\partial \phi}{\partial x} = \frac{\mu}{\gamma} \frac{\partial u}{\partial y} + C \tag{4.5a}$$

$$y \frac{\partial \phi}{\partial z} = \frac{\mu}{\gamma} \frac{\partial w}{\partial y} + C \tag{4.5b}$$

The constant of integration, C, is found to be zero by observing that at the center of the flow region, where y = 0 both $\frac{\partial u}{\partial y}$ and $\frac{\partial w}{\partial y}$ are also zero, so that

$$y \frac{\partial \phi}{\partial x} = \frac{\mu}{\gamma} \frac{\partial u}{\partial y} \tag{4.6a}$$

$$y \frac{\partial \phi}{\partial z} = \frac{\mu}{\gamma} \frac{\partial w}{\partial y} \tag{4.6b}$$

Integrating these equations again with respect to y gives

$$\frac{y^2}{2} \frac{\partial \phi}{\partial x} = \frac{\mu}{\gamma} u + C_1 \tag{4.7a}$$

$$\frac{y^2}{2} \frac{\partial \phi}{\partial z} \quad \frac{\mu}{\gamma} w + C_1 \tag{4.7b}$$

Here, the constant of integration, C_1, is found by requiring that, at the surface of the plates, where $y = \pm d/2$, $u = w = 0$. With these boundary conditions the expressions for the velocity distribution across the gap are found to be

$$u = \frac{\gamma}{2\mu} \left(y^2 - \frac{d^2}{4}\right) \frac{\partial \phi}{\partial x} \tag{4.8a}$$

$$w = \frac{\gamma}{2\mu} \left(y^2 - \frac{d^2}{4}\right) \frac{\partial \phi}{\partial z} \tag{4.8b}$$

where d is the thickness of the gap between the plates. Now, in order to find a velocity analogous to Darcy's discharge velocity for flow through porous media, equations (4.8) must be averaged across the thickness of the gap as follows

$$q_x = \frac{1}{d} \int_{-d/2}^{d/2} u \, dy = - \frac{d^2}{12} \frac{\gamma}{\mu} \frac{\partial \phi}{\partial x} \tag{4.9a}$$

$$q_z = \frac{1}{d} \int_{-d/2}^{d/2} w \, dy = - \frac{d^2}{12} \frac{\gamma}{\mu} \frac{\partial \phi}{\partial z} \tag{4.9b}$$

If the constant coefficients in equations (4.9) are used to define an effective hydraulic conductivity, K_m, for the model

$$K_m = \frac{d^2}{12} \frac{\gamma}{\mu} \tag{4.10}$$

then the governing equations for flow between the plates become

$$q_x = - K_m \frac{\partial \phi}{\partial x} \tag{4.11a}$$

$$q_z = - K_m \frac{\partial \phi}{\partial z} \tag{4.11b}$$

in which the resemblance to the two dimensional form of Darcy's law is obvious. In further analogy to groundwater flow, an intrinsic permeability for the Hele-Shaw model, k_m, can be defined as

$$k_m = d^2/12 \tag{4.12}$$

so that

$$K_m = k_m \frac{\gamma}{\mu} \tag{4.13}$$

The continuity equation for the flow between the plates is

$$\frac{\partial u}{\partial x} + \frac{\partial w}{\partial z} = 0 \tag{4.14}$$

since there is no velocity in the y direction. Averaging these velocities across the gap, as before, results in

$$\frac{\partial}{\partial x} \left(K_m \frac{\partial \phi}{\partial x} \right) + \frac{\partial}{\partial z} \left(K_m \frac{\partial \phi}{\partial z} \right) = 0 \tag{4.15}$$

which has the same form as the governing equation for two dimensional flow in an incompressible porous medium. The model hydraulic conductivity, K_m, is a constant depending only on the spacing, d, of the plates and the unit weight and viscosity of the fluid. Consequently, for parallel plates and homogeneous fluids the flow is homogeneous and isotropic, so that equation (4.15) reduces to the Laplace equation in

two dimensions

$$\frac{\partial^2 \phi}{\partial x^2} + \frac{\partial^2 \phi}{\partial z^2} = 0 \tag{4.16}$$

Since K_m is a function of physical parameters which are relatively easy to measure and control, the Hele-Shaw model is a very convenient tool for the scale modelling of two dimensional groundwater flow.

Model Scaling

In the preceding section it was shown that two dimensional groundwater flow can be modeled by the Hele-Shaw analog because the governing equations for the two cases are of the same form. If quantitative results are to be obtained from the model, however, the scaling ratios between model and prototype must be chosen so that the governing equations are actually identical. In order to achieve this, the model laws which fit the Hele-Shaw model to the prototype case of groundwater flow must be developed.

Since the present case involves the modeling of two immiscible liquids separated by an interface the equations on which the model laws depend are Darcy's law, the continuity equation and the boundary condition for interface flow. Letting the subscript m denote model parameters and p denote those in the prototype, Darcy's law for the model is

$$q^i_{xm} = -K_m \frac{\partial \phi^i_m}{\partial x_m} \tag{4.17a}$$

$$q^i_{zm} = -K_m \frac{\partial \phi^i_m}{\partial z_m} \tag{4.17b}$$

where the superscript $i = \begin{cases} f \text{ for the lighter fluid} \\ s \text{ for the heavier fluid} \end{cases}$

The corresponding equations for the prototype are

$$q^i_{xp} = -K_p \frac{\partial \phi^i_p}{\partial z_p} \tag{4.18a}$$

$$q^i_{zp} = -K_p \frac{\partial \phi^i_p}{\partial z_p} \tag{4.18b}$$

Let the scaling ratios between model parameters and prototype parameters be denoted by the subscript r, so that

$$K_r = K_m/K_p \tag{4.19a}$$

$$q_r = q_m/q_p \tag{4.19b}$$

$$x_r = x_m/x_p \tag{4.19c}$$

etc.

Then, substituting these relationships into equations (4.18) gives

$$q^i_{xm}/q^i_{xr} = - \frac{K_m}{K_r} \frac{X_r}{\phi^i_r} \frac{\partial \phi^i_m}{\partial x_m} \tag{4.20a}$$

$$q^i_{zm}/q^i_{zr} = - \frac{K_m}{K_r} \frac{Z_r}{\phi^i_r} \frac{\partial \phi^i_m}{\partial z_r} \tag{4.20b}$$

If these are to be identical to equations (4.17) then it must be ture that

$$q^i_{xr} = \frac{K_r \phi^i_r}{X_r} \tag{4.21a}$$

$$q^i_{zr} = \frac{K_r \phi^i_r}{z_r} \tag{4.21b}$$

Equations (4.21) provide one of the model laws which allow results from the model to be transferred to the prototype.

The continuity equations for isotropic flow in the model and prototype are

$$\frac{\partial^2 \phi^i_m}{\partial x^2_m} + \frac{\partial^2 \phi^i_m}{\partial z^2_m} = 0 \tag{4.22}$$

and

$$\frac{\partial^2 \phi^i_p}{\partial x^2_p} + \frac{\partial^2 \phi^i_p}{\partial z^2_p} = 0 \tag{4.23}$$

Substituting the appropriate parameter ratios into equation (4.23) and requiring that it be identical to equation (4.22) results in

$$x_r = z_r \tag{4.24}$$

The third similitude requirement is that the boundary conditions at the moving interface be given by identical equations in both model and prototype. These interface equations were given in Chapter 3. For the model they are

$$n_m \frac{\gamma^f_m}{\Delta\gamma_m} \frac{\partial \phi^f_m}{\partial t_m} - n_m \frac{\gamma^s_m}{\Delta\gamma_m} \frac{\partial \phi^s_m}{\partial t_m} - K_m \frac{\gamma^f_m}{\Delta\gamma_m} (\nabla\phi^f_m)^2 + K_m \frac{\gamma^s_m}{\Delta\gamma_m} (\nabla\phi^f_m \cdot \nabla\phi^s_m) -$$

$$- K_m \frac{\partial \phi^f_m}{\partial z_m} = 0 \tag{4.25a}$$

and

$$n_m \frac{\gamma_m^f}{\Delta\gamma_m} \frac{\partial \phi_m^f}{\partial t_m} - n_m \frac{\gamma_m^s}{\Delta\gamma} \frac{\partial \phi_m^s}{\partial t} + K_m \frac{\gamma_m^s}{\Delta\gamma_m} (\nabla\phi_m^s)^2 + K_m \frac{\gamma_m^f}{\Delta\gamma_m} (\nabla\phi_m^f \cdot \nabla\phi_m^s) -$$

$$- K_m \frac{\partial \phi_m^s}{\partial z_m} = 0 \qquad (4.25b)$$

The corresponding equations for the prototype are the same as equations (4.25) except that the m subscripts are replaced by p. When the parameter ratios are substituted into the prototype equations and equality is required with the model equations, 16 groupings of parameter ratios are generated, which must all be equal to unity. Many of these groupings are repetitive and, since they provide no new information, they will not be listed here. The groupings which are useful are

$$\frac{1}{n_r} \frac{\Delta\gamma_r}{\gamma_r^f} \frac{t_r}{\phi_r^f} = \frac{1}{n_r} \frac{\Delta\gamma_r}{\gamma_r^s} \frac{t_r}{\phi_r^s} = \frac{1}{K_r} \frac{\Delta\gamma_r}{\gamma_r^f} \frac{x_r^2}{\phi_r^{f2}} = \frac{1}{K_r} \frac{z_r}{\phi_r^f} = \frac{1}{K_r} \frac{z_r}{\phi_r^s} = 1 \qquad (4.26)$$

The equality of the first and third terms of this equation gives the time scale for the model

$$t_r = \frac{n_r \; x_r^2}{K_r \; \phi_r^f} \qquad (4.27)$$

Equality of the first, second, and fourth terms of equation (4.26) together with equation (4.27) results in

$$\gamma_r^f \; \phi_r^f = \gamma_r^s \; \phi_r^s = \Delta\gamma_r \; z_r \qquad (4.28)$$

Finally, the equality between the last two groupings in equation (4.26) requires that

$$\phi_s^f = \phi_r^s \tag{4.29}$$

which, in turn, means that

$$\gamma_r^f = \gamma_r^s \tag{4.30}$$

The complete list of similitude requirements for matching the prototype to the model is given in Table (4.1).

Model Construction

The design of the Hele-Shaw model involved the following consideration:

1. The plates must be transparent, relatively inflexible and demonstrably flat.
2. Provision must be made for the controlled introduction of the viscous fluids and the release of entrapped air.
3. The model must be easily disassembled for cleaning between tests.
4. It must be possible to rotate the model from horizontal to vertical so that the initial shape of the interface can be controlled.

The availability of materials and the requirement for transparency dictated that the material to be used for the flat plates be either 1/4 inch plate glass or 1/2 plexiglass. Since 1/2 plexiglass is more than 2.5 times more flexible than 1/4 inch plate glass, it was decided to use the latter.

TABLE 4.1

SUMMARY OF SIMILITUDE REQUIREMENTS FOR VERTICAL HELE-SHAW MODEL WITH TWO IMMISCIBLE FLUIDS

Velocity Ratios:

$$q^i_{xr} = \frac{K_r \phi^i_r}{x_r} \quad \text{and} \quad q^i_{zr} = \frac{K_r \phi^i_r}{z_r}$$

where $i = \begin{cases} f, \text{ for the lighter fluid} \\ s, \text{ for the heavier fluid} \end{cases}$

Geometric Ratios:

$$x_r = z_r$$

Time Ratio:

$$t_r = \frac{n_r x_r^2}{K_r \phi^f_r}$$

Head and Density Ratios:

$$\gamma^f_r \phi^f_r = \gamma^s_r \phi^s_r = \Delta\gamma_r z_r$$

and

$$\gamma^f_r = \gamma^s_r$$

It was originally thought that all plate glass was very flat and that its flatness must be controlled to very close tolerances during its manufacture. Conversations with production engineers at several glass factories revealed, however, that most emphasis is placed on the uniformity of thickness of the glass and not on its flatness. Essentially, all standard plate glass is now produced by the flotation process. This gives it a very smooth surface and uniform thickness and it is simply assumed to be flat enough for most purposes. Numerous pieces of commercially available plate glass were optically tested for flatness, and it was found that some pieces are much flatter than others. The tests were run by placing the carefully cleaned surfaces of two glass plates together and illuminating them with monochromatic light from a sodium vapor lamp. The uniformity of the interference fringes produced gives a qualitative indication of the flatness of the two glass panes. Three pieces of special plate glass were obtained which were manufactured by the traditional process of mechanical grinding and polishing. The manufacturer claimed that this glass was flat to within two interference fringes per inch, where one interference fringe represents a deviation from the mean surface of approximately 2.75×10^{-4} millimeters. When these pieces of plate glass were observed under the sodium vapor lamp, their superior flatness was evident. Selected pieces of the commercially available glass, however, were nearly as good. These were used in the construction of the Hele-Shaw model.

In order to provide for the controlled infusion of the viscous liquids into the gap between the plates, it was necessary to glue a section of machined plexiglass to each end of both glass plates. In

this way, an infusion reservoir was created on either end of the model so that the liquids could be injected uniformly into the test section. This is shown in Figure 4.2.

The gap between the two glass plates was maintained at a uniform thickness by a series of brass spacers 1/16 of an inch (1.59 mm) thick placed at intervals around the edges of the model. The plates were held in position by C-clamps which pressed them tightly against the spacers. The model was sealed by a length of surgical rubber tubing which was placed around the edges, just inside of the spacers, and crushed flat by the action of the C-clamps. The wall thickness of this tubing was approximately 1/32 of an inch so that it could be crushed between the plates without exerting much force against the glass.

The assembled model, mounted on its stand is shown in Figure 4.3. The length of the test section is 76 centimeters and its height is 38 centimeters. With the rubber seal in place, however, the actual height available for flow is 35.6 centimeters.

The viscous liquids are supplied to the infusion reservoirs on either end of the model through plastic tubes. The plexiglass end pieces on the back plate are each supplied with four fittings for 1/2 inch (1.27 cm) plastic tubing. The heavier fluid is conducted to the model through this tubing from constant head tanks mounted on a ring stand. This is shown in Figure 4.4. On the front plate, the end pieces are provided with air vents on one end, and four nipples for the connection of 1/4 inch (0.64 cm) plastic tubing on the other. The lighter viscous fluid is injected through this tubing into one of the infusion reservoirs by a positive displacement syringe pump. This setup is illustrated in Figure 4.5.

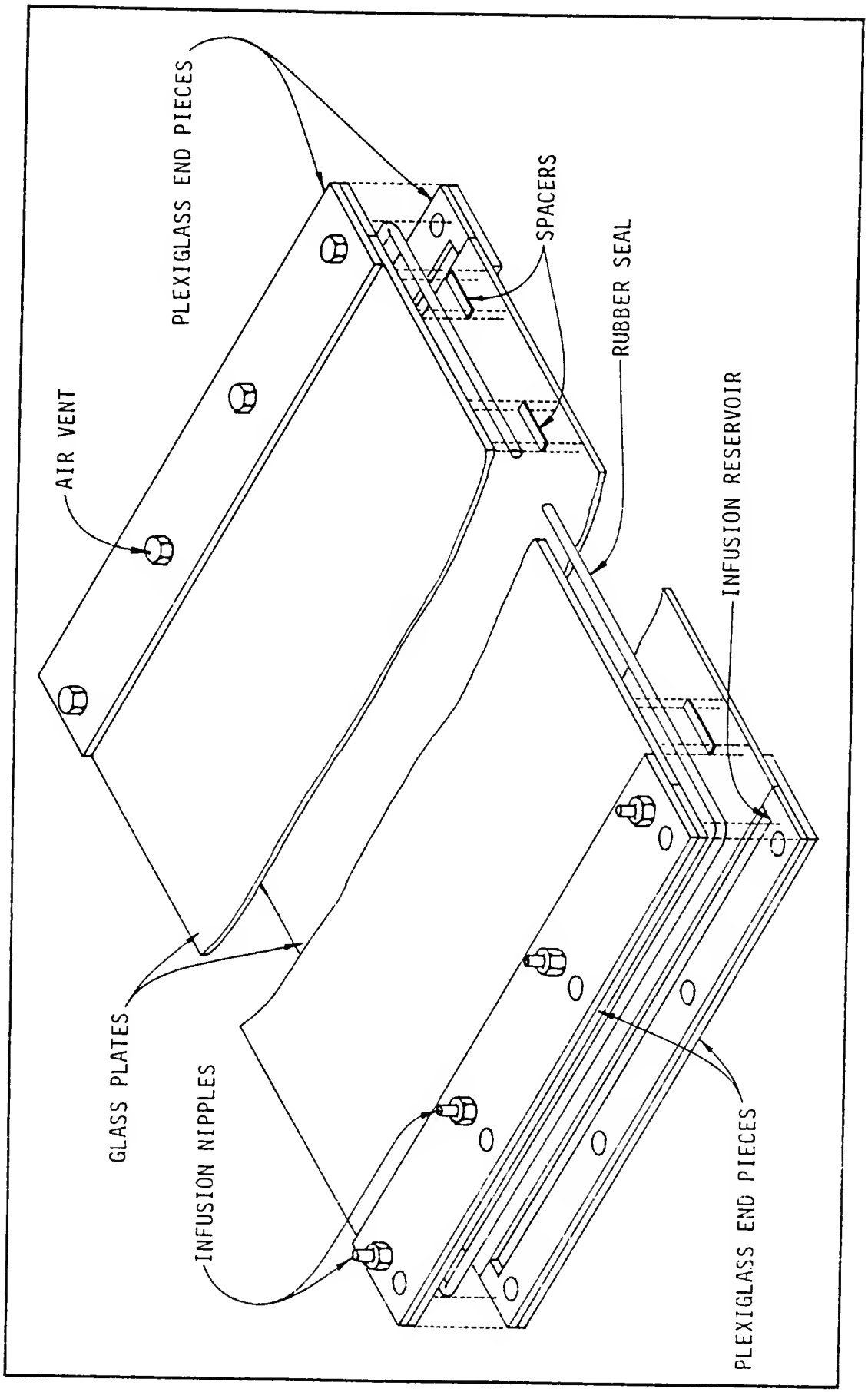

FIGURE 4.2. GLASS PLATES WITH INFUSION RESERVOIRS AND SEAL

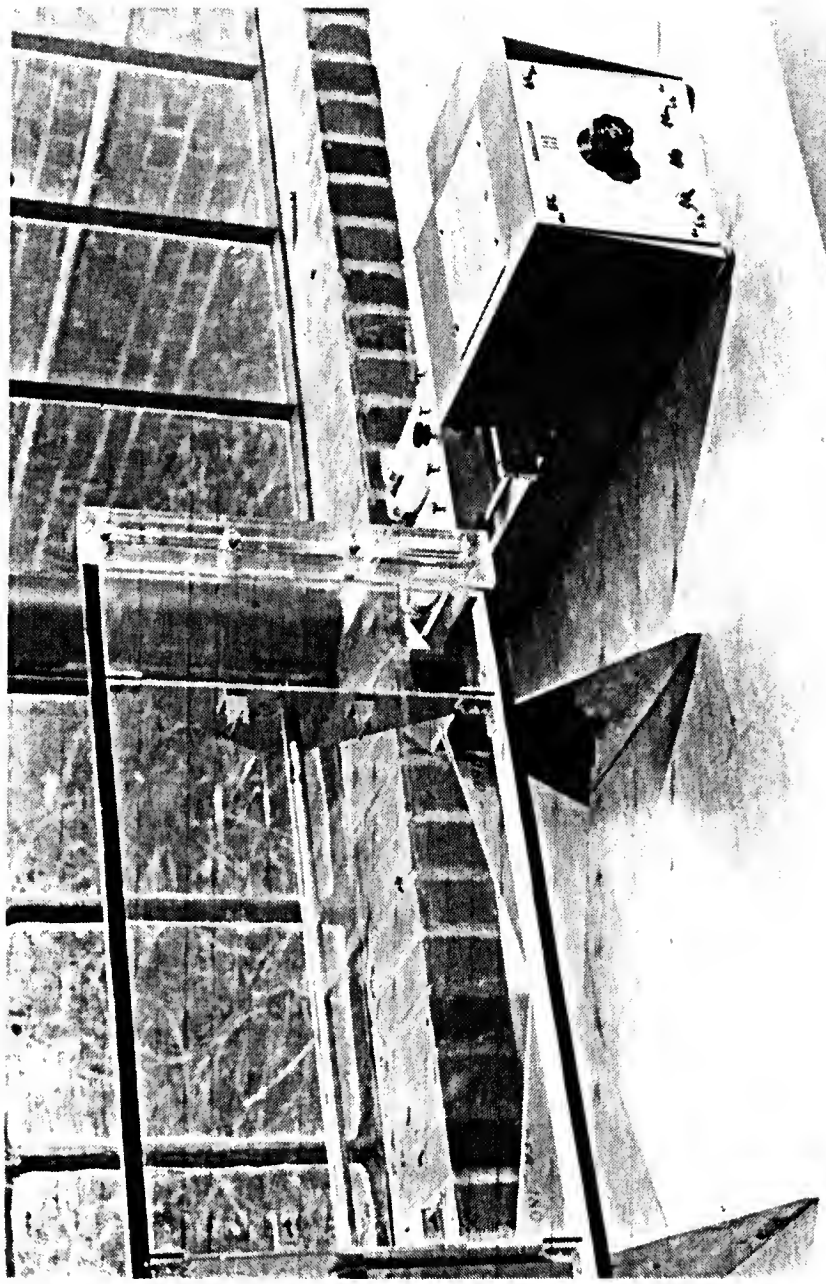

FIGURE 4.3. ASSEMBLED MODEL ON ITS STAND

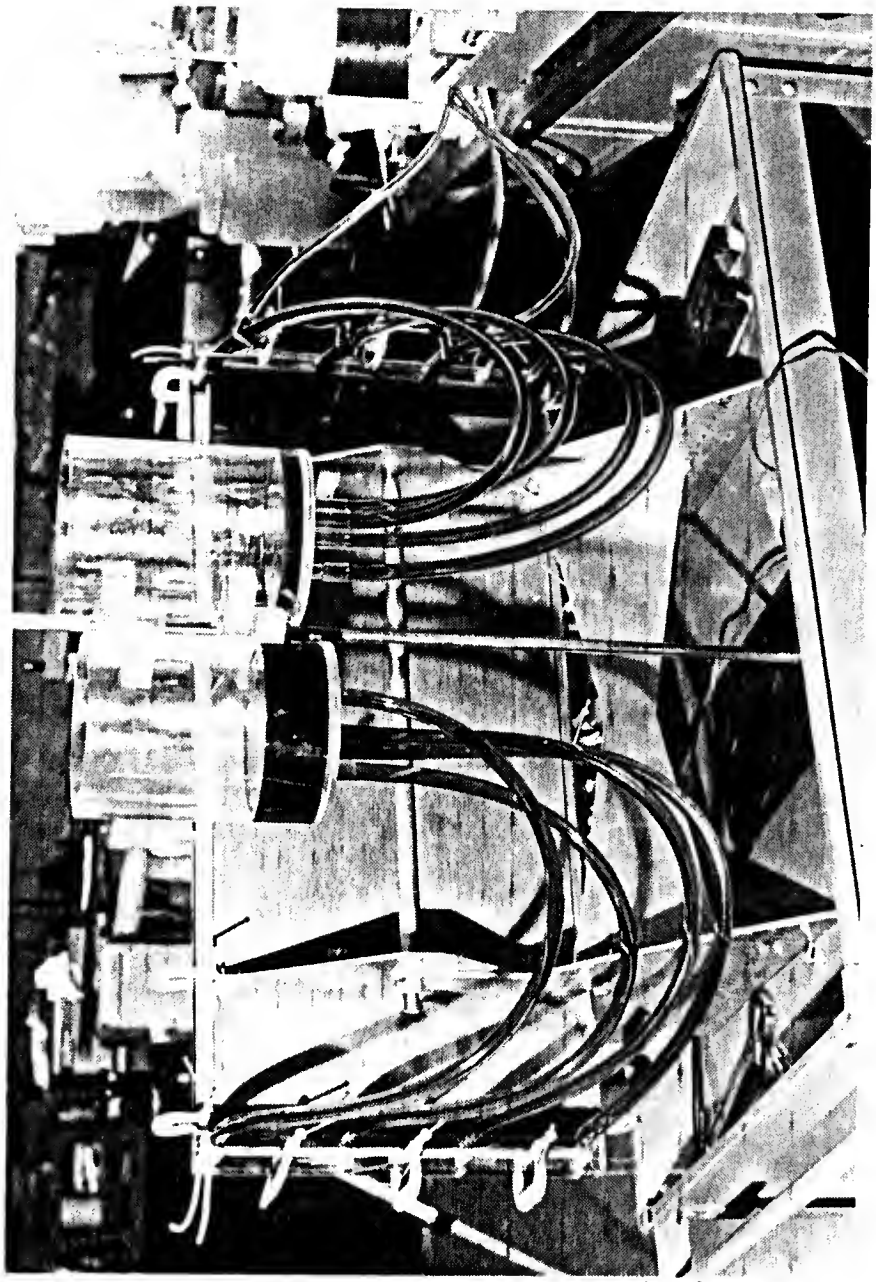

FIGURE 4.4. BACK SIDE OF MODEL WITH CONSTANT HEAD TANKS

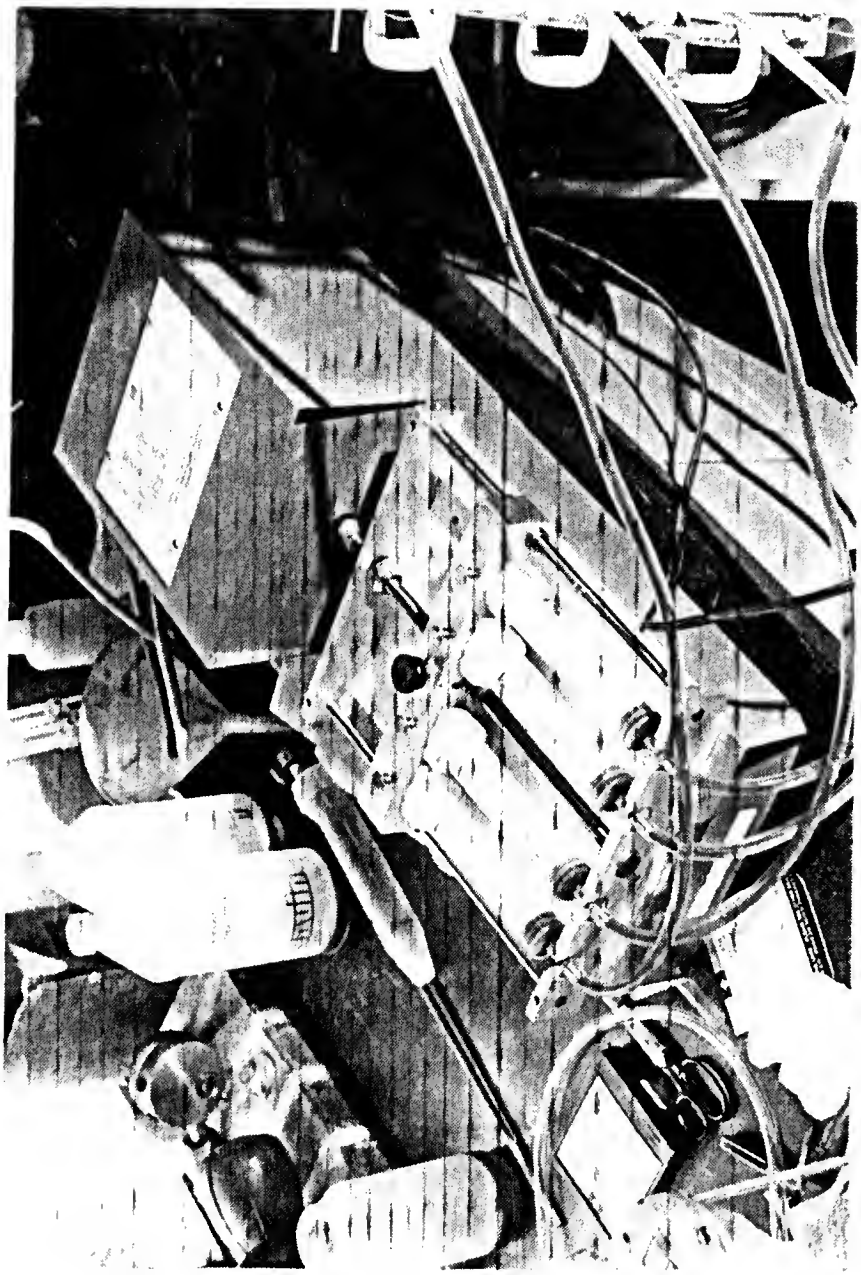

FIGURE 4.5. INFUSION PUMP CONNECTED TO MODEL

Properties of the Viscous Fluids

Dow Corning Corporation Series 200 silicone oil was used as the heavier fluid in the model. This is a clear dimethyl siloxane which is characterized by oxidation resistance and low vapor pressure. Its specific gravity is 0.977 and its kinematic viscosity is nominally 500 centistokes at 25°C. For the lighter fluid in the model, a mixture of 90 SAE and 30 SAE non-detergent motor oils was used. This mixture was adjusted until its kinematic viscosity was the same as that of the silicone oil at a temperature of 24.5°C. The temperature versus viscosity relationships for the two fluids in the neighborhood of 25°C is shown in Figure 4.6. This data was obtained with a Cannon-Zietfuchs viscometer with calibration traceable to the National Bureau of Standards. The specific gravity of the light oil mixture was 0.890 at 25°C.

These two fluids are not readily miscible, yet the surface tension effects between the two are not so great that capillary action at the interface is noticeable.

Operation of the Model

The Hele-Shaw model is a versatile analytical tool and its mode of operation depends somewhat on the type of test being run. In the present case the object of the tests was to observe the shape and rate of rotation of the initially vertical interface between the two fluids of different density. The idea was that the behavior of such an interface would be similar to that of the interface formed by the injection of freshwater from a well into a confined saline aquifer, neglecting dispersion. Of course, the two processes are not the same because the flow away from a well is radial while the Hele-Shaw model

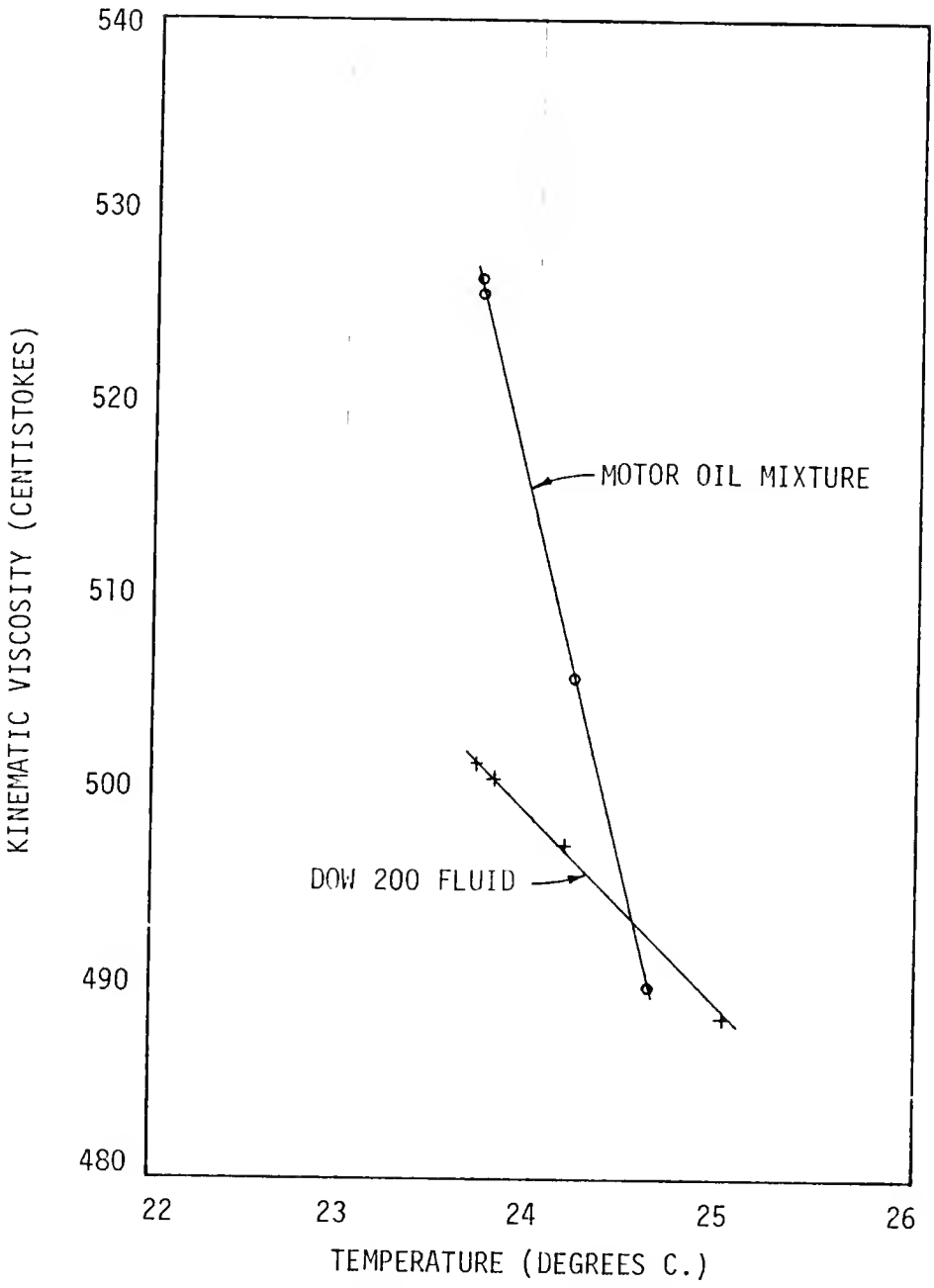

FIGURE 4.6. TEMPERATURE VS. VISCOSITY FOR THE TWO VISCOUS FLUIDS

is limited to two-dimensional flow in cartesian coordinates. Direct application of the Hele-Shaw results to a prototype well situation is, therefore, not possible. With increasing distance from the well, however, the two flows become more and more similar so that the model tests are useful for the qualitative description of interface movement. The results of the model tests are also useful for comparison with numerical models which can be made to work in either radial or cartesian coordinate systems.

In setting up the model for a test, it is necessary first to be sure that all parts of it are clean and dry. This can only be done by completely disassembling it and washing each part. A commercial preparation of trichloroethane cleaning solution was found useful in washing the oils from the glass and plastic parts. After the model had been cleaned and reassembled, with the plates rotated to the horizontal position, the heavier oil was introduced at the downstream end; the upstream end being the one into which the lighter oil would be injected. During this process the upstream end was raised a few centimeters so that all of the air in the test section would be expelled. Air entrapped in the downstream infusion reservoir was released by loosening the brass plugs provided for this purpose. The introduction of silicone oil was continued until the oil reached the end of the glass and was just ready to run into the upstream infusion reservoir. At this point, the flow was stopped and the oil front was held at the edge of the glass by proper adjustment of the constant head supply tank. The 1/2 inch (1.27 cm) plastic tubes on the bottom side of the upstream end were then clamped off tightly with hose clamps. Three of the 1/4 inch (0.635 cm) tubes from the syringe pump were then

hooked up and the upstream infusion reservoir was filled with motor oil. The fourth nipple was left open for the escape of air. After all of the air had escaped and the model was entirely filled with the two viscous fluids, the fourth tube was attached and the interface between the two oils was driven into the model to the starting point for the test. It was found helpful to let the interface sit in this position for several hours so that any irregularities in it would be straightened out by gravity. The elevated end of the model was then lowered to a level position and the test begun.

The test was started by simultaneously rotating the model to the vertical position, turning on the syringe pump and starting the timer. The movement of the interface could then be photographed until the downstream end of the model was reached.

Several variations of this procedure were used. The first test was run with the model left in its horizontal position so that the straightness of the advancing interface could be checked. It was found that, with higher rates of injection of the lighter fluid, the interface moved faster in the center of the model. This indicated that the higher pressure required to drive the viscous fluids across the model could cause the glass plates to bend, changing the thickness of the gap. Figures 4.7 and 4.8 show the shape of the interface when advancing at rates of 3.65 cm/min and 7.28 cm/min, respectively. Since the straightness of the interface at the lower speed was considered acceptable most of the remaining tests were run at this rate of injection.

Figures 4.9 and 4.10 show a test which was run at a higher injection rate with the model in the vertical position. The bowing out of the glass plates caused the center section of the interface to advance

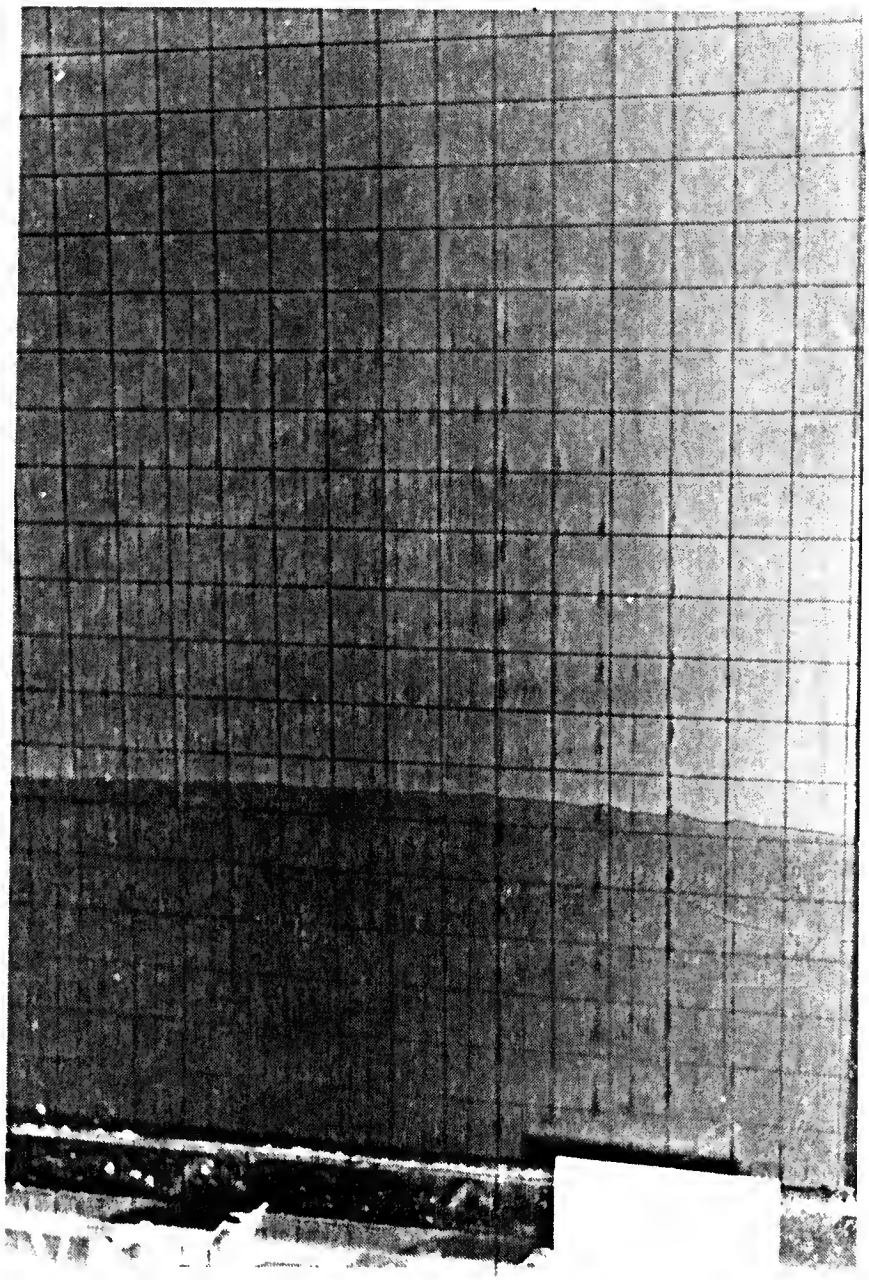

FIGURE 4.7. TEST RUN WITH HORIZONTAL MODEL. INJECTION RATE = 20.44 CC/MIN

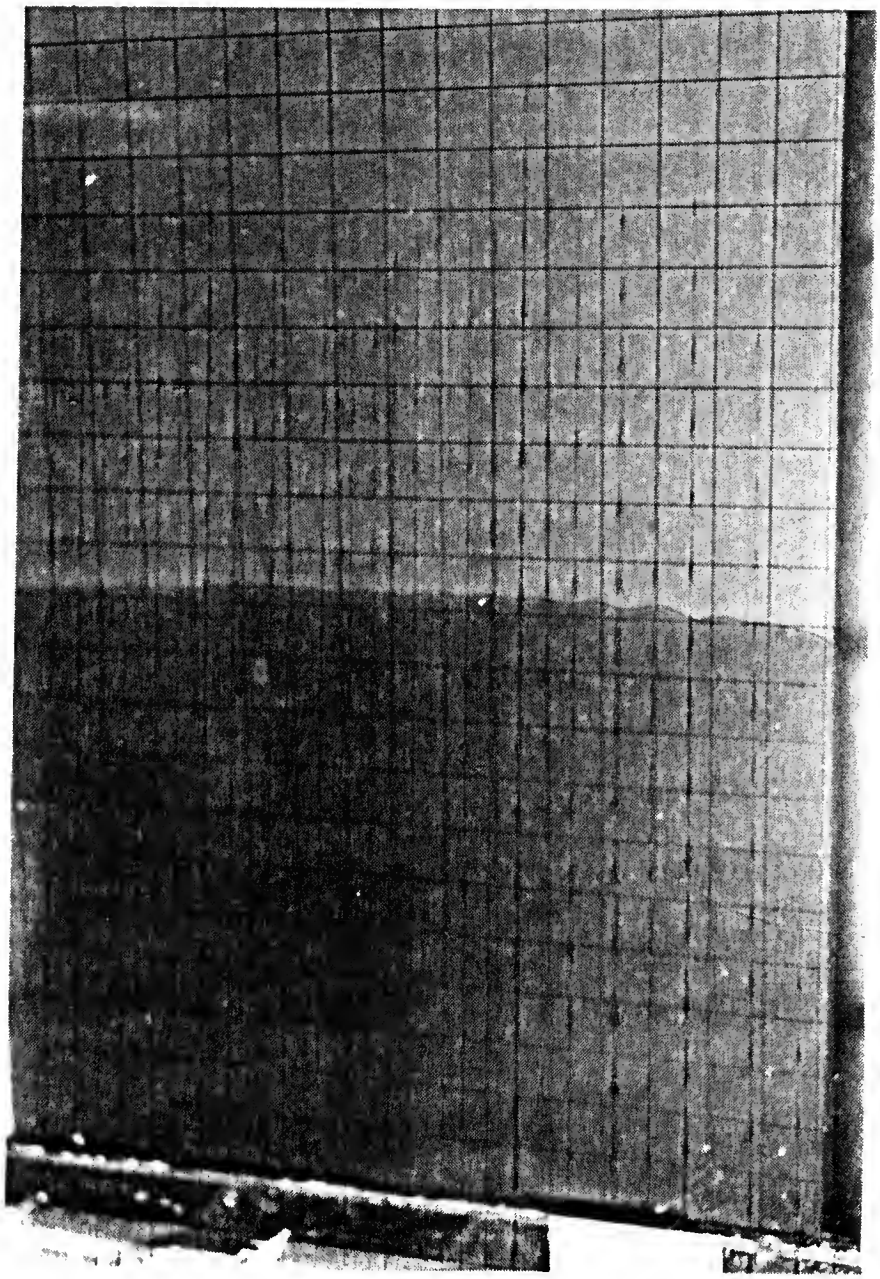

FIGURE 4.8. TEST RUN WITH HORIZONTAL MODEL. INJECTION RATE = 41.04 CC/MIN

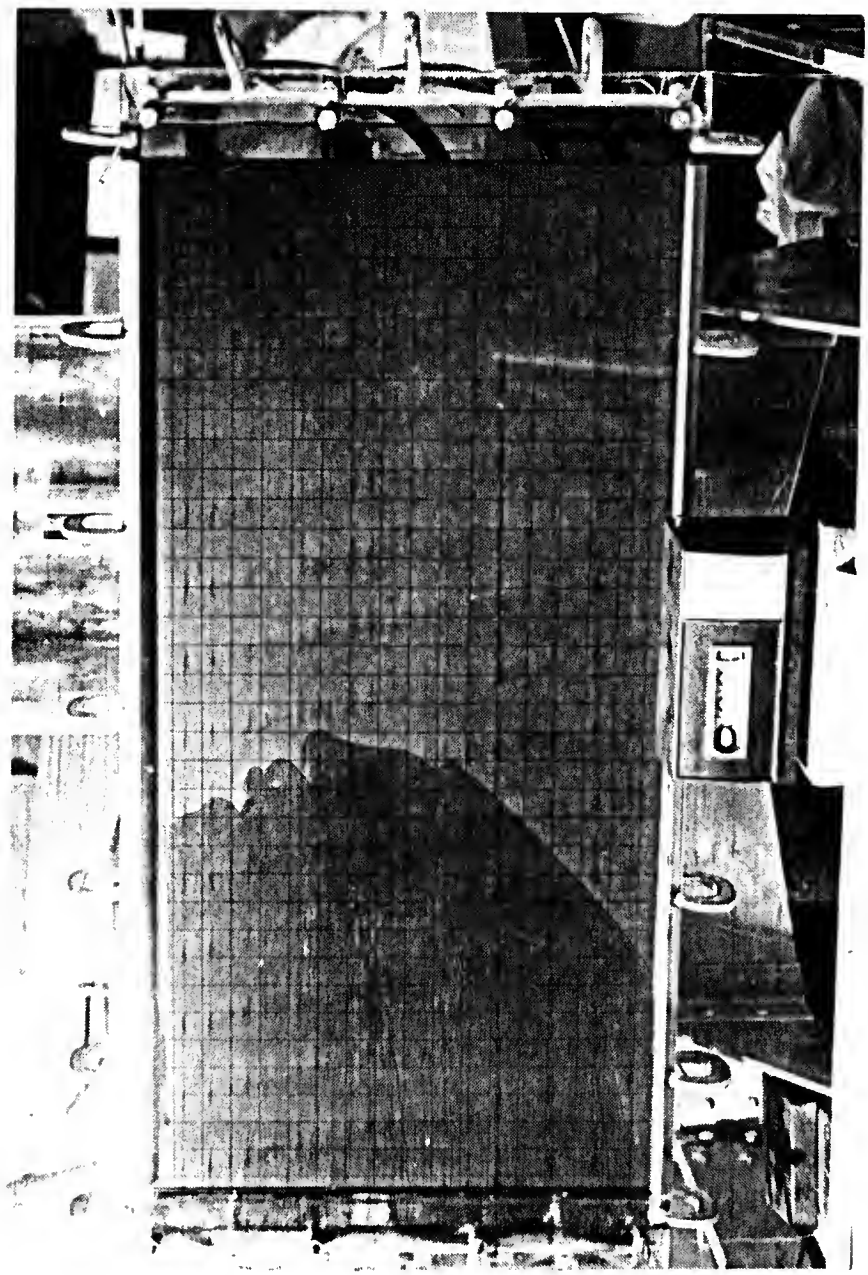

FIGURE 4.9. INSTABILITY DEVELOPING AFTER 50 SECONDS. INJECTION RATE = 81.72 CC/MIN

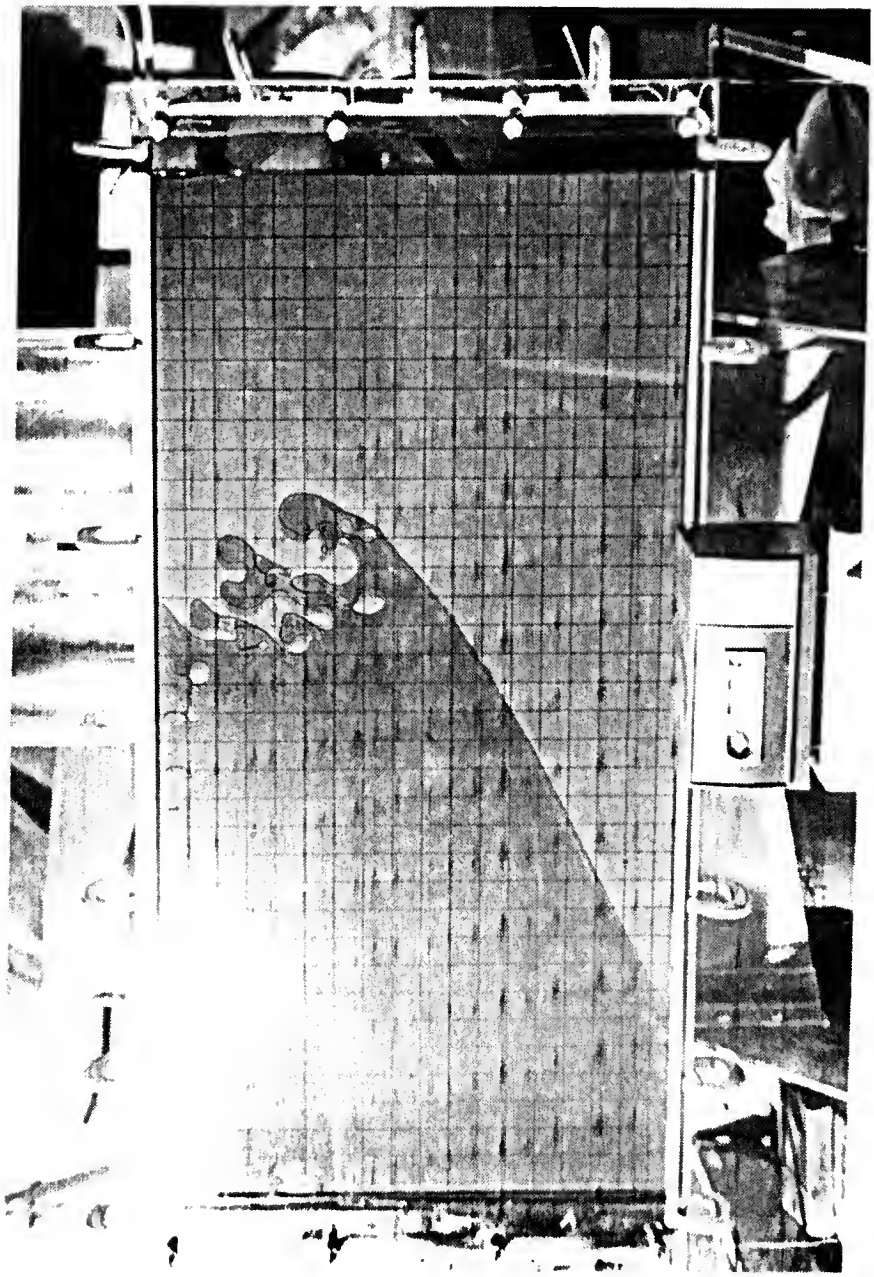

FIGURE 4.10. UNSTABLE INTERFACE AFTER 3 MINUTES. INJECTION RATE = 81.72 CC/MIN

more rapidly than the ends. Rotation of the upper part of the interface past the vertical results in instability, which is clearly evident here.

The sequence of Figures 4.11 through 4.16 shows a test that was run with an injection rate of 20.44 cubic centimeters per minute. This is the same injection rate that resulted in the relatively straight interface shown in Figure 4.7 when the model was horizontal.

The sequence of Figures 4.17 through 4.23 shows a test in which only the lower half of the model was used. This was accomplished by inserting a barrier composed of rubber splicing compound and silicon rubber sealant between the glass plates to reduce the width of the test section by half. The injection rate used here was 8.16 cubic centimeters per minute.

Analysis of Test Results

The rotation of an initially vertical interface between two fluids of different density has been studied in several previous investigations. Gardner, Downie and Kendall (1962) proposed an equation to predict the rate of interface rotation which, for an isotropic aquifer and fluids of equal viscosity, has the form

$$\left(\frac{X}{b}\right)^2 = \frac{16}{3}\,\frac{(t/t')^2}{1 + t/t'} \qquad (4.31)$$

where

X = projection of the interface on the horizontal

b = thickness of the aquifer

t = time

$t' = 4/3\,\frac{nb\bar{\rho}}{K\Delta\rho}$

$\bar{\rho}$ = average density of the two fluids.

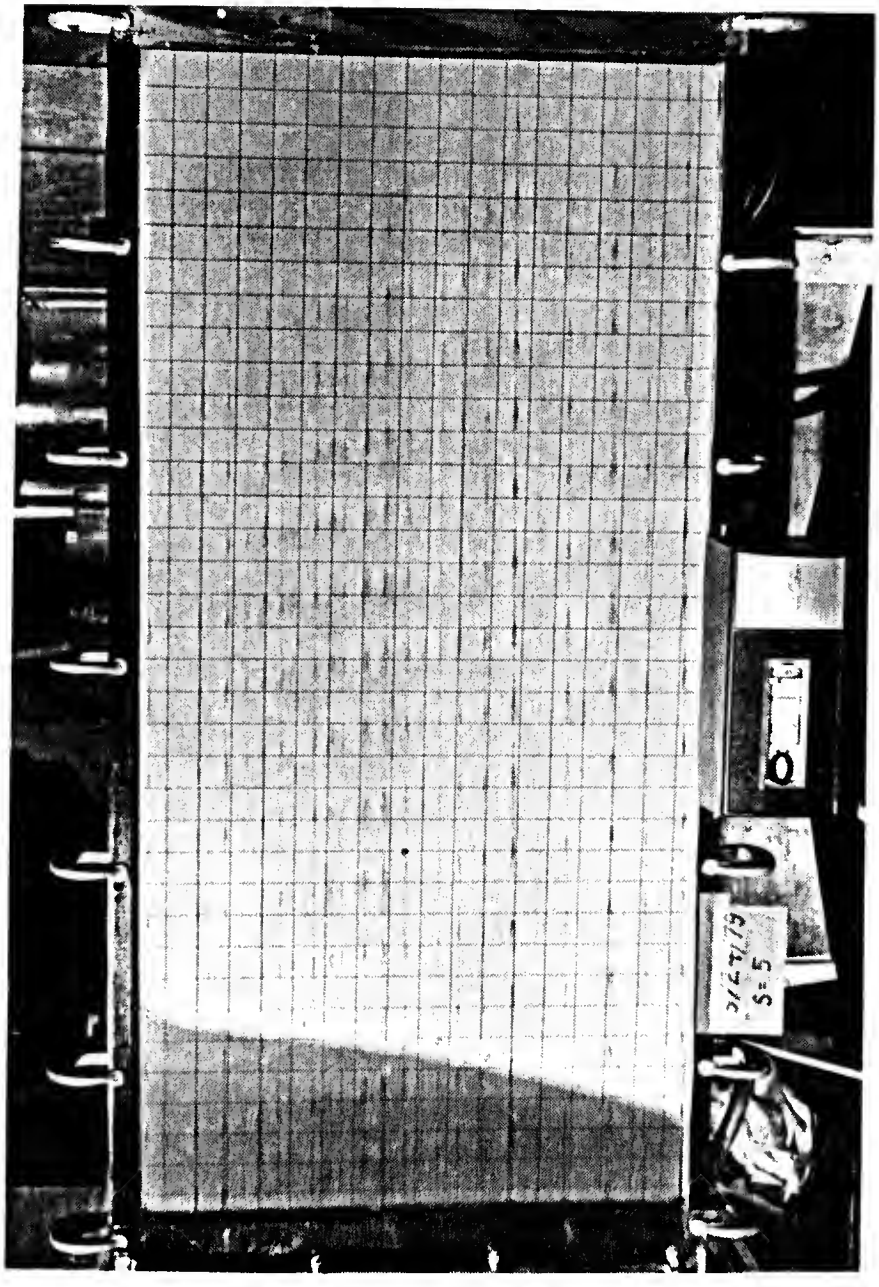

FIGURE 4.11. INTERFACE AFTER 1 MINUTE. INJECTION RATE = 20.44 CC/MIN

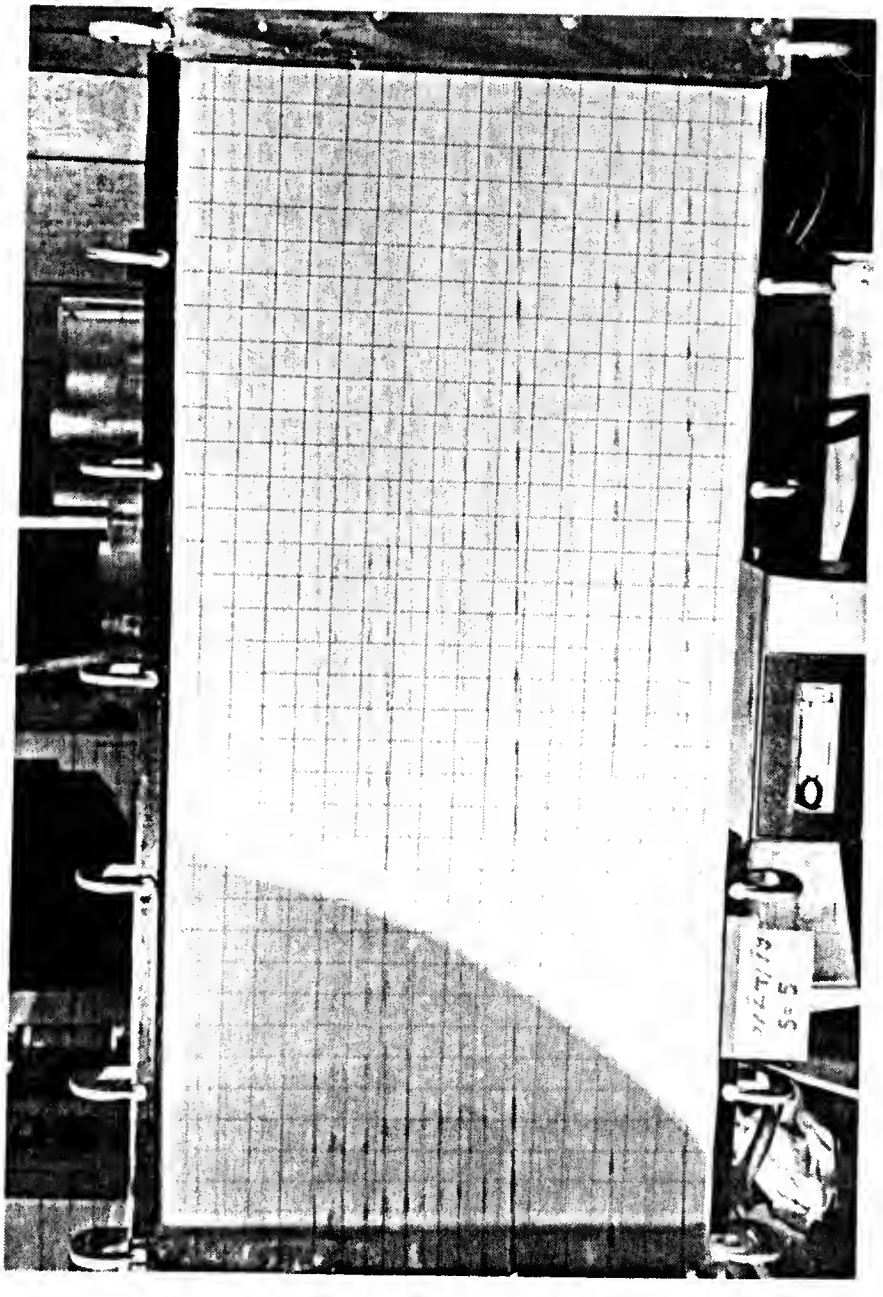

FIGURE 4.12. INTERFACE AFTER 3 MINUTES. INJECTION RATE = 20.44 CC/MIN

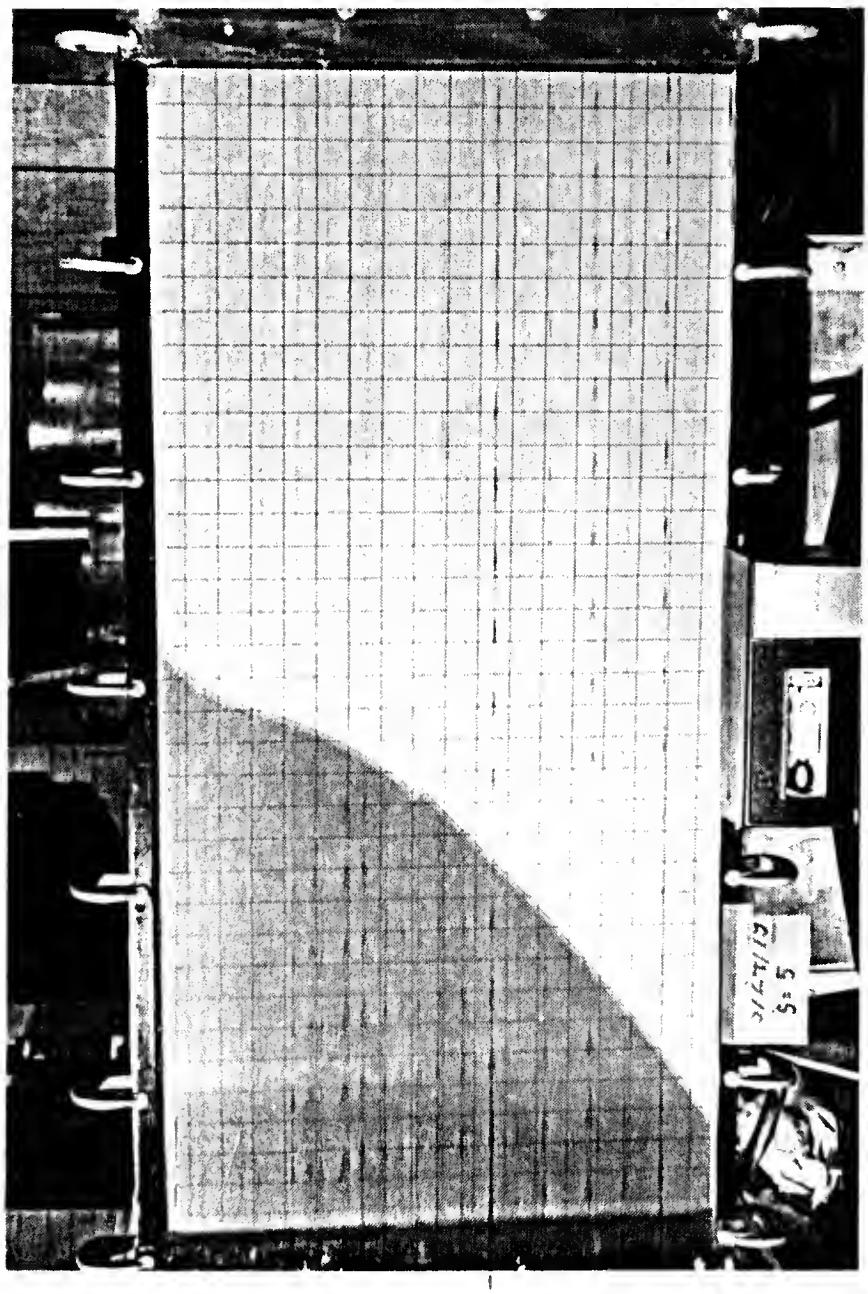

FIGURE 4.13. INTERFACE AFTER 5 MINUTES. INJECTION RATE = 20.44 CC/MIN

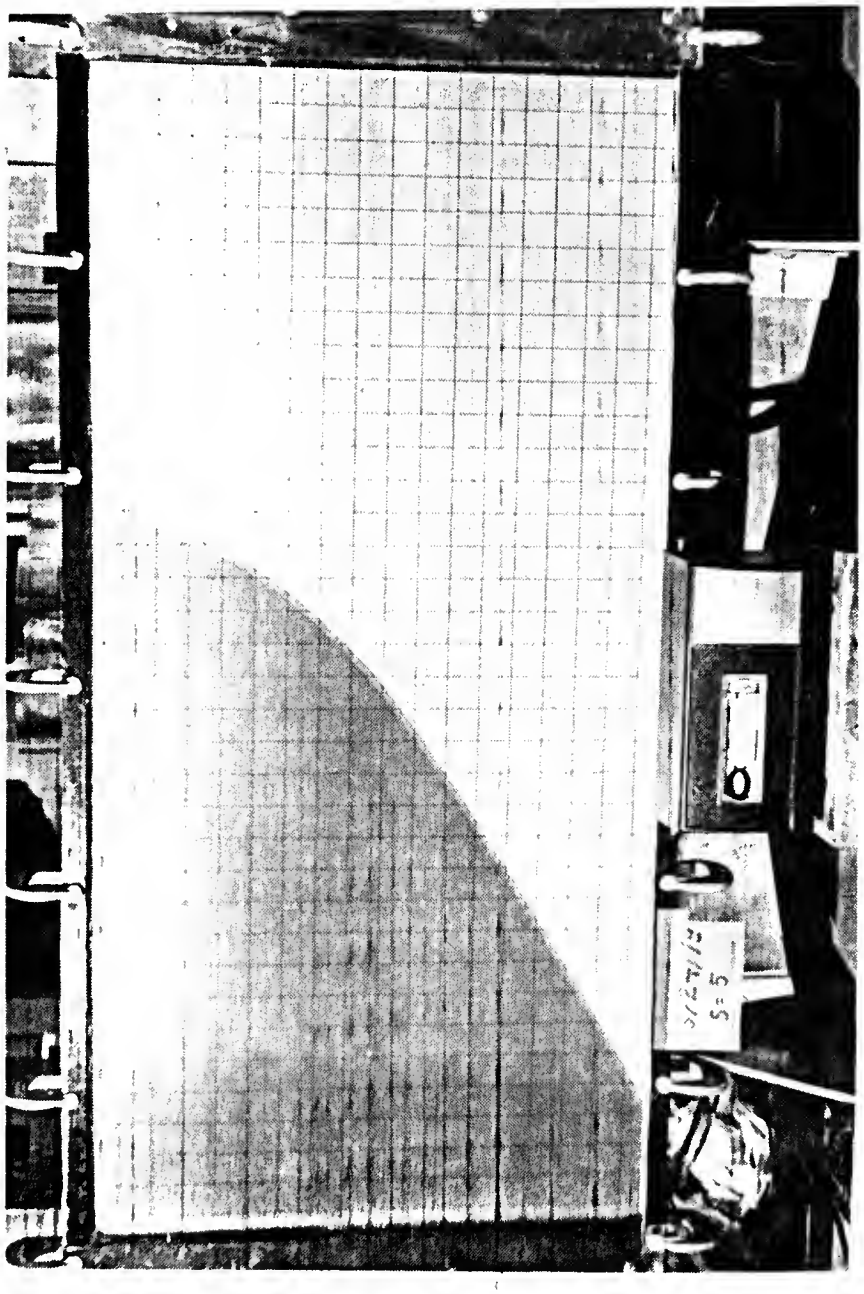

FIGURE 4.14. INTERFACE AFTER 7 MINUTES. INJECTION RATE = 20.44 CC/MIN

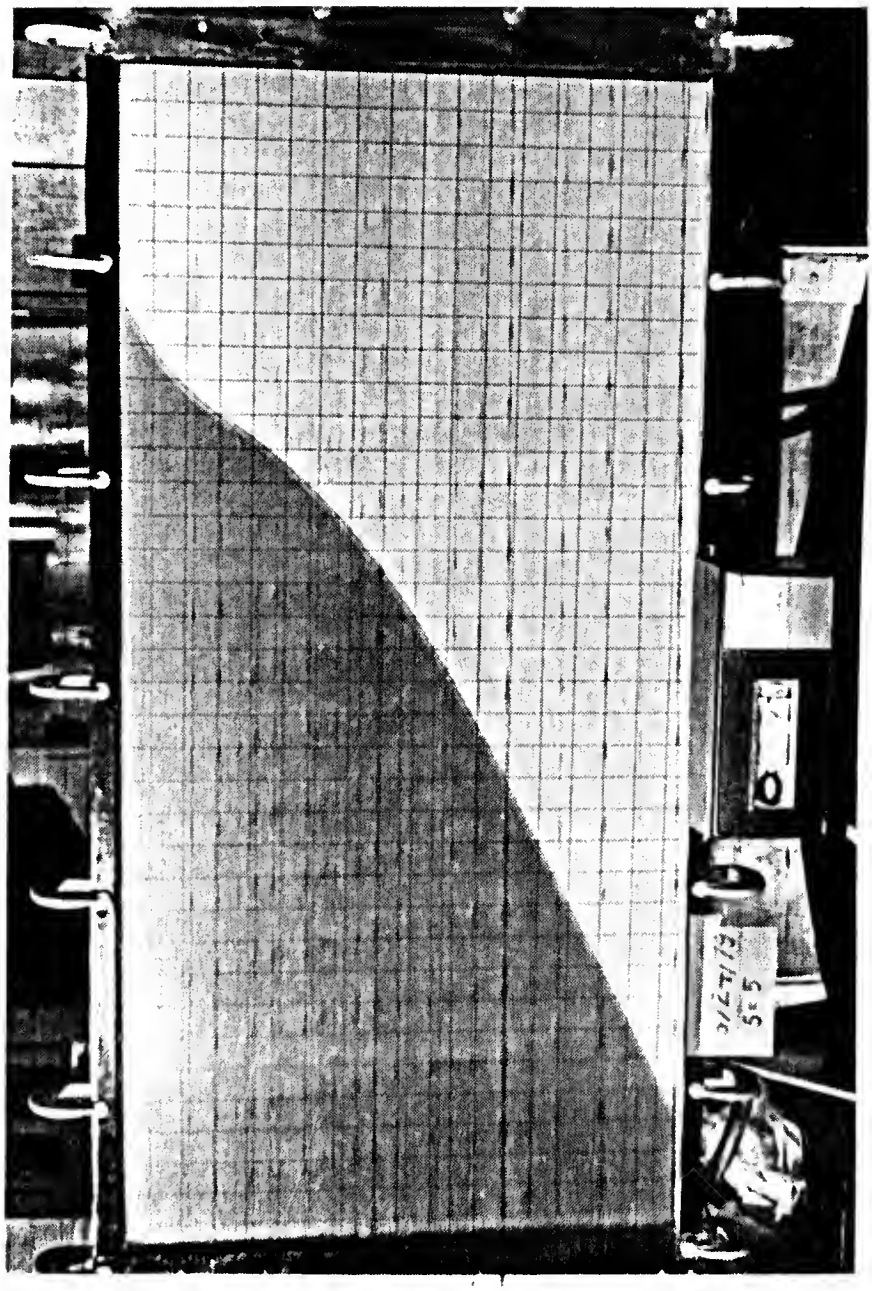

FIGURE 4.15. INTERFACE AFTER 9 MINUTES. INJECTION RATE = 20.44 CC/MIN

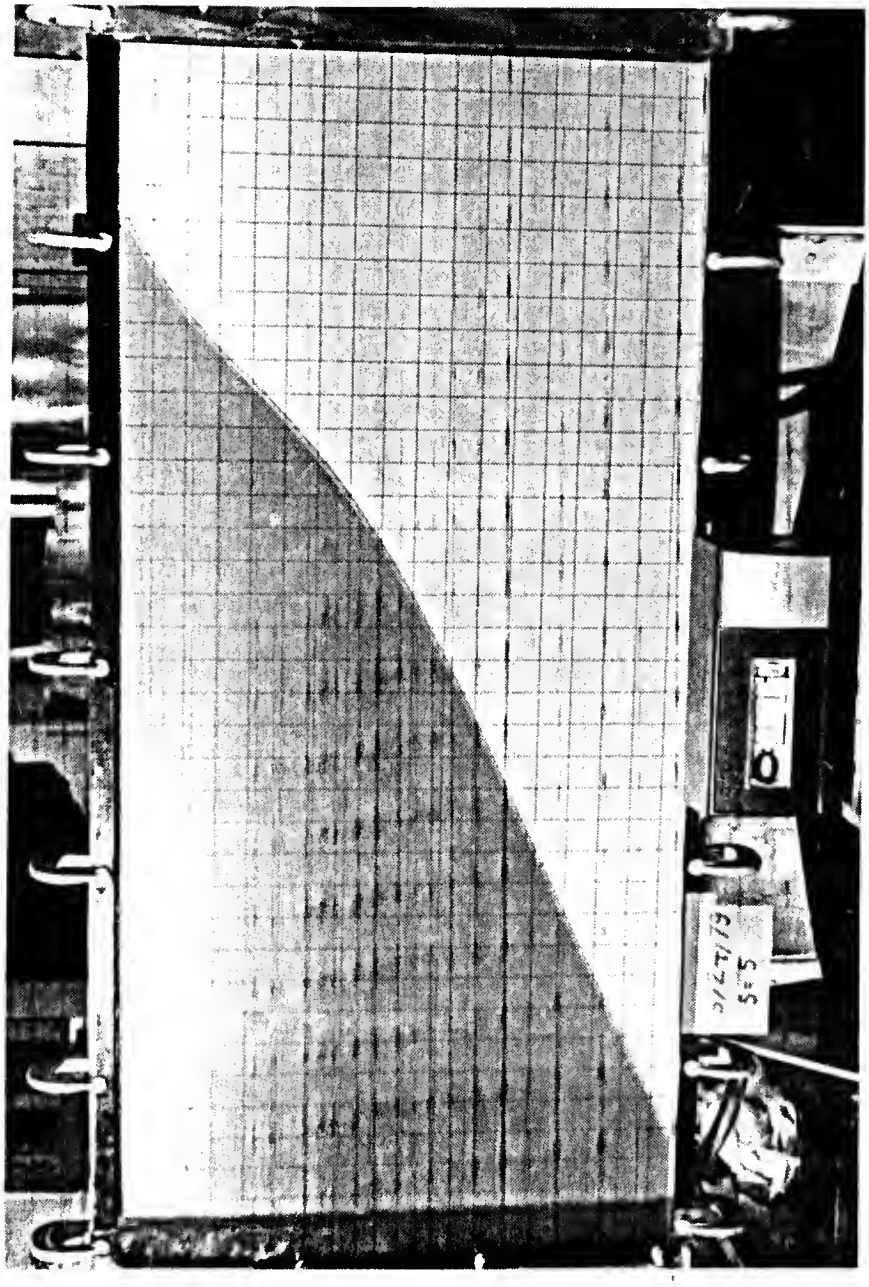

FIGURE 4.16. INTERFACE AFTER 11 MINUTES. INJECTION RATE = 20.44 CC/MIN

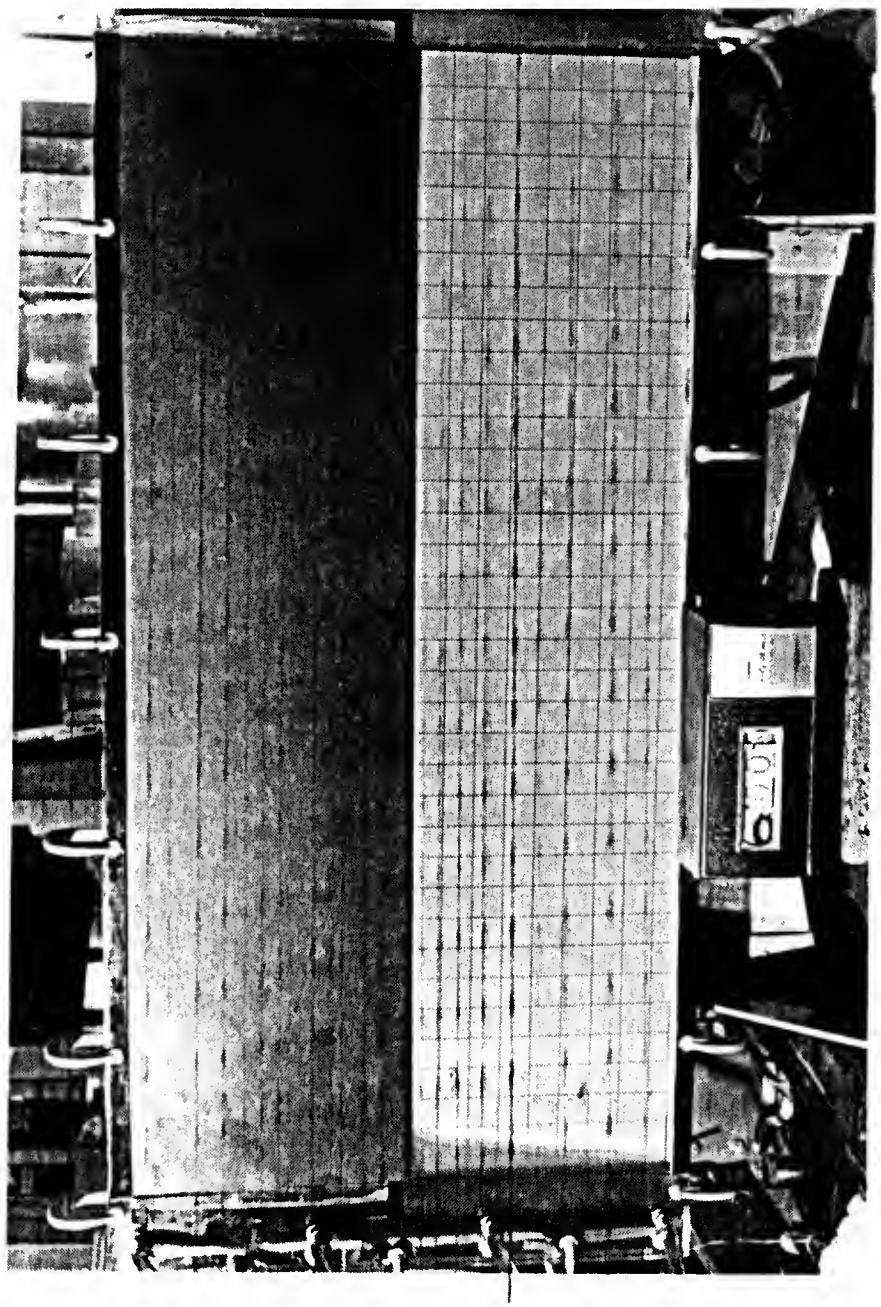

FIGURE 4.17. INTERFACE AFTER 10 SECONDS. INJECTION RATE = 8.16 CC/MIN
MODEL DEPTH REDUCED BY HALF

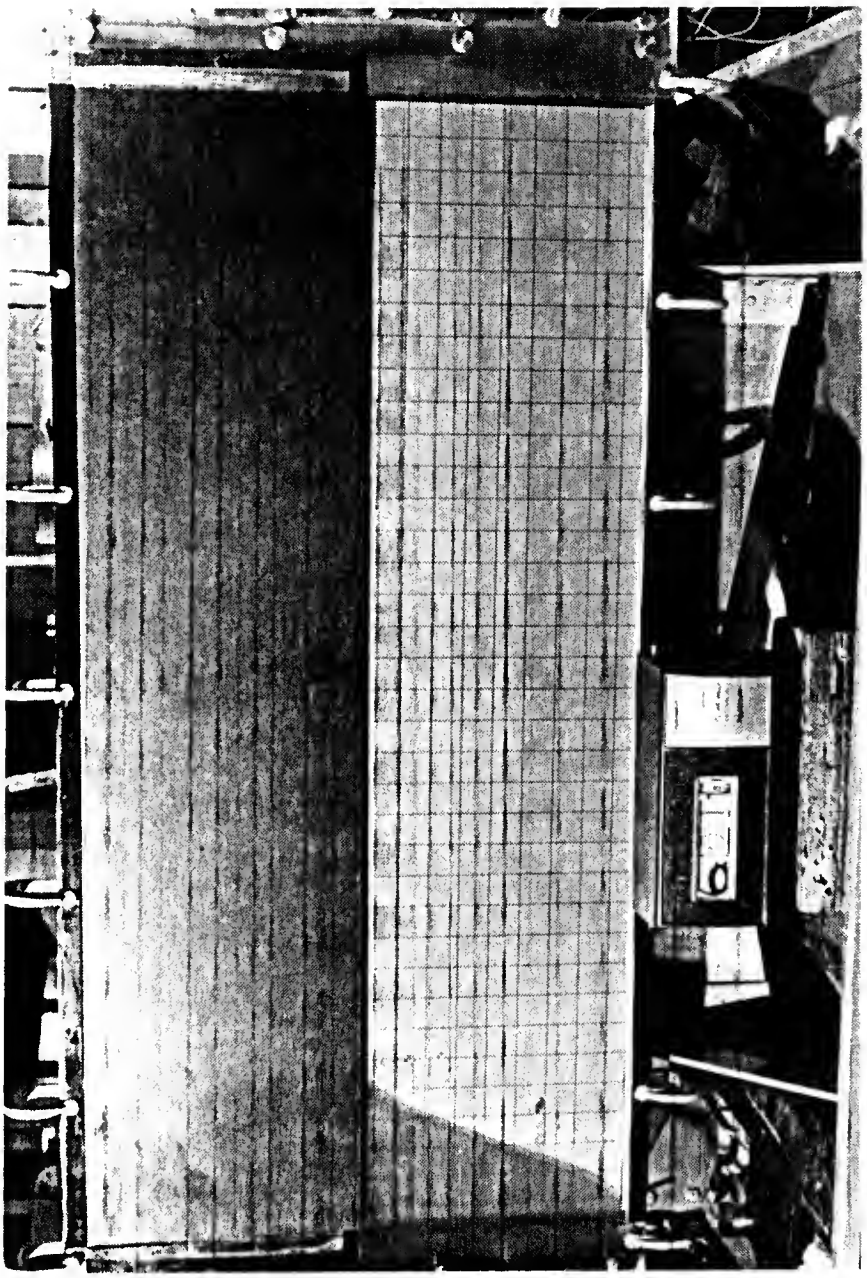

FIGURE 4.18. INTERFACE AFTER 1 MINUTE. INJECTION RATE = 8.16 CC/MIN
MODEL DEPTH REDUCED BY HALF

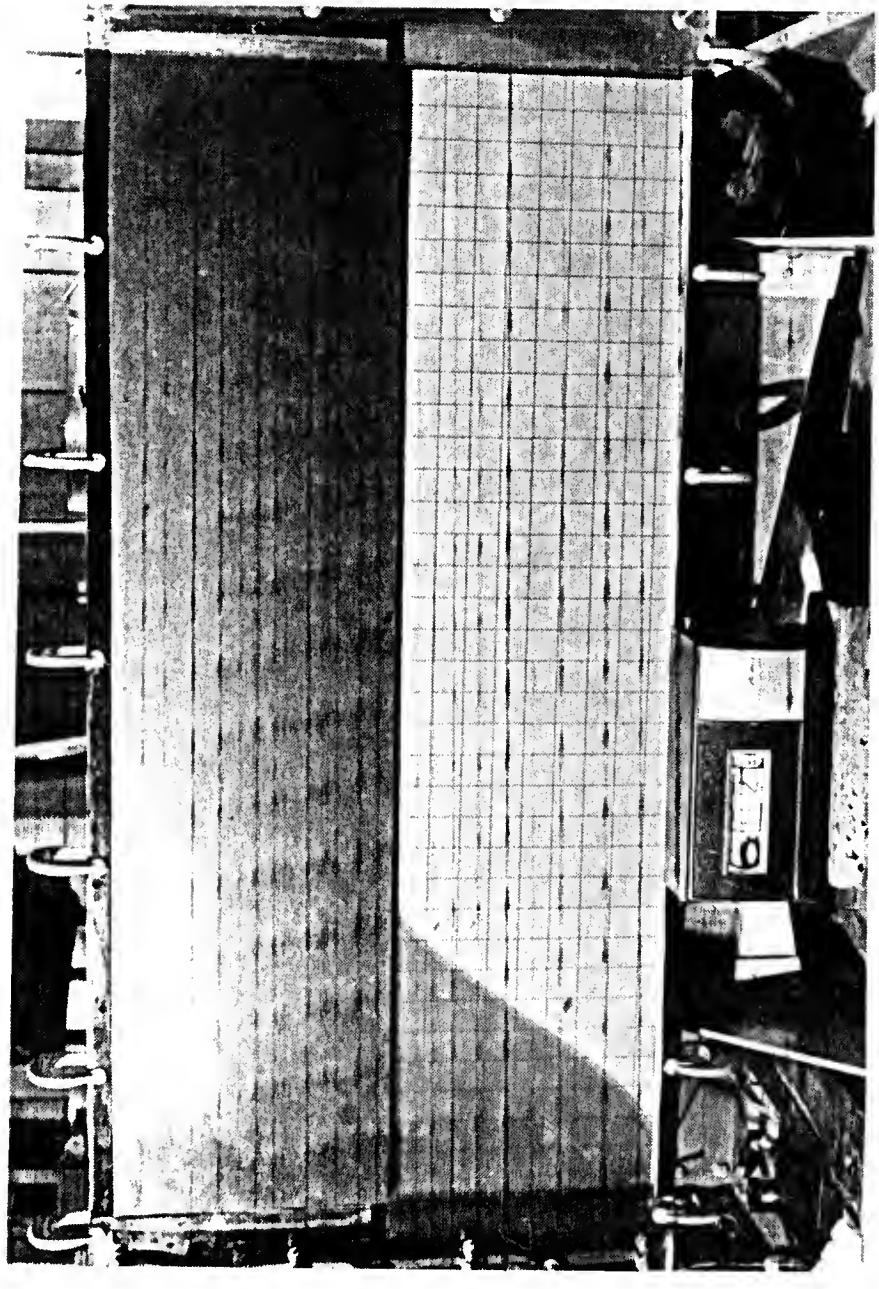

FIGURE 4.19. INTERFACE AFTER 2 MINUTES. INJECTION RATE = 8.16 CC/MIN
MODEL DEPTH REDUCED BY HALF

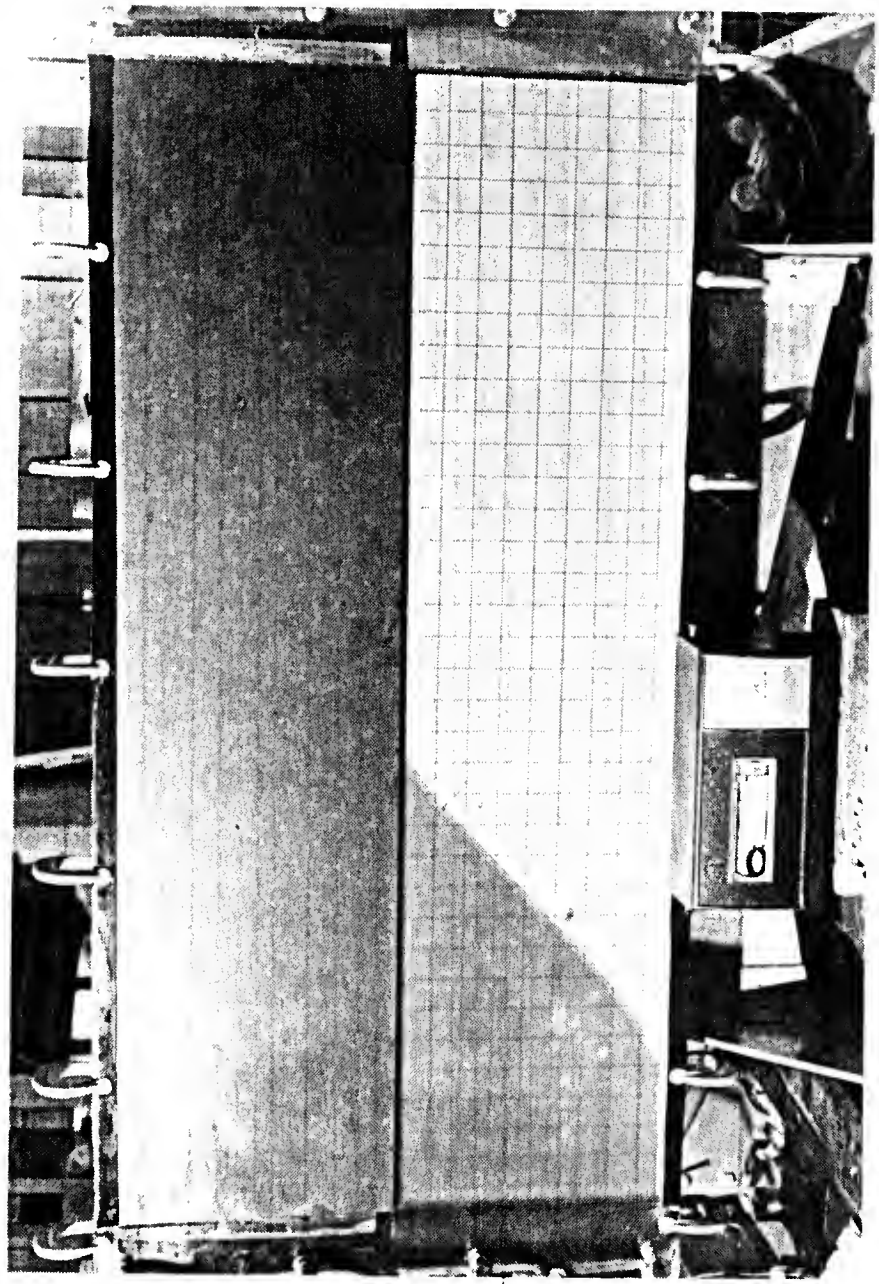

FIGURE 4.20. INTERFACE AFTER 3 MINUTES. INJECTION RATE = 8.16 CC/MIN
MODEL DEPTH REDUCED BY HALF

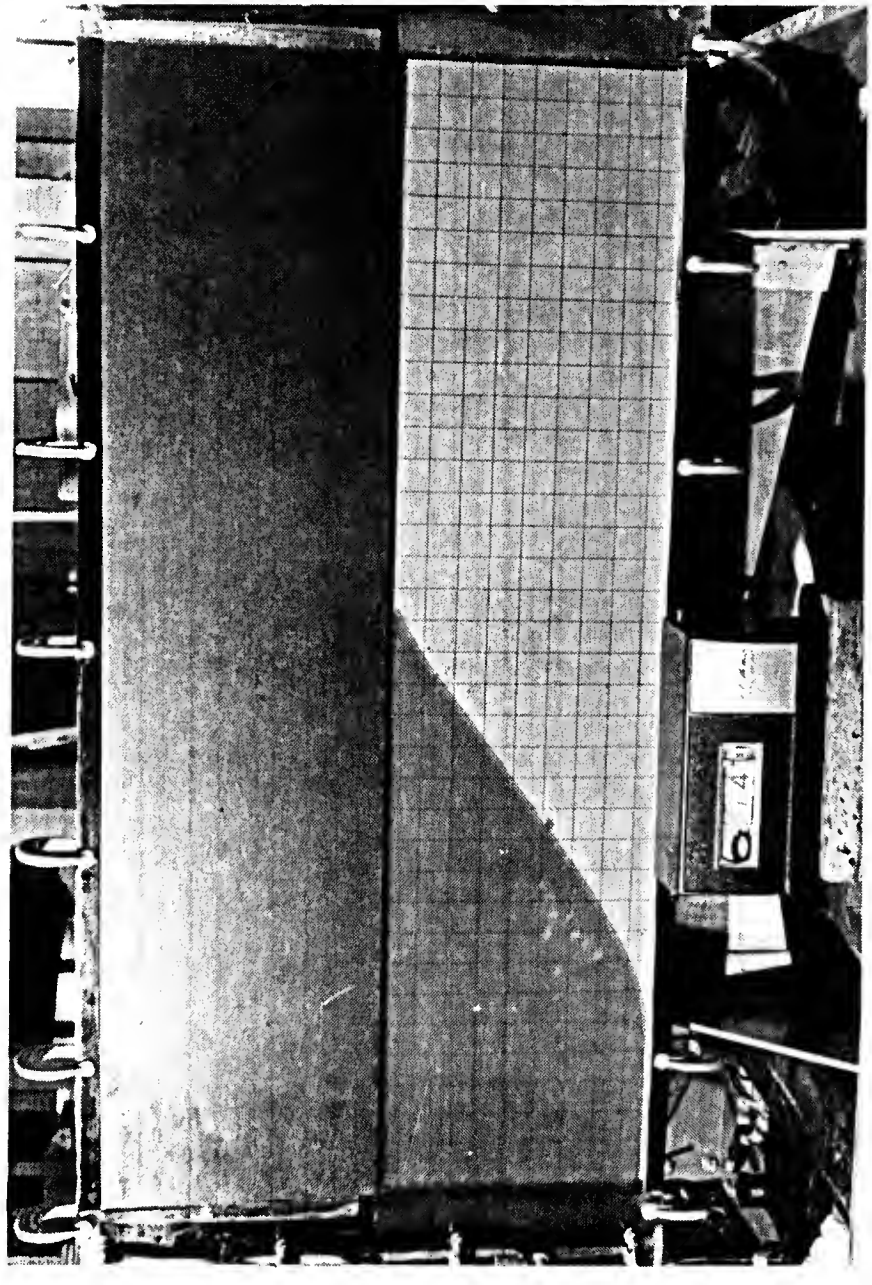

FIGURE 4.21. INTERFACE AFTER 4 MINUTES. INJECTION RATE = 8.16 CC/MIN
MODEL DEPTH REDUCED BY HALF

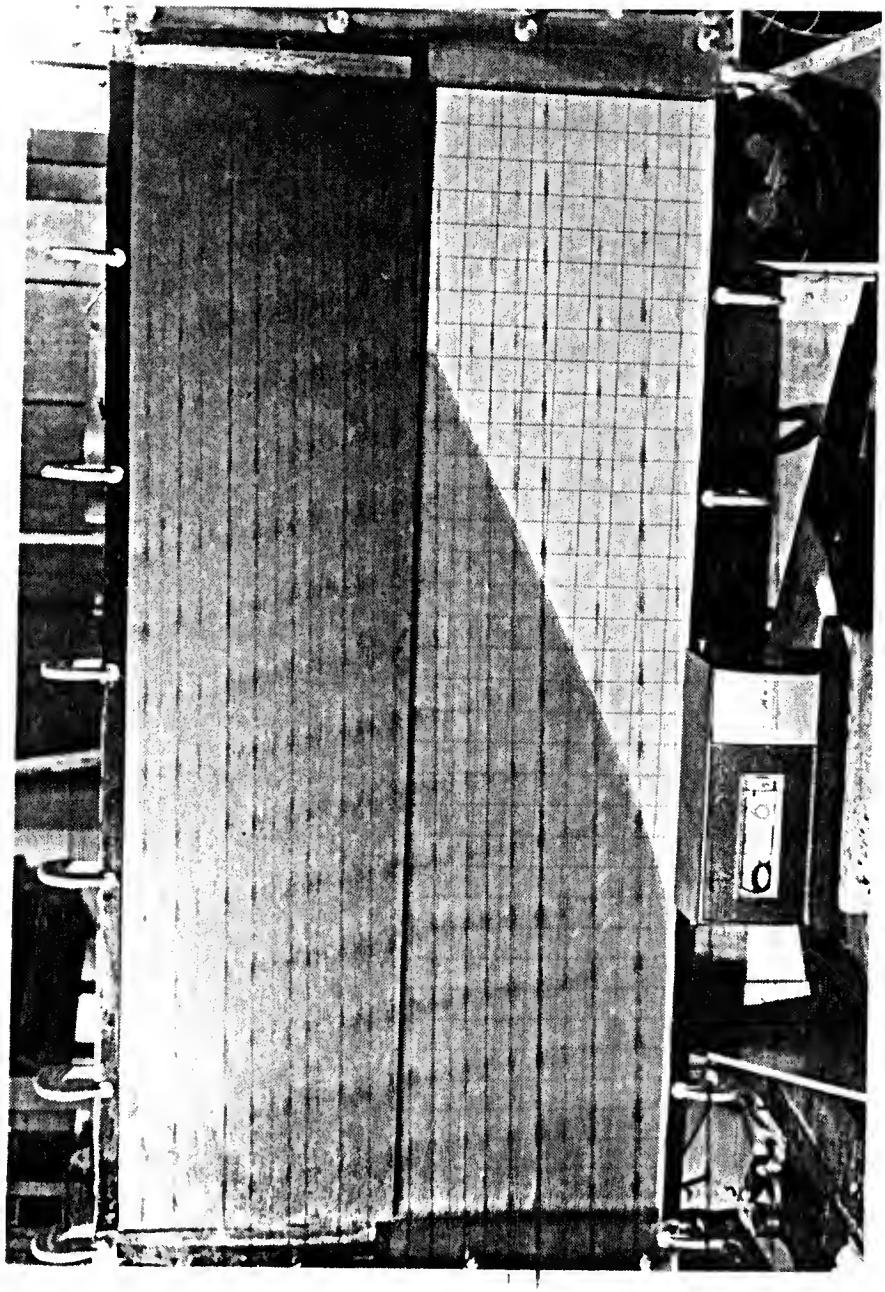

FIGURE 4.22. INTERFACE AFTER 6 MINUTES. INJECTION RATE = 8.16 CC/MIN
MODEL DEPTH REDUCED BY HALF

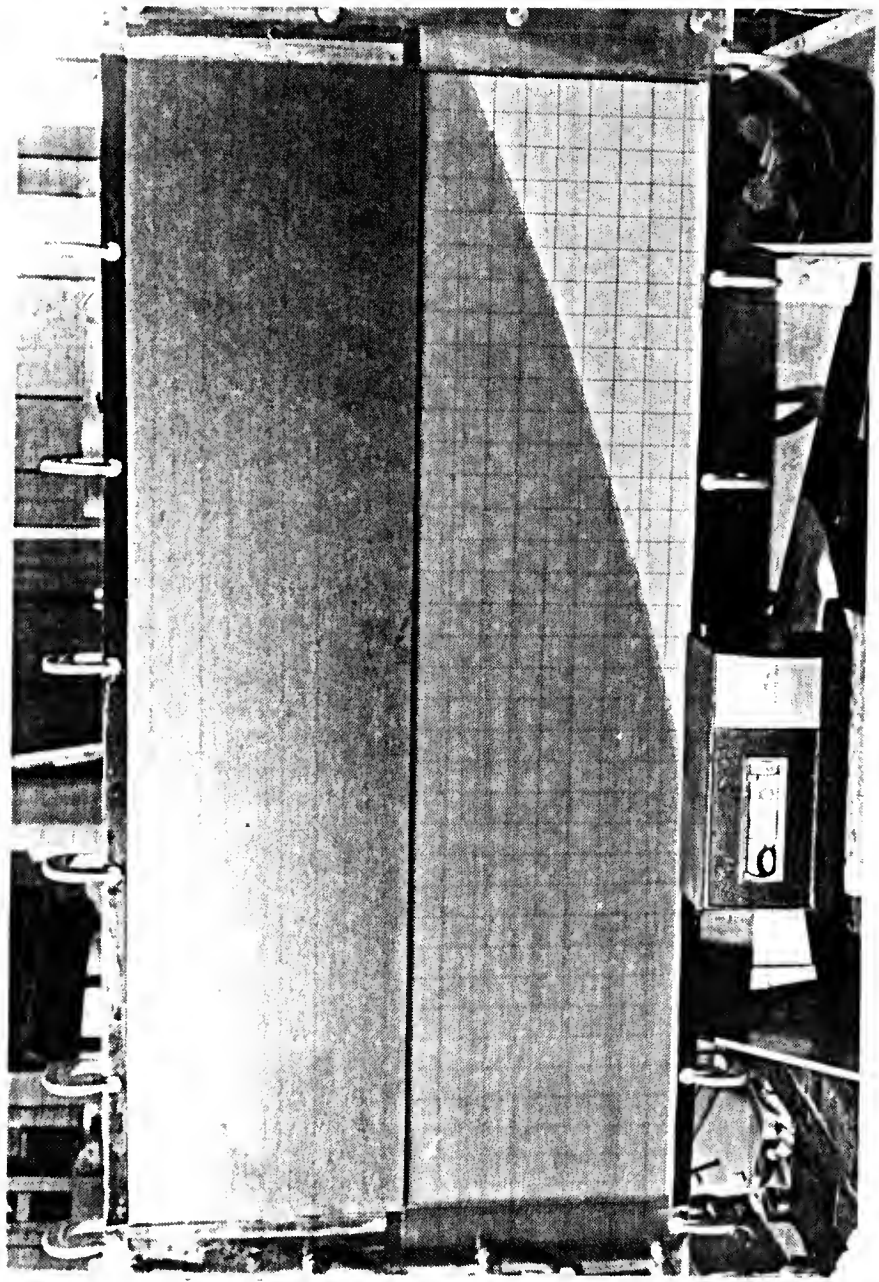

FIGURE 4.23. INTERFACE AFTER 8 MINUTES. INJECTION RATE = 8.16 CC/MIN
MODEL DEPTH REDUCED BY HALF

Equation (4.31) was constructed intuitively by joining the solutions to the extreme cases of nearly vertical and nearly horizontal interfaces. The solutions to these extreme cases were based on the assumptions of no vertical flow and no curvature of the interface.

Another equation for the movement of an initially vertical interface was given by Harleman and Rumer (1962). Once again, assuming a straight interface and no vertical flow, they obtained

$$\left(\frac{X}{b}\right)^2 = 8/3\ \frac{t}{t'} \tag{4.32}$$

This equation is of the same form as the one for nearly horizontal interfaces from which equation (4.31) was derived.

Figure (4.24) shows the comparison of equations (4.31) and (4.32) with data taken from three runs of the vertical Hele-Shaw model. Runs number two and three are shown in Figures 4.11 through 4.16 and 4.17 through 4.23, respectively. Run number one was performed in the same manner as run number two except that the injection rate was twice as high. The third run gave the best fit to equation (4.31). Runs number one and two, while fairly consistent between themselves, do not fit either equation very well. Since the main difference between these two runs and the third run is in the depth of the flow region, it is most logical to suspect that it is caused by the existance of vertical velocity components which were ignored in the derivation of the equations. The greater curvature of the interface which is apparent in the first two runs tends to support this view.

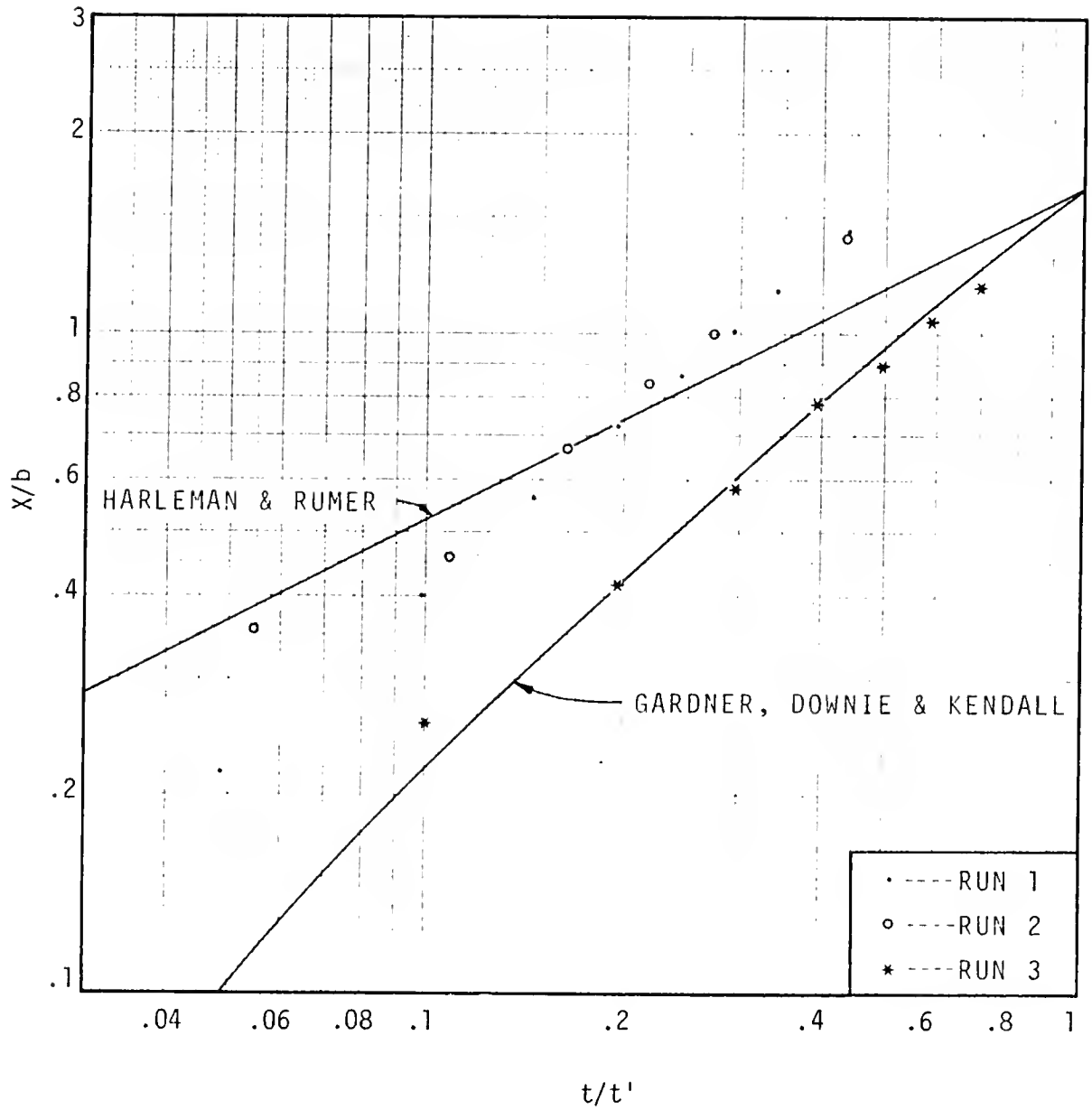

FIGURE 4.24. COMPARISON OF EXPERIMENTAL RESULTS WITH EQUATIONS FOR INTERFACE ROTATION

CHAPTER 5

SIMPLE CASES INVOLVING STEADY FLOW

General

It was shown in Chapter 3 that the general problem of locating a moving interface between two fluids of different density is very complex even when the standard simplifying assumptions involving homogeneity, isotropy and immiscibility are used. It requires the solution of two coupled flow problems, one in the freshwater and one in the saltwater, joined by a nonlinear boundary condition on the interface, of which the position is unknown. The only methods presently available for getting a solution to such a problem are by physical and numerical modeling. However, if the problem is limited to the special case of a stationary freshwater lens in a static saline aquifer, then it becomes much more tractable. In this special case, it is only necessary to solve the continuity and motion equations in the freshwater region and the location of the interface, while still not initially known, can be treated by the Ghyben-Herzberg principle. This makes it possible to formulate some problems which can be solved analytically.

Steady flow in a freshwater lens is not possible unless the aquifer possesses a constant head boundary which permits freshwater to flow out of the lens at the same rate that it is being injected. One such constant head boundary is found at the sea coast where injection wells may be used to create freshwater lenses in aquifers affected by saltwater intrusion. Another case is that of injection into a leaky saline aquifer

where the leaky layer serves as a boundary which permits efflux of freshwater from the lens. Even in these cases, steady flow may only occur during a small part of the history of the lens. It represents a condition of equilibrium in which buoyant forces are counteracted by the loss of energy due to the flow resistance of the porous medium. It is useful to study this condition because it indicates the limiting size of lens that can be achieved under the given flow conditions.

It should also be noted that, in the operation of a storage lens, certain advantages can be gained by maintaining the lens in a steady state through continuous freshwater injection. The first is that continuous injection is necessary to preserve the potential energy of the lens so that the maximum amount of freshwater can be withdrawn when it is needed. Note that as soon as injection is stopped, the lens begins to decay into a thin layer of freshwater at the top of the aquifer which could not be selectively retrieved even if fresh and saltwater did not mix. The second advantage is that the continuous injection of freshwater to the lens tends to wash out the saltwater which had remained in the pores and adhered to the particles of the porous medium after the passage of the mixing zone as the lens was being formed. In this way, the salinity of the freshwater and the thickness of the mixing zone are reduced.

Freshwater Injection in a Coastal Aquifer

Saltwater Intrusion

It is commonly observed in coastal aquifers which discharge to the sea that a wedge of nearly static saltwater extends inland from the coast underneath the flowing freshwater. Actually, it was the study of

this phenomenon which led W. Badon Ghyben and A. Herzberg to develop their hydrostatic theory for interfaces. Numerous subsequent investigators have brought forth more refined methods for analyzing saltwater wedges (Glover, 1959; Henry, 1959; Bear and Dagan, 1964; Van Der Veer, 1977) and have found the Ghyben-Herzberg results to be quite accurate except for that part of the interface closest to the sea.

The application of this principle, combined with the Dupuit assumption, to a confined aquifer of constant thickness gives the following relationship between h and x.

$$x = Kh^2/(2\delta Q_x) \tag{5.1}$$

in which the symbols are as shown in Figure 5.1. The position of the toe of the interface is given by

$$x_t = \frac{-Kb^2}{2\delta Q_x} \tag{5.2}$$

Injection Into a Coastal Aquifer

If an injection well pumps freshwater at a constant rate into the coastal aquifer pictured in Figure 5.2 then the equilibrium position of the saline wedge will be modified and a steady freshwater lens will be formed in what was formerly a saline part of the aquifer. This is a case of injection into an aquifer in which only the freshwater is flowing, so that the Ghyben-Herzberg principles can still be used. The flow pattern around a well in a uniformly flowing aquifer is customarily studied by the methods of potential theory in which the velocity potentials for source flow and uniform flow are superimposed. However, in the presence of the saltwater wedge, even though the vertical velocity components are neglected, flow is not two dimensional because of the

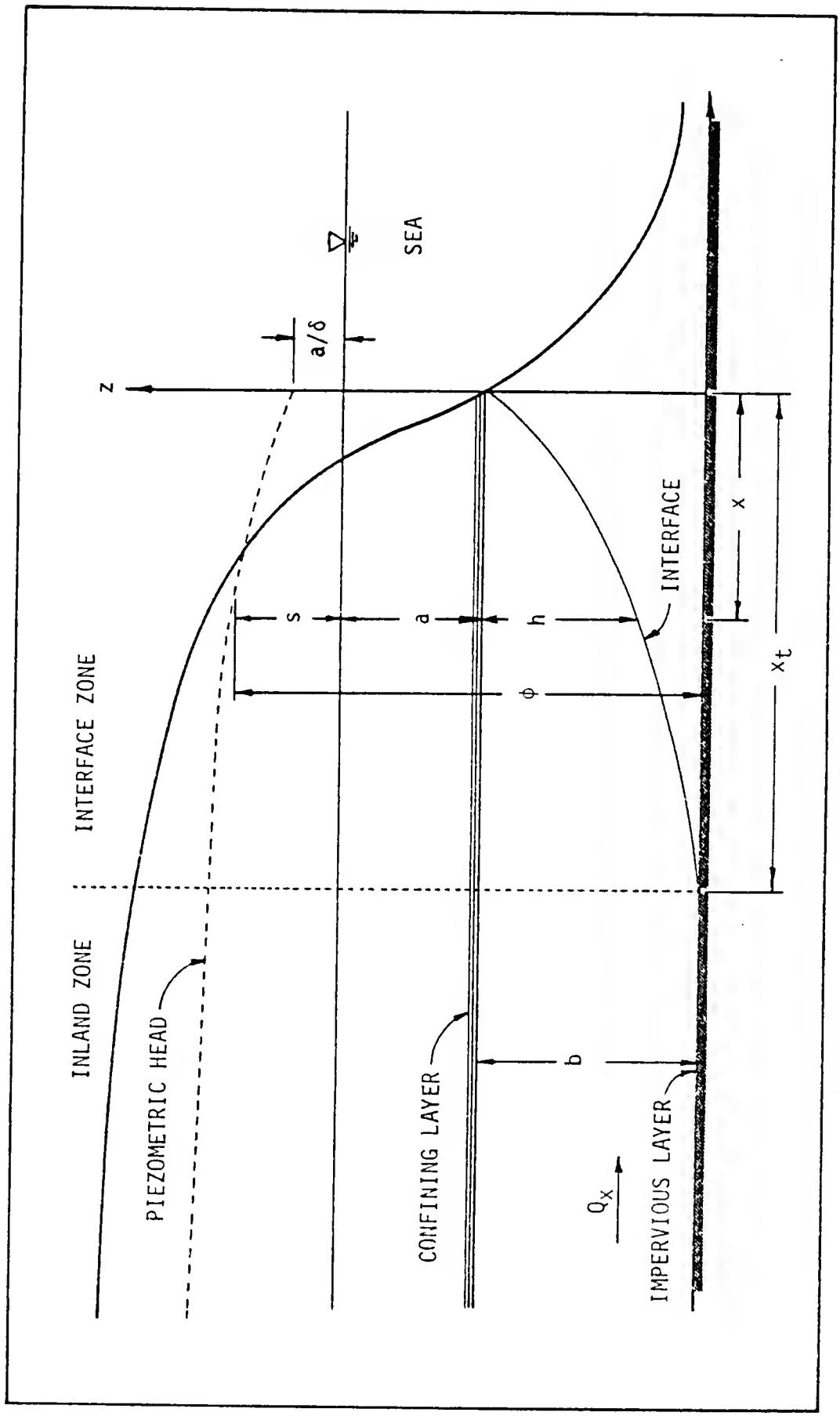

FIGURE 5.1. SHAPE OF SALTWATER WEDGE (DUPUIT PARABOLA)

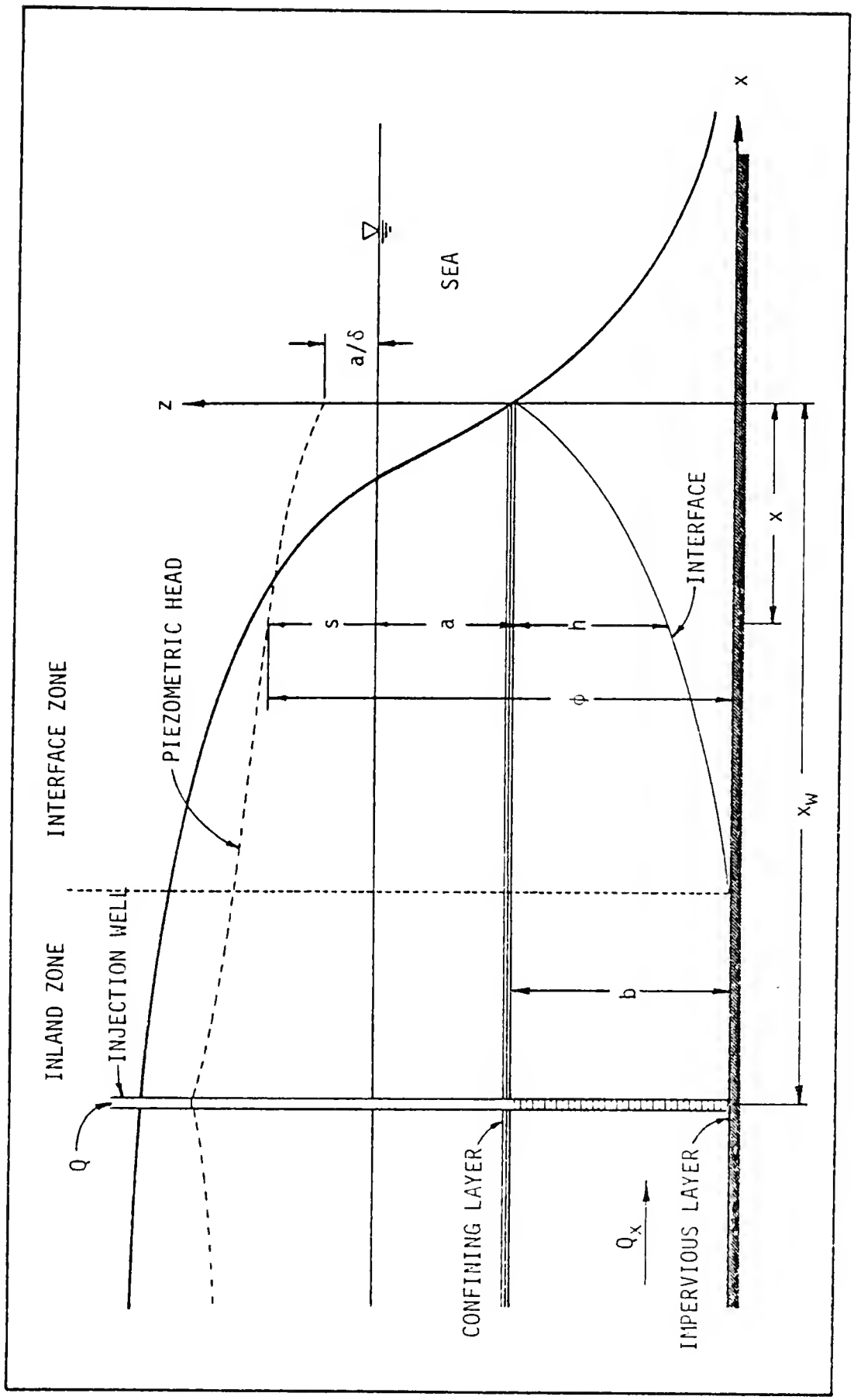

FIGURE 5.2. INJECTION INTO A CONFINED COASTAL AQUIFER

changing thickness of the flow region. Strack (1976) has found a modified form of the vertically integrated potentials originally proposed by Girinskii (see Bear, 1972; p. 157) which can account for the presence of the interface. If the thickness of the flow region is a linear function of the piezometric head, ϕ, i.e.,

$$h = \alpha\phi + \beta \tag{5.3}$$

then Strack gives the potential for the interface zone as

$$\Phi_i = 1/2\alpha K(\phi + \beta/\alpha)^2 \tag{5.4}$$

For the inland part of the aquifer where there is no interface, the potential is defined by

$$\Phi = Kb\phi + c \tag{5.5}$$

where the constant, c, is used to make the potential function continuous at the toe of the interface. It is easily verified from equations (5.4) and (5.5) that the discharge components in the x and y directions are obtained from Φ in the usual way.

$$Q_x = -\partial\Phi/\partial x \qquad \text{and} \qquad Q_y = -\partial\Phi/\partial y \tag{5.6}$$

in which Q_x and Q_y represent the discharge through a unit width and the total thickness of the aquifer in the x and y directions, respectively. From equations (5.6) it follows that the continuity condition for the confined coastal aquifer is given by the Laplace equation

$$\partial^2\Phi/\partial x^2 + \partial^2\Phi/\partial y^2 = 0 \tag{5.7}$$

and Φ is a harmonic function of x and y. The effect of this is that

through use of Girinskii's potential, variations in the vertical direction have been integrated out of the problem. The resulting potential function can be manipulated, using the theory of complex variables to describe a two-dimensional flow field with the desired boundary conditions. At the same time, the numerical value of the potential function at any point gives the depth to the interface at that point through the Ghyben-Herzberg relation and thereby supplies three-dimensional information about the freshwater lens. Before this can be done, however, it is necessary to determine the constants α and β in equation (5.4) and c in equation (5.5).

Confined coastal aquifer. From the geometry of the saltwater wedge, as shown in Figure 5.2, it is seen that

$$s = \phi - b - a \tag{5.8}$$

The thickness of the freshwater region, h, is related to the "push up", s, through

$$h = \delta s - a \tag{5.9}$$

which is a consequence of the Ghyben-Herzberg principle.

The combination of equations (5.8) and (5.9) results in

$$h = \delta\phi - \delta b - (1 + \delta)a \tag{5.10}$$

But it has already been assumed that the relationship between h and ϕ in the interface zone is given by equation (5.3). Consequently the values of α and β must be:

$$\alpha = \delta \quad \text{and} \quad \beta = -\delta b\ (1 + \delta)a \tag{5.11}$$

Substituting these values into equation (5.4) gives the definition of

the potential function in the interface zone for a confined coastal aquifer.

$$\Phi_i = \frac{1}{2} \delta K[\phi - b - (1 + 1/\delta)a]^2 \tag{5.12}$$

Now, in order that the potential function may be continuous throughout the aquifer, it is necessary to determine c in equation (5.5). Note that at the toe of the saltwater edge

$$s = (a + b)/\delta \tag{5.13}$$

which along with equation (5.8) gives

$$\phi = (a + b)\ (1 + 1/\delta) \tag{5.14}$$

Using this value of ϕ in both equations (5.5) and (5.12) and requiring that they be equal at the toe of the wedge results in

$$c = \frac{Kb^2}{2\delta} - Kb(a + b)\ (1 + 1/\delta) \tag{5.15}$$

The definition of the potential function in the inland zone of a confined coastal aquifer then becomes

$$\Phi = Kb[\phi + 1/2\ b/\delta - (a + b)\ (1 + 1/\delta)] \tag{5.16}$$

At the toe of the saltwater wedge this reduces to

$$\Phi_t = 1/2\ Kb^2/\delta \tag{5.17}$$

In order to construct the complex potential function for flow in the aquifer the boundary condition at the sea coast must be known. From Figure 5.2 it is seen that $s = a/\delta$ at the coast. Substituting this into equation (5.12) gives the boundary condition

$$\Phi = 0 \quad \text{at} \quad x = 0 \tag{5.18}$$

This condition can be satisfied by locating an image well, with the same strength as the injection well but opposite sign, on the other side of the boundary at the same distance from it, x_w, as the injection well. The superposition of the velocity potential for the two wells and the uniform seaward flow results in

$$\Phi = -xQ_x + \frac{Q}{4\pi} \ln \left\{ \frac{(x - x_w)^2 + y^2}{(x + x_w)^2 + y^2} \right\} \tag{5.19}$$

When particular values of Φ are computed from equation (5.12) and substituted into equation (5.19) which is then solved for the particular equipotential line, the shape of the freshwater lens produced by the injection well is outlined. Such a case is shown in Figure 5.3.

From a practical point of view it is most important to locate the toe of the saltwater wedge around the periphery of the lens because this is the outer boundary of the usable portion of the freshwater. The equipotential line which delineates this outer boundary has the value given by equation (5.17). Solutions for this line can be made dimensionless by defining the following dimensionless parameters:

$$x' = \frac{Q_x}{\Phi_t} x \tag{5.20a}$$

$$y' = \frac{Q_x}{\Phi_t} y \tag{5.20b}$$

$$x'_w = \frac{Q_x}{\Phi_t} x_w \tag{5.20c}$$

$$Q' = \frac{Q}{\Phi_t} \tag{5.20d}$$

A series of such dimensionless solutions for various conditions of injection is shown in Figure 5.4. and Figure 5.5.

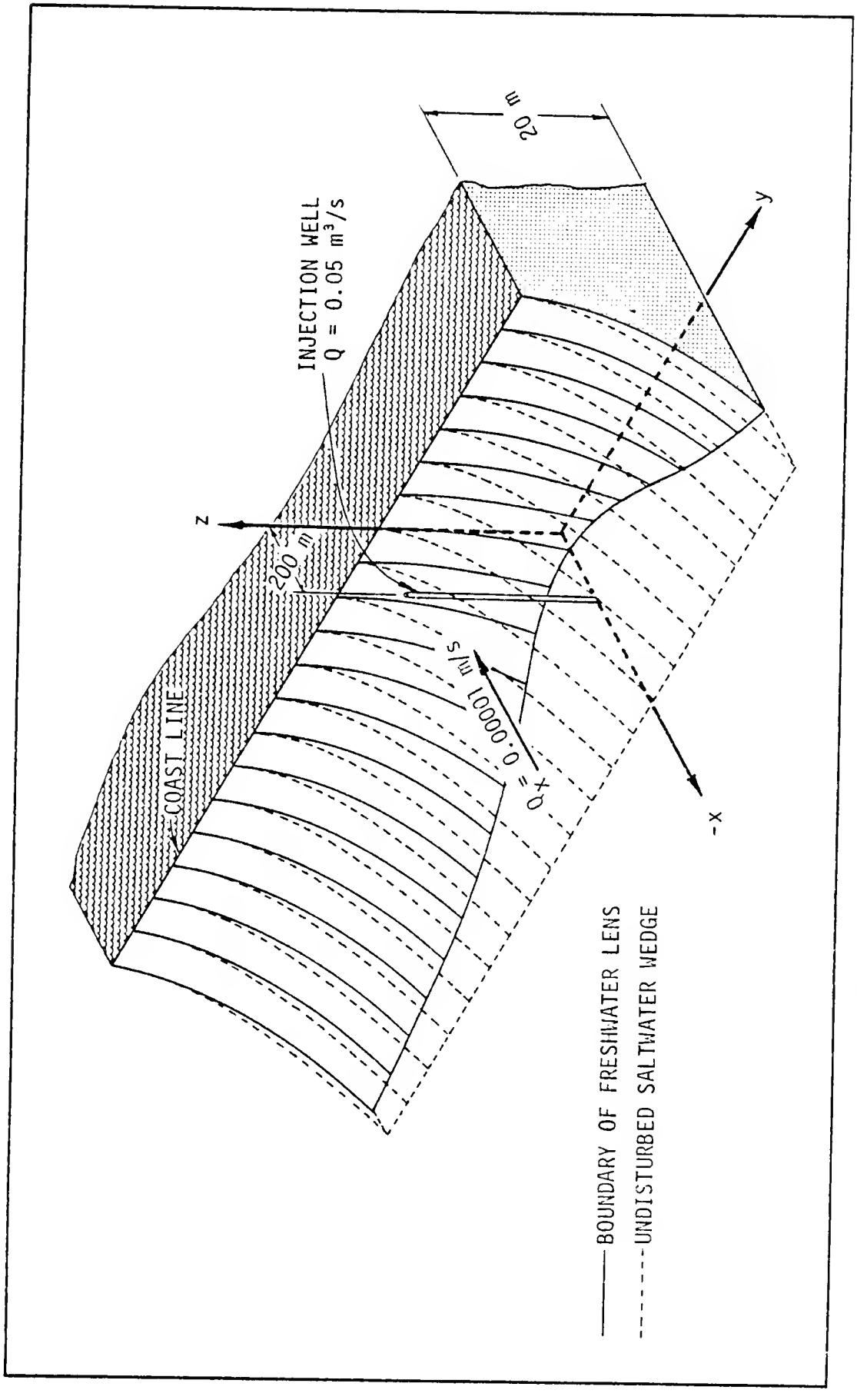

FIGURE 5.3. FRESHWATER LENS PRODUCED BY INJECTION INTO A CONFINED COASTAL AQUIFER

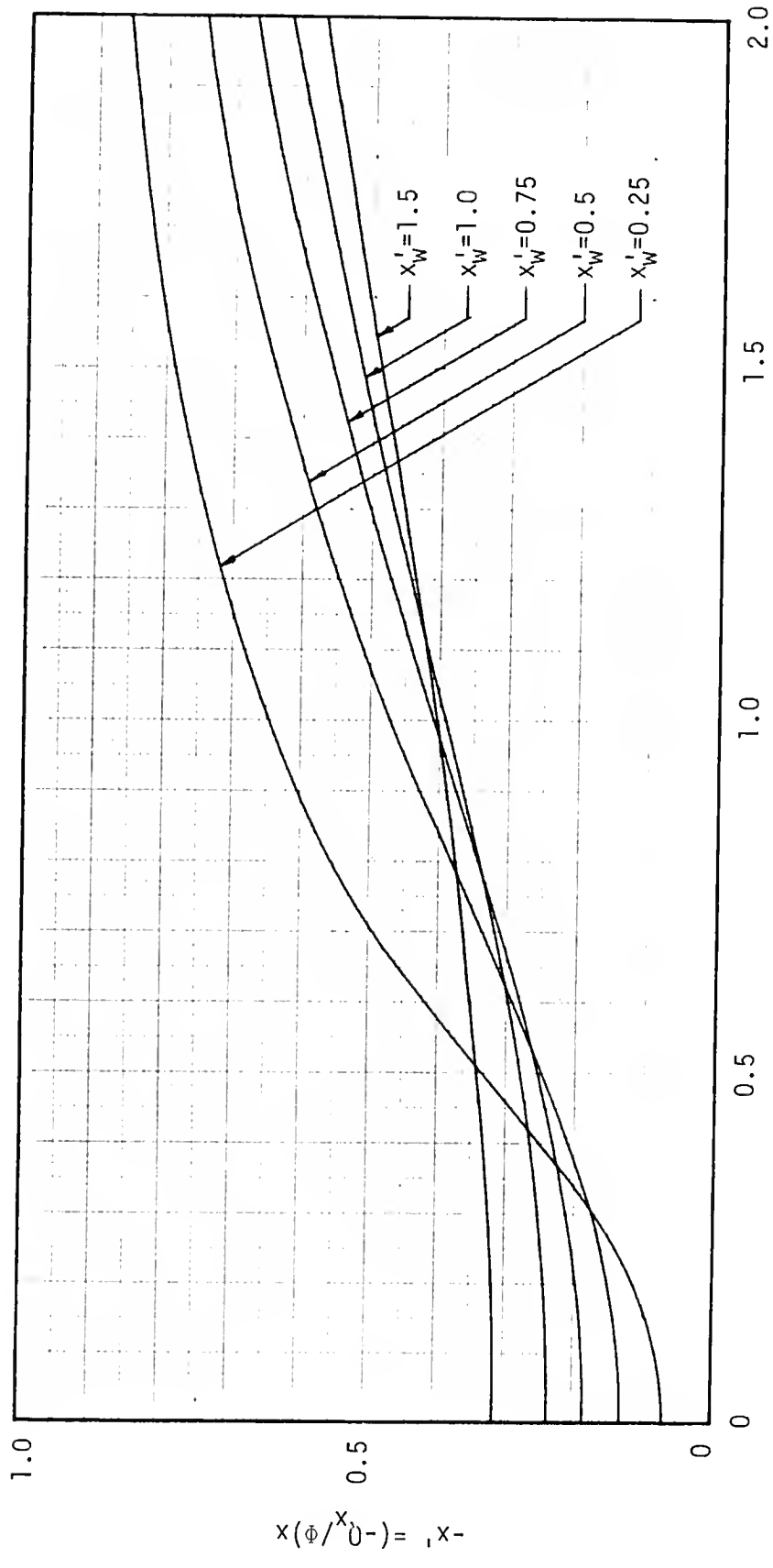

FIGURE 5.4. DIMENSIONLESS REPRESENTATION OF INTERFACE TOE, $Q' = Q/\Phi = 10.0$

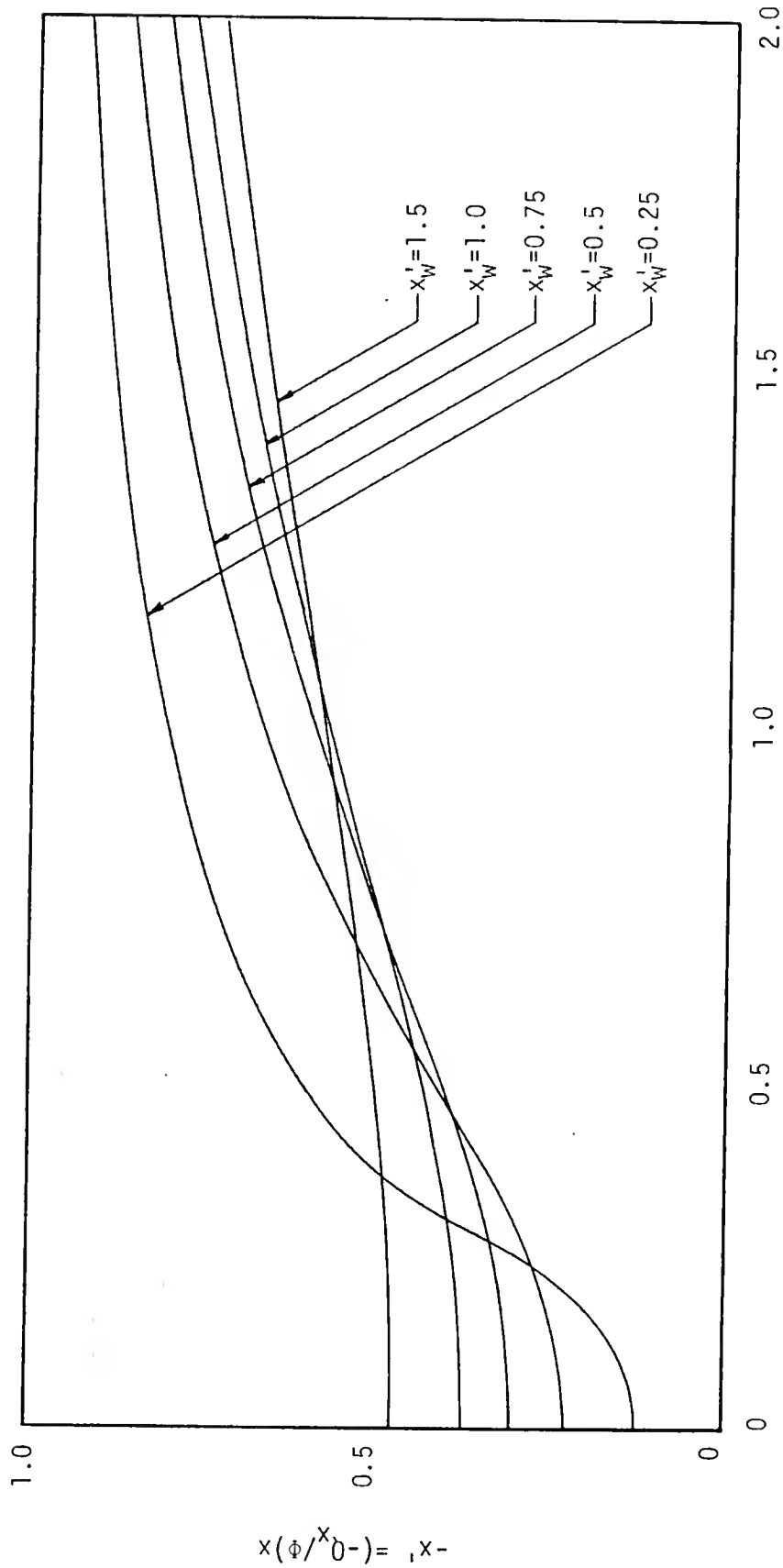

FIGURE 5.5. DIMENSIONLESS REPRESENTATION OF INTERFACE TOE, $Q' = Q/\Phi = 5.0$

Phreatic coastal aquifer. The Girinskii potentials defined by Strack for interface flow can also be used in aquifers which have no upper confining layer because the thickness of the freshwater region is still a linear function of the piezometric head. The linear function is not the same as for a confined aquifer, however, so the potentials must be redefined to conform to the aquifer geometry shown in Figure 5.6. In the inland zone the specific discharge, Q_x is given by

$$Q_x = -\phi K \frac{\partial \phi}{\partial x} = -\frac{K}{2} \frac{\partial \phi^2}{\partial x^2} \tag{5.21}$$

The potential for this region, then, should be defined as

$$\Phi = 1/2\ K\phi^2 + c \tag{5.22}$$

In the interface zone, note that

$$s = \phi - b \tag{5.23}$$

and from the Ghyben-Herzberg principle the thickness of the flow region is

$$h = s(1 + \delta) \tag{5.24}$$

which leads to

$$h = (1 + \delta)\phi - (1 + \delta)b \tag{5.25}$$

If this is to be in the form of equation (5.3) then the constants α and β must be

$$\alpha = (1 + \delta) \quad \text{and} \quad \beta = -(1 + \delta)b \tag{5.26}$$

Substituting these values into equation (5.4) results in a definition

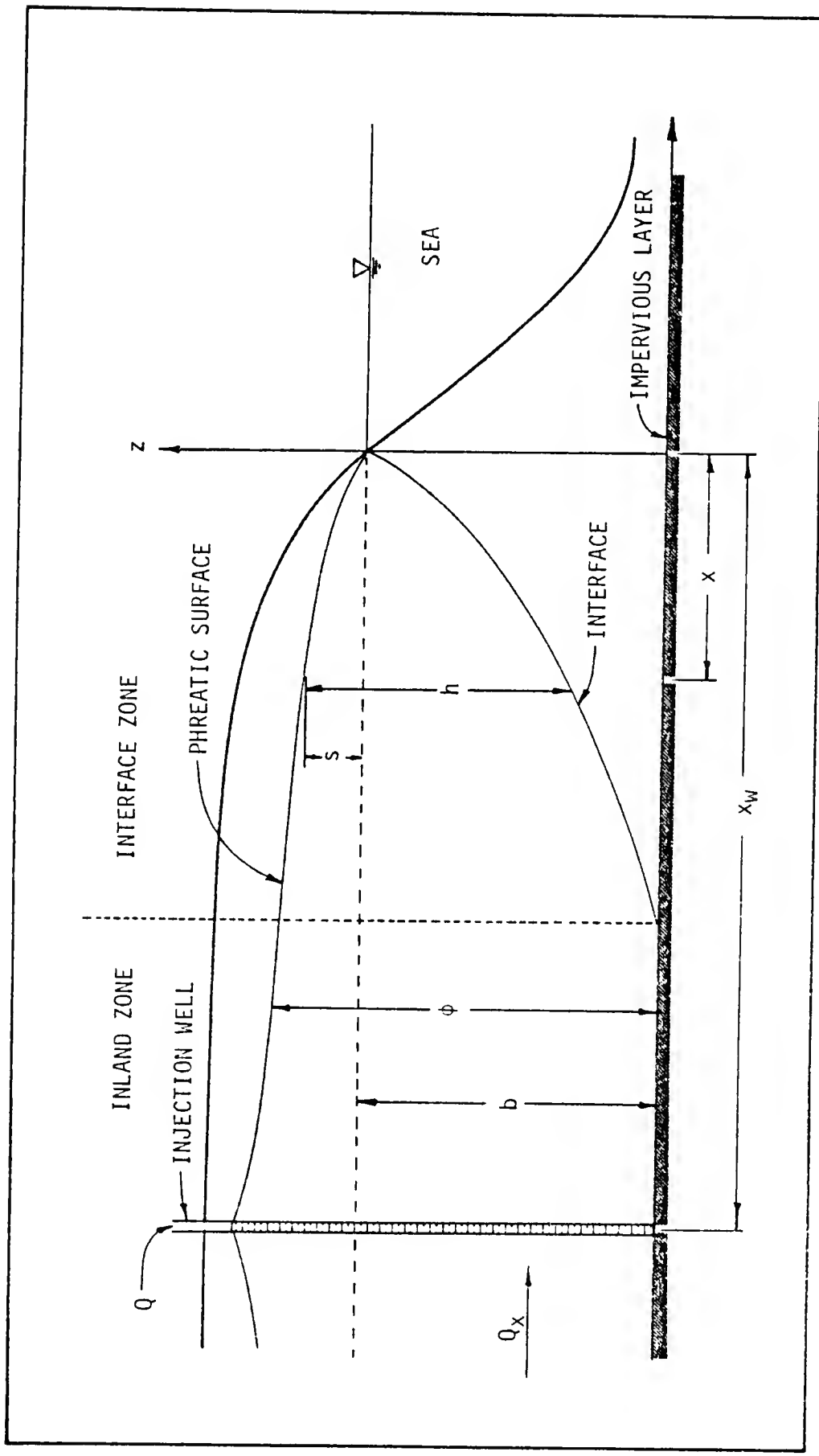

FIGURE 5.6. INJECTION INTO A PHREATIC AQUIFER

for the velocity potential in the interface zone

$$\Phi_i = 1/2\ (1 + \delta)\ K(\phi - b)^2 \tag{5.27}$$

At the toe of the saltwater wedge the piezometric head is

$$\Phi_t = b(1 + 1/\delta) \tag{5.28}$$

Substituting this into equations (5.22) and (5.27) and requiring that be single valued at this point leads to the value of the constant c in equation (5.22).

$$c = -1/2\ Kb^2\ (1 + 1/\delta) \tag{5.29}$$

The definition of the velocity potential in the inland zone of the phreatic aquifer then becomes

$$\Phi = 1/2\ K[\phi^2 - (1 + 1/\delta)b^2] \tag{5.30}$$

At the toe of the saltwater wedge this reduces to

$$\Phi_t = 1/2\ Kb^2(1 + \delta)/\delta^2 \tag{5.31}$$

which is greater than the corresponding value for a confined aquifer by a factor of $(1 + 1/\delta)$.

Axisymmetric Flow in a Leaky Aquifer

Consider a homogeneous saline aquifer with hydraulic conductivity, K, of uniform thickness, b, and unlimited areal extent. It is confined

at the bottom by a horizontal impervious layer and at the top by a horizontal aquitard of thickness, b', and hydraulic conductivity, K'. A fully penetrating well injects freshwater at a constant rate, Q, forming a freshwater lens, which remains centered on the well since there is no pre-existing flow in the surrounding salt water. Injection continues until a steady state is eventually reached in which the injection rate is matched by the rate of leakage through the aquitard. The mixing zone at the boundary of the lens then becomes relatively thin and can be approximated by a sharp interface. This situation is depicted in Figure 5.7.

The flow region is divided into two zones, each of which has its own governing equation. In zone 1, which is occupied entirely by freshwater, the customary analysis for well flow in leaky aquifers can be used. This includes the assumption of 90 degree streamline refraction at the aquitard so that flow in the aquifer is horizontal while in the aquitard it is vertical. The governing equation is (see De Weist, 1965, p. 264)

$$\frac{d^2s}{dr^2} + \frac{1}{r}\frac{ds}{dr} - \left(\frac{1}{B}\right)^2 s = 0 \qquad (5.32)$$

where

$$B^2 = Kbb'/K'$$

This is a modified Bessel equation of order zero, for which the general solution is given by

$$s = C_1 I_0(r/B) + C_2 K_0(r/B) \qquad (5.33)$$

where I_0 and K_0 are the modified zeroth order Bessel functions of the first and second kinds, respectively. The boundary condition at the

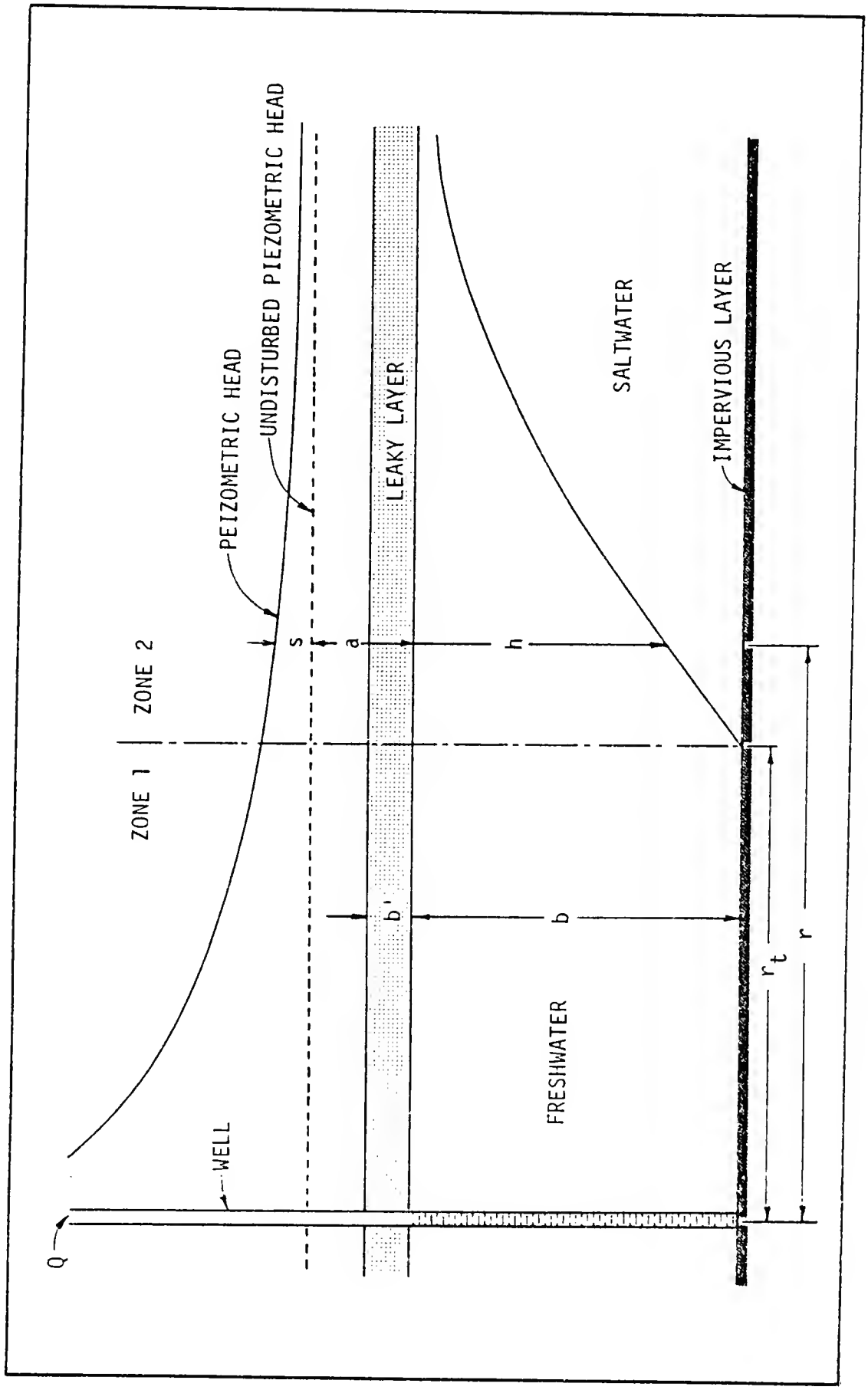

FIGURE 5.7. STEADY FRESHWATER LENS IN A LEAKY SALINE AQUIFER

outer edge of zone 1 is complicated by the fact the position of the boundary is unknown. Since the Ghyben-Herzberg relationship is being used, the value of s at the toe of the interface is known, though, and this will be used to determine the boundary location. The boundary conditions for zone 1, then, are

$$1) \quad \lim_{r \to 0} \left(r \frac{ds}{dr}\right) = - Q/(2\pi Kb) \tag{5.34a}$$

$$2) \quad s = \frac{b+a}{\delta} \quad \text{at} \quad r = r_t \tag{5.34b}$$

Differentiating equation (5.33) and applying the first boundary condition gives

$$C_1 \lim_{r \to 0} [r/B \, I_1(r/B)] - C_2 \lim_{r \to 0} [r/B \, K_1(r/B)] = -Q/(2\pi Kb) \tag{5.35}$$

in which I_1 and K_1 are modified Bessel functions of order 1. The first limit in equation (5.35) is zero and the second is one, which leads to a value for the constant, C_2.

$$C_2 = \frac{Q}{2\pi Kb} \tag{5.36}$$

Substituting this and the second of equations (5.34) into equation (5.33) gives the other required constant

$$C_1 = [\frac{b+a}{\delta} - \frac{Q}{2\pi Kb} K_0(r_t/B)]/I_0(r_t/B) \tag{5.37}$$

The solution for s in zone 1 is then

$$s = [\frac{b+a}{\delta} - \frac{Q}{2\pi Kb} K_0 (r_t/B)] \frac{I_0(r/B)}{I_0(r_t/B)} + \frac{Q}{2\pi Kb} K_0(r/B) \tag{5.38}$$

in which the value of r_t is as yet undetermined.

The flow in zone 2 is complicated by the presence of the interface so that a new equation must be derived for it. In this, the Dupuit assumption will be used so that, as before, only head loss due to horizontal flow in the aquifer will be considered.

Applying the principle of mass conservation to the differential wedge of aquifer shown in figure 5.8 gives

$$uhrd\theta - (u+du)(h+dh)(r+dr)d\theta - w(s)rdrd\theta = 0 \tag{5.39}$$

expanding this, cancelling terms where possible, and dividing by $drd\theta$ results in

$$hr\frac{du}{dr} + ur\frac{dh}{dr} + r\frac{du}{dr}dh + uh + dhu + dudh + rw(s) = 0 \tag{5.40}$$

Taking the limit as the differentials go to zero, this becomes

$$hr\frac{du}{dr} + ur\frac{dh}{dr} + uh + rw(s) = 0 \tag{5.41}$$

Substituting Darcy's law

$$u = -K\frac{ds}{dr} \tag{5.42}$$

into equation (5.41) and dividing by Khr gives

$$\frac{d^2s}{dr^2} + \frac{1}{h}\frac{dh}{dr}\frac{ds}{dr} + \frac{1}{r}\frac{ds}{dr} - \frac{w(s)}{Kh} = 0 \tag{5.43}$$

But the Gyben-Herzberg principle gives the following relationship between h and s

$$h = (\delta s - a) \tag{5.44}$$

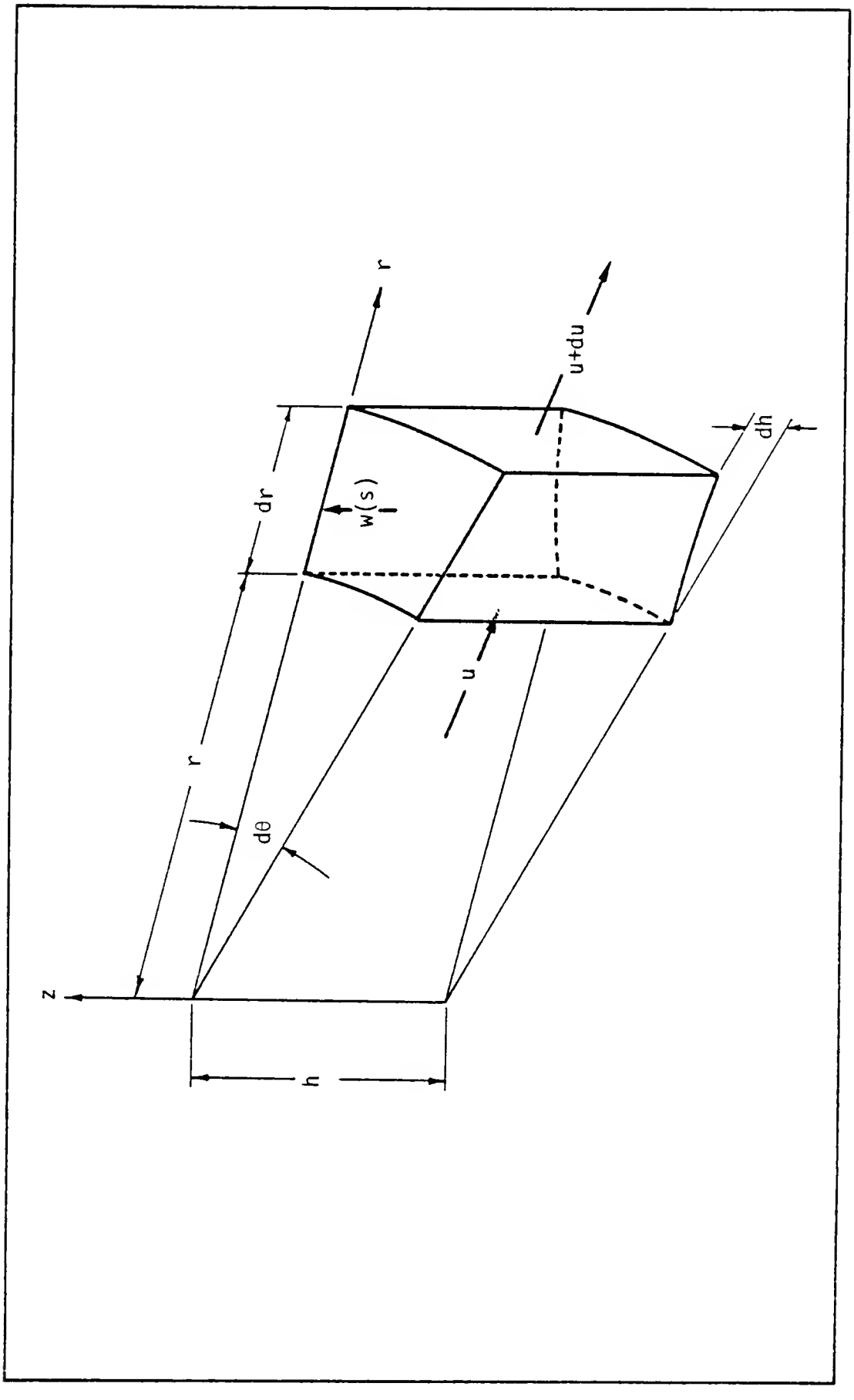

FIGURE 5.8. DIFFERENTIAL WEDGE OF LEAKY AQUIFER

Substituting this into equation (5.43) gives

$$\frac{d^2s}{dr^2} + \frac{\delta}{(\delta s-a)}\left(\frac{ds}{dr}\right)^2 + \frac{1}{r}\frac{ds}{dr} - \frac{w(s)}{Kh} = 0 \qquad (5.45)$$

Noting that

$$w(s) = K's/b' \qquad (5.46)$$

the governing equation for flow in zone 2 is obtained

$$\frac{d^2s}{dr^2} + \frac{\delta}{(\delta s-a)}\left(\frac{ds}{dr}\right)^2 + \frac{1}{r}\frac{ds}{dr} - \frac{K's}{(\delta s-a)b'K} = 0 \qquad (5.47)$$

Equation (5.47) is non-linear and is not one of the few types of non-linear equations for which analytical methods of solution are available. There are several routine numerical methods which can handle such an equation, but first it is necessary to find the correct boundary conditions by which the flow in zone 2 can be coupled to that in zone 1. Those conditions are partially provided by the requirement that the piezometric head, s, and its slope, $\frac{ds}{dr}$, must be continuous at the radius, r_t, where the two zones join. Now, the value of s at that point has already been given, and its slope can be found by differentiating equation (5.38). These requirements can be stated as:

1) $$s(r_t) = \frac{b+a}{\delta} \qquad (5.48a)$$

2) $$\left.\frac{ds}{dr}\right|_{r_t} = \left[\frac{b+a}{\delta} - \frac{Q}{2\pi Kb} K_0(r_t/B)\right] \frac{I_1(r_t/B)}{BI_0(r_t/B)} - \frac{Q}{2\pi KbB} K_1(r_t/B) \qquad (5.48b)$$

These are only partial boundary conditions, however, because they contain the unknown, r_t. One final boundary condition is needed which can

be described as the requirement that as r approaches infinity, s and all of its derivatives should approach zero. The truth of this is not immediately apparent, but it will be demonstrated after some of the integral curves to the set of coupled equations (5.32) and (5.47) have been obtained.

The integral curves can be obtained by choosing values for the variable, r_t. When this is done, the solution for zone 1 is immediately obtained from equation (5.38). The boundary conditions (5.48) then provide the necessary starting point for a numerical treatment of equation (5.47). The integral curves shown in Figure 5.9 were obtained by the Adams-Bashforth type predictor-corrector method using the Runge-Kutta method as a starter for the first four distance steps. Figure 5.9 reveals two different kinds of integral curves representing solutions for equation (5.47) in terms of s vs. r for different values of r_t. In the upper curves, s first starts to decrease with increasing r, then a minimum value is reached and s starts to increase. This is obviously not a physically possible solution to the problem. The lower curves, on the other hand, continue to approach zero until they reach it. This is not a physically possible steady state solution either because as s approaches zero along this line, its slope becomes increasingly negative which means that the flow velocity is increasing. If this were true, it would mean that the flow field engendered by the injection well has a finite boundary and that the flow rate at that boundary is very high. It is instructive here to consider the equation for the curvature of the piezometric head line in the special case of $a = 0$.

$$\frac{d^2s}{dr^2} = \frac{K'}{\delta b' K} - \frac{1}{s}\left(\frac{ds}{dr}\right)^2 - \frac{1}{r}\frac{ds}{dr} \qquad (5.49)$$

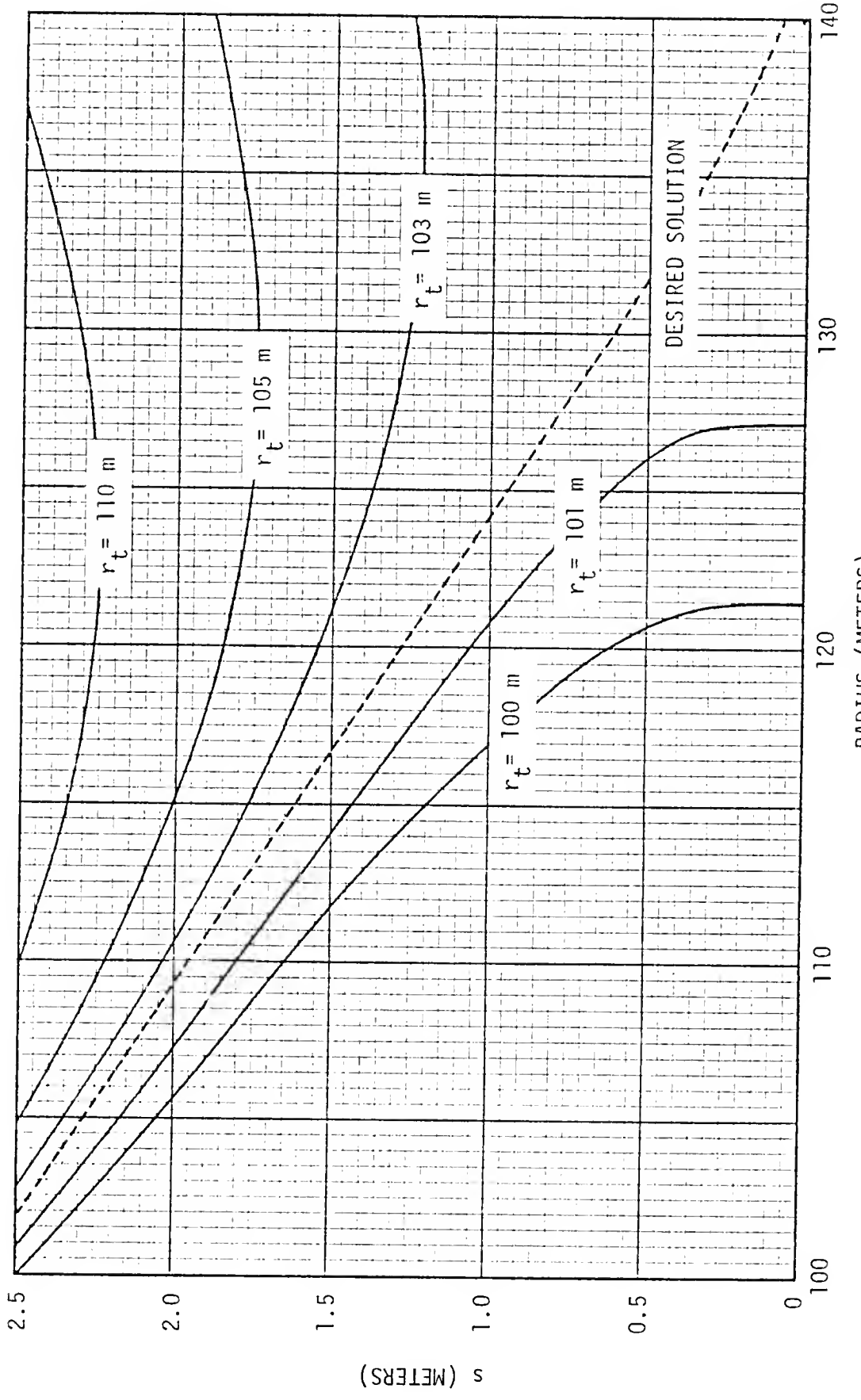

FIGURE 5.9. INTEGRAL CURVES FOR EQUATION (5.47)

This shows that as s approaches zero with non-zero slope, the curvature becomes negatively infinite. This is what is happening in the lower set of integral curves. However, if both s and $\frac{ds}{dr}$ approach zero in the right way, the curvature $\frac{d^2s}{dr^2}$ will approach zero also. This happens somewhere in the area between the upper and lower integral curves, and it represents the only physically possible solution. While it is not possible to exhibit this solution precisely, it is possible to obtain the upper and lower integral curves as close to it as one may desire.

Figure 5.10 shows solutions for the toe of the interface, r_t, which were claculated by this method for a variety of flow conditions. They are presented in the form of dimensionless variables $\delta Q/(2\pi Kb^2)$ vs. r_t/B for several values of the density ratio, a/b, on each figure. Of course, knowledge of the value of r_t does not constitute a complete solution to the problem. One would also like to know the shape of the interface and consequently of the entire lens. Examples of such solutions are shown in Figure 5.11. It should be noted, however, that from a practical standpoint, the position of the toe of the interface is most important, since the freshwater located in that part of the lens beyond, r_t, cannot be recovered unmixed with salt water. In fact, it will not be possible even to recover all of the water inside r_t because of dispersion and further tilting of the interface when the lens departs from its equilibrium position.

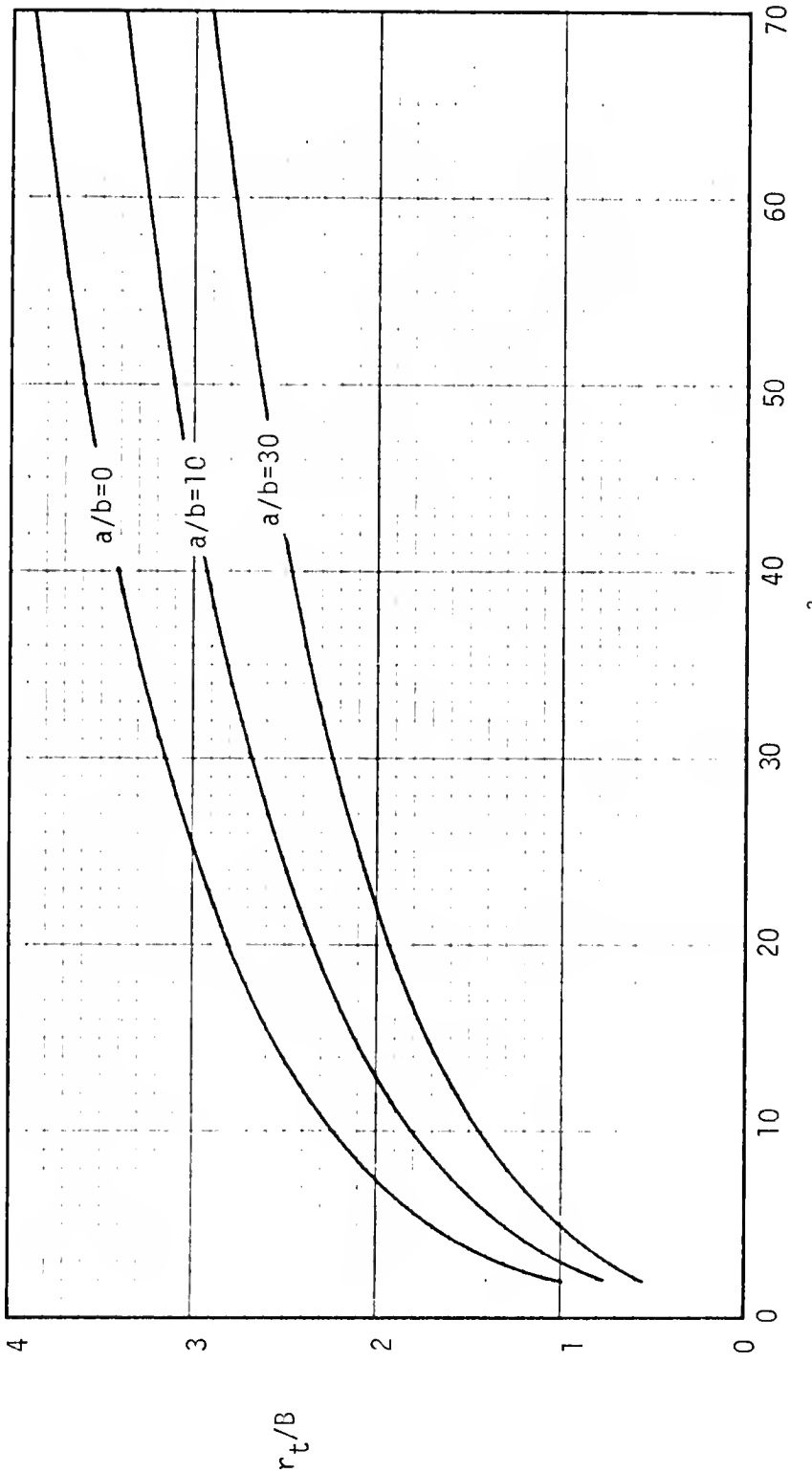

FIGURE 5.10. $Q\delta/(2\pi Kb^2)$ vs. r_t/B FOR THREE VALUES OF a/b

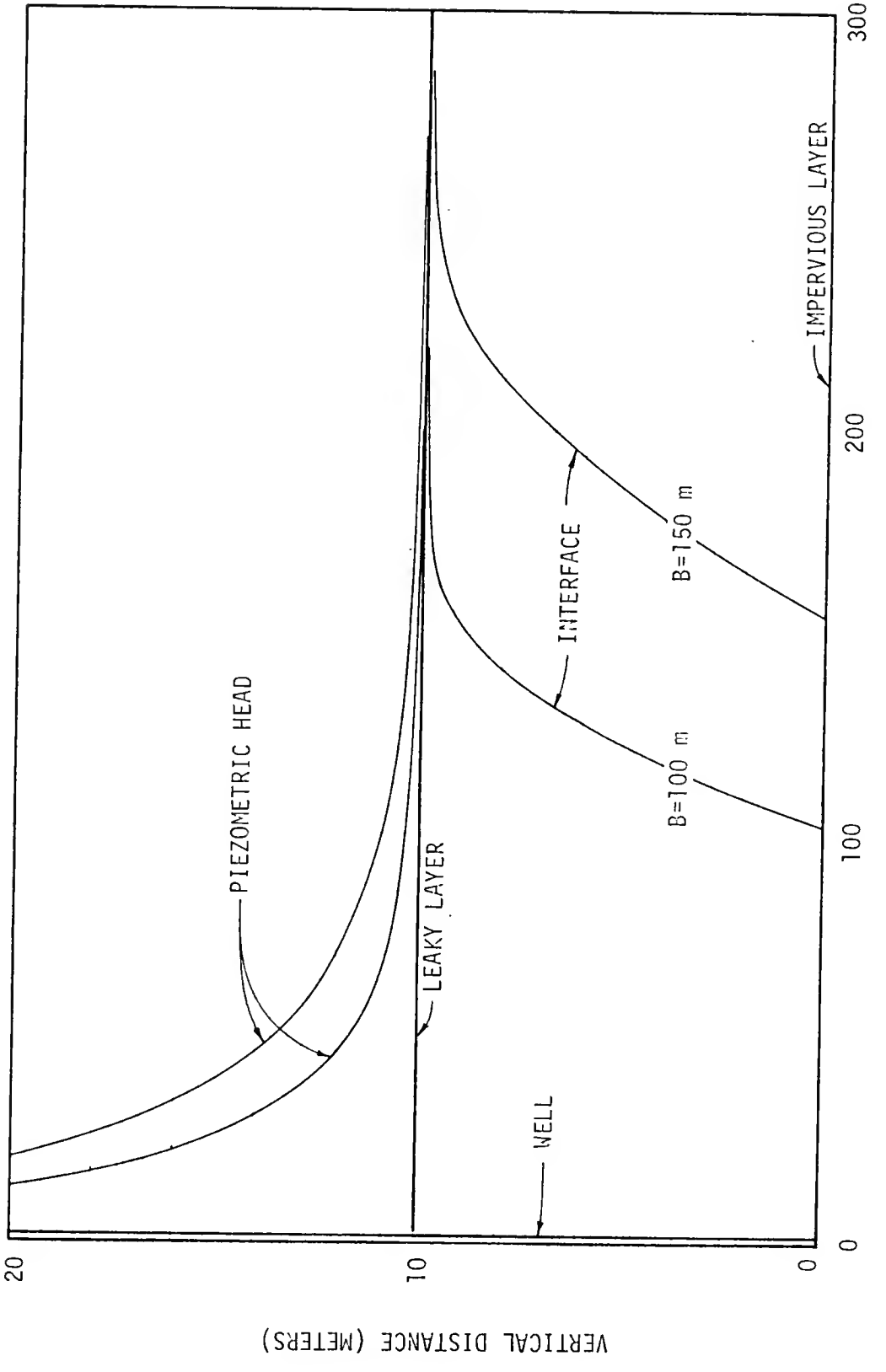

FIGURE 5.11. SECTION THROUGH STEADY FRESHWATER LENS FOR TWO VALUES OF LEAKAGE, B,: a = 0

CHAPTER 6

A FINITE ELEMENT MODEL FOR THE STEADY FLOW CASE

General

The solutions to steady state problems given in the preceeding chapter depended on the assumption of horizontal streamlines and static conditions in the saline part of the aquifer. These two simplifications were required so that the Ghyben-Herzberg principle could be used for location of the position of the interface. If the horizontal streamline restriction is lifted, a three-dimentional boundary value problem must be solved and the interface must be located by a trial and error process. If flow is permitted in the saline portion of the aquifer as well, then a pair of coupled three-dimensional boundary value problems must be solved. In this chapter the method of finite elements will be used to obtain numerical solutions to such problems.

Description of the Galerkin Finite Element Scheme

The Fundamental Concept

The boundary value problem within a steady freshwater lens can be posed in terms of the piezometric head $\phi = \phi(x, y, z)$, a dependent variable which is a continuous function of position inside the boundaries of the lens. In the finite element method this continuous function is approximated by a set of piecewise continuous polynomial functions, each of which is defined on a discrete subregion, or element, of the flow domain. In order to do this, the flow region must first be divided up into elements with a finite number of nodal points denoting

the boundaries of the elements. The values of the continuous quantity, ϕ, at all of these nodal points form a set of unknown variables for which the boundary value problem is to be solved. The piecewise continuous polynomial functions are defined over the elements in terms of these unknown nodal values of ϕ. For this reason, they are called interpolation functions.

Once the set of interpolating functions is obtained the values of the nodal unknowns must be determined in such a way that the interpolation polynomials will provide the closest possible approximation to the governing differential equation. There are several ways of doing this. The method used here is to minimize the error of the approximating functions when integrated over the flow domain by the Galerkin weighted residual technique.

The Element and its Shape Functions

The type of element to be used is illustrated in Figure 6.1. It is a three-dimensional element with 20 nodes. The presence of the mid-side nodes on each side permits the dependent variable, ϕ, to be approximated by an interpolation function that is quadratic in all three coordinate directions. The form of this interpolation polynomial is

$$\begin{aligned}\hat{\phi} = {} & \alpha_1 + \alpha_2 x + \alpha_3 y + \alpha_4 z + \alpha_5 xy + \alpha_6 xz + \alpha_7 yz \\ & + \alpha_8 xyz + \alpha_9 x^2 + \alpha_{10} y^2 + \alpha_{11} z^2 + \alpha_{12} x^2y + \alpha_{13} x^2z \\ & + \alpha_{14} xy^2 + \alpha_{15} y^2z + \alpha_{16} xz^2 + \alpha_{17} yz^2 + \alpha_{18} x^2yz \\ & + \alpha_{19} xy^2z + \alpha_{20} xyz^2 \end{aligned} \tag{6.1}$$

where $\hat{\phi}$ is the approximation to ϕ and the 20 coefficients $\alpha_1 \cdots \alpha_{20}$ must be defined in terms of the element shape and the unknown values of

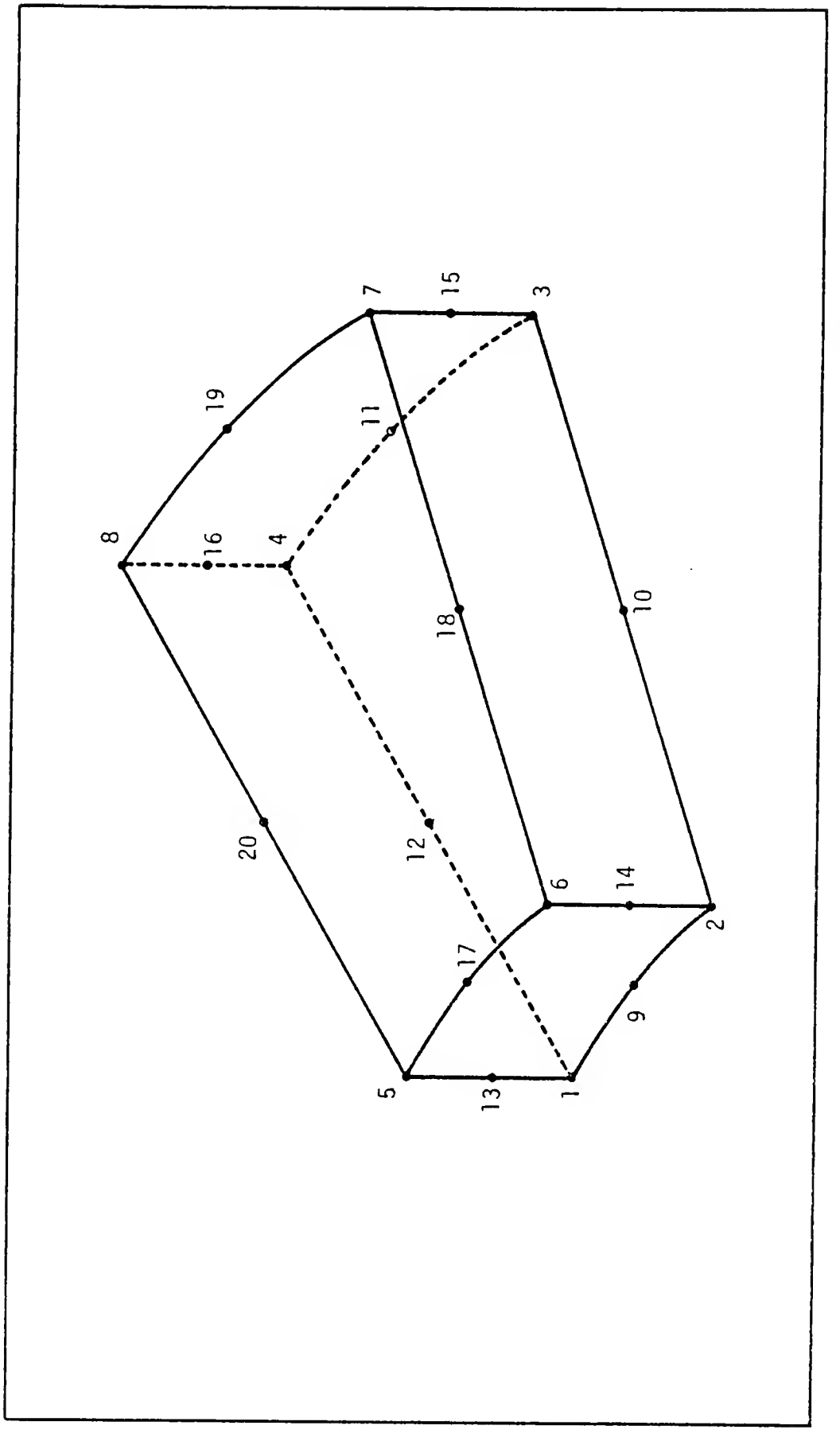

FIGURE 6.1. THREE-DIMENSIONAL ELEMENT SHOWING NODE NUMBERS

$\hat{\phi}$ at the 20 nodes, $\Phi_1 \ldots \Phi_{20}$. The definition of these coefficients must be done in such a way that the values of $\hat{\phi}$ given by equation (6.1) will satisfy

$$\hat{\phi}\,(x, y, z) = \Phi_i \quad \text{when} \quad (x, y, z) = (X_i, Y_i, Z_i) \tag{6.2}$$

where X_i, Y_i and Z_i are the coordinates of the i^{th} node. It is possible to apply the condition of equation (6.2) to equation (6.1) for all 20 nodes and solve the resulting 20 equations for $\alpha_1 \ldots \alpha_{20}$. Substituting the results of this into equation (6.1) it can be rearranged into the following form:

$$\hat{\phi} = \sum_{i=1}^{20} N_i \, \Phi_i \tag{6.3}$$

where the 20 coefficients $N_i \cdots N_{20}$ are called shape functions because they depend only on the geometry of the element. Since equation (6.3) must also satisfy the requirement of equation (6.2) it is obvious that at the i^{th} node $N_i = 1$ and all the other N's are zero. The values of the shape functions between nodes must be such that $\hat{\phi}$ will be continuous over the element. The distributions of two quadratic shape functions over a two-dimensional element are illustrated in Figure 6.2.

The element and its shape functions can be considered to adequately represent the flow domain and the dependent variable, ϕ, if they result in a description which converges to the true distribution of ϕ as the flow domain is subdivided into finer and finer elements. It can be shown (Zienkiewicz, 1971) that the solution will be convergent if two conditions are satisfied. First, the element shape functions must be capable of correctly describing a constant distribution of the dependent variable throughout the element. If the dependent variable were constant

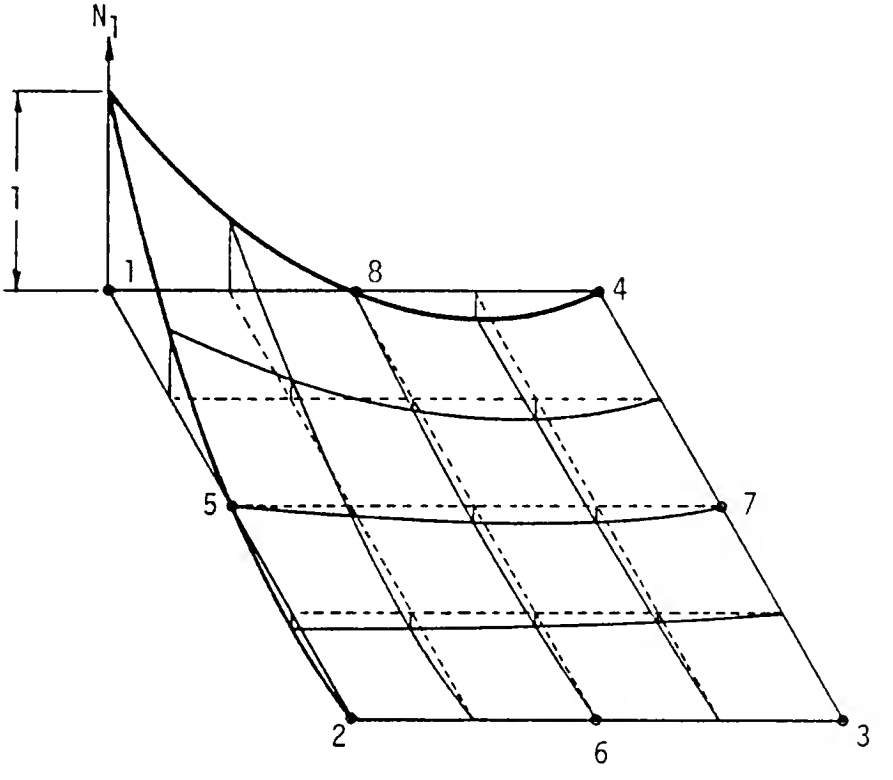

a. Distribution of shape function N_1

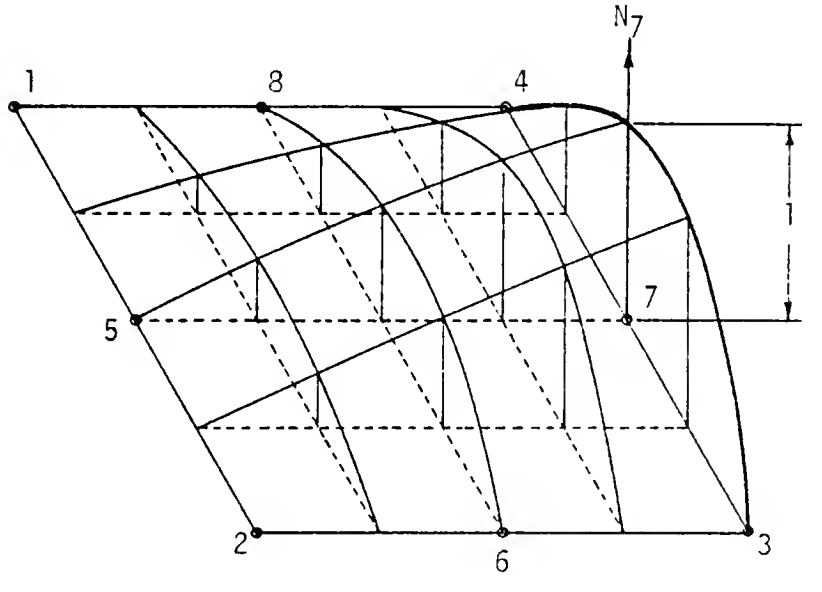

b. Distribution of shape function N_7

FIGURE 6.2. DISTRIBUTION OF TWO QUADRATIC SHAPE FUNCTIONS OVER A TWO-DIMENSIONAL QUADRILATERAL ELEMENT

then all twenty values of Φ_1, Φ_2, . . . Φ_{20} would be equal and $\hat{\phi}$ would be correctly described if

$$\sum_{i=1}^{20} N_i (x, y, z) = 1 \qquad (6.4)$$

for all values of x, y, and z in the element. Second, the predicted values of the dependent variable, $\hat{\phi}$, must be continuous across the boundaries between adjacent elements. In order that this may be assured, it is necessary that the shape function values for the adjacent elements must be equal along their common boundaries. The 20 node element shown in Figure 6.1 is one of a family called the Serendipity family of elements because 20 shape functions can be found for it by inspection which satisfy all of the above requirements.

The 20 shape functions are defined in terms of the local coordinate system shown in Figure 6.3. The adoption of a local coordinate system is necessary for the quadrilateral family of elements to insure inter-element continuity when the element boundaries are not parallel to the global x, y, z coordinates (Segerlind, 1976). The shape functions are given in Table 6.1.

Finite Element Formulation of the Governing Equation

The governing equation for steady groundwater flow in a homogeneous leaky aquifer is

$$L(\phi) = K_{xx} \frac{\partial^2 \phi}{\partial x^2} + K_{yy} \frac{\partial^2 \phi}{\partial y^2} + K_{zz} \frac{\partial^2 \phi}{\partial z^2} + Q - \frac{\phi - \phi_0}{\beta^2} = 0 \qquad (6.5)$$

where Q is the strength of a fluid source at the surface of the flow region, $\beta^2 = b'/K'$ is a modified form of the leakage coefficient, B^2, and ϕ_0 is the piezometric head in the phreatic aquifer above the

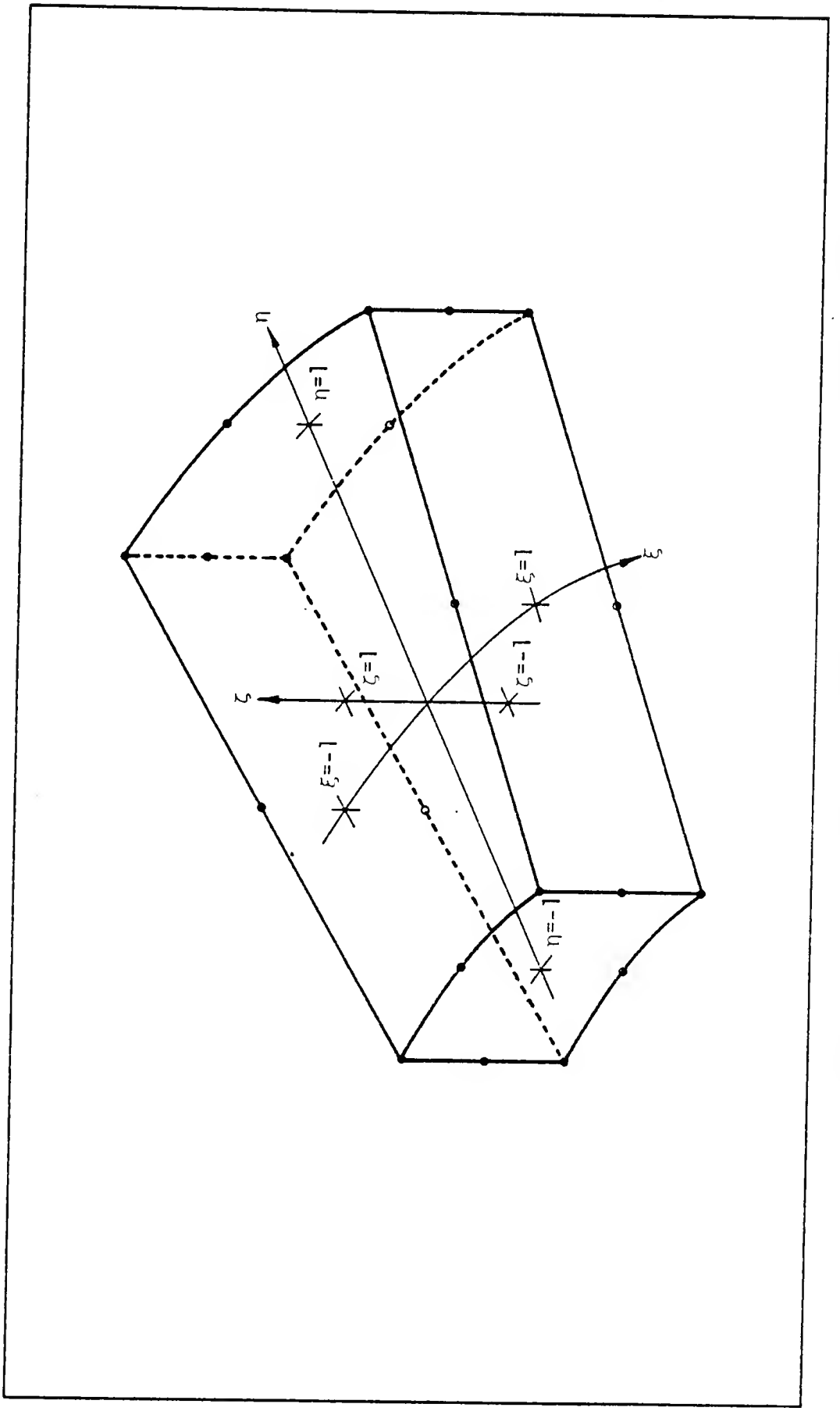

FIGURE 6.3. LOCAL COORDINATE SYSTEM FOR THE THREE-DIMENSIONAL ELEMENT

TABLE 6.1

SHAPE FUNCTIONS FOR THE 20 NODES ELEMENT

$$N_1 = 1/8\ (1 - \xi)\ (1 - \eta)\ (1 - \zeta)\ (-\xi - \eta - \zeta - 2)$$

$$N_2 = 1/8\ (1 + \xi)\ (1 - \eta)\ (1 - \zeta)\ (\xi - \eta - \zeta - 2)$$

$$N_3 = 1/8\ (1 + \xi)\ (1 - \eta)\ (1 - \zeta)\ (\xi + \eta - \zeta - 2)$$

$$N_4 = 1/8\ (1 - \xi)\ (1 + \eta)\ (1 - \zeta)\ (-\xi + \eta - \zeta - 2)$$

$$N_5 = 1/8\ (1 - \xi)\ (1 - \eta)\ (1 + \zeta)\ (-\xi - \eta + \zeta - 2)$$

$$N_6 = 1/8\ (1 + \xi)\ (1 - \eta)\ (1 + \zeta)\ (\xi - \eta + \zeta - 2)$$

$$N_7 = 1/8\ (1 + \xi)\ (1 + \eta)\ (1 + \zeta)\ (\xi + \eta + \zeta - 2)$$

$$N_8 = 1/8\ (1 - \xi)\ (1 + \eta)\ (1 + \zeta)\ (-\xi + \eta + \zeta - 2)$$

$$N_9 = 1/4\ (1 - \xi^2)\ (1 - \eta)\ (1 - \zeta)$$

$$N_{10} = 1/4\ (1 - \eta^2)\ (1 + \xi)\ (1 - \zeta)$$

$$N_{11} = 1/4\ (1 - \xi^2)\ (1 + \eta)\ (1 - \zeta)$$

$$N_{12} = 1/4\ (1 - \eta^2)\ (1 - \xi)\ (1 - \zeta)$$

$$N_{13} = 1/4\ (1 - \zeta^2)\ (1 - \xi)\ (1 - \eta)$$

$$N_{14} = 1/4\ (1 - \zeta^2)\ (1 + \xi)\ (1 - \eta)$$

$$N_{15} = 1/4\ (1 - \zeta^2)\ (1 + \xi)\ (1 + \eta)$$

$$N_{16} = 1/4\ (1 - \zeta^2)\ (1 - \xi)\ (1 + \eta)$$

$$N_{17} = 1/4\ (1 - \xi^2)\ (1 - \eta)\ (1 + \zeta)$$

$$N_{18} = 1/4\ (1 - \eta^2)\ (1 + \xi)\ (1 + \zeta)$$

$$N_{19} = 1/4\ (1 - \xi^2)\ (1 + \eta)\ (1 + \zeta)$$

$$N_{20} = 1/4\ (1 - \eta^2)\ (1 - \xi)\ (\ \ + \zeta)$$

leaky layer. As described in a previous section, the finite element method is to approximate the variable ϕ by the piecewise continuous function $\hat{\phi}$. If this could be done perfectly then equation (6.5) could be written in terms of $\hat{\phi}$ as

$$L\,(\hat{\phi}) = 0 \tag{6.6}$$

for every point in the flow domain. In reality, the best that can be done is to minimize the operation $L\,(\hat{\phi})$ in an average sense over every element by the Galerkin weighted residual method, so that

$$\int_V N_j\, L\,(\hat{\phi})\, dV = 0; \quad \text{for} \quad j = 1, 2, \ldots 20 \tag{6.7}$$

in which the weighting functions N_j are the same as the element shape functions. In expanded form this is

$$\int_V \left[K_{xx}\, N_j \frac{\partial^2\hat{\phi}}{\partial x^2} + K_{yy}\, N_j \frac{\partial^2\hat{\phi}}{\partial y^2} + K_{zz}\, N_j \frac{\partial^2\hat{\phi}}{\partial z^2} + N_j Q - N_j \frac{(\hat{\phi}-\phi_0)}{\beta^2}\right] dV = 0 \tag{6.8}$$

It should be recalled that the element shape functions listed in Table 6.1 were required to satisfy the condition that only the value of $\hat{\phi}$ need be continuous between elements. Since the continuity of the first derivative of $\hat{\phi}$ is not guaranteed the integral in equation (6.8), which contains second derivatives of $\hat{\phi}$, may not necessarily exist. For this reason the order of the derivaties in equation (6.8) must be reduced by one. This is done through the use of the divergence theorem and the product rule for derivatives which states that

$$\frac{\partial}{\partial x}\left(N_j \frac{\partial\hat{\phi}}{\partial x}\right) = \frac{\partial N_j}{\partial x}\frac{\partial\hat{\phi}}{\partial x} + N_j \frac{\partial^2\hat{\phi}}{\partial x^2} \tag{6.9}$$

Rearranging this and substituting into equation (6.8) results in

$$\int_V \left[K_{xx} \frac{\partial}{\partial x} \left(N_j \frac{\partial \hat{\phi}}{\partial x}\right) + K_{yy} \frac{\partial}{\partial y} \left(N_j \frac{\partial \hat{\phi}}{\partial y}\right) + K_{zz} \frac{\partial}{\partial z} \left(N_j \frac{\partial \hat{\phi}}{\partial z}\right)\right] dV$$

$$+ \int_V \left[N_j Q + (\hat{\phi} - \phi_0) N_j / \beta^2\right] dV$$

$$= \int_V \left[K_{xx} \frac{\partial N_j}{\partial x} \frac{\partial \hat{\phi}}{\partial x} + K_{yy} \frac{\partial N_j}{\partial y} \frac{\partial \hat{\phi}}{\partial y} + K_{zz} \frac{\partial N_j}{\partial z} \frac{\partial \hat{\phi}}{\partial z}\right] dV \qquad (6.10)$$

Noting that, by Darcy's law,

$$K_{xx} \frac{\partial}{\partial x} \left(N_j \frac{\partial \hat{\phi}}{\partial x}\right) = \frac{\partial}{\partial x} \left(N_j q_x\right) \qquad (6.11)$$

the first integral in equation (6.10) can be changed by the divergence theorem into

$$\int_S N_j \vec{q} \cdot \vec{n} \, dA$$

when $\vec{n}$ is the outward unit vector normal to the boundary, S.

Now consider the terms in the second integral of equation (6.10). The first term, containing Q, refers to the addition of fluid at the bounding surface of the flow domain. The second refers to fluid lost from the aquifer by leakage through the boundary in contact with the leaky layer. The second integral, then, can be changed to a surface integral because the integral is zero everywhere except on the surface of the flow region. Equation (6.10) then becomes

$$\int_V \left[K_{xx} \frac{\partial N_j}{\partial x} \frac{\partial \hat{\phi}}{\partial x} + K_{yy} \frac{\partial N_j}{\partial y} \frac{\partial \hat{\phi}}{\partial y} + K_{zz} \frac{\partial N_j}{\partial z} \frac{\partial \hat{\phi}}{\partial z}\right] dV$$

$$= \int_S \left[N_j \vec{q} \cdot \vec{n} + N_j Q - (\hat{\phi} - \phi_0) N_j / \beta^2\right] dA \qquad (6.12)$$

It was shown in the previous section that the approximated piezometric head, $\hat{\phi}$, is defined over each element in terms of the element shape functions and the nodal unknowns by equation (6.3). Applying this definition to equation (6.12) gives the finite element formulation of the governing equation for an element

$$\Phi_i \int_V \left(K_{xx} \frac{\partial N_i}{\partial x} \frac{\partial N_j}{\partial x} + K_{yy} \frac{\partial N_i}{\partial y} \frac{\partial N_j}{\partial y} + K_{zz} \frac{\partial N_i}{\partial z} \frac{\partial N_j}{\partial z} \right) dV$$

$$+ \Phi_i \int_S N_i N_j / \beta^2 \, dA = \int_S \left(N_j \vec{q} \cdot \vec{n} + N_j Q + N_j \phi_0 / \beta^2 \right) dA \qquad (6.13)$$

for

$$i = 1, 2, \ldots 20$$

$$j = 1, 2, \ldots 20$$

In matrix form this can be written as

$$[k] \{\Phi\} = \{f\} \qquad (6.14)$$

where [k] is a 20 x 20 matrix known as the element stiffness matrix, {f}, is a column matrix of forcing functions given by the right hand side of equation (6.13), and {Φ} is the matrix of nodal unknowns, Φ_1, Φ_2, . . . Φ_{20}.

In accordance with the fundamental concept of the finite element method, a similar equation can be written for the entire flow domain by a proper summation of matrix equations for the individual elements. This results in

$$[K] \{\Phi\} = \{F\} \qquad (6.15)$$

in which [K] is the global stiffness matrix, {F} is the global matrix of forcing functions, and {Φ} is the matrix of unknown values of piezometric head at all nodes. These matrices are obtained from the element matrices by standard methods of assembly which can be found in any finite element textbook.

Development of the Element Matrices

The terms of the element stiffness matrix are given by the integrals on the left hand side of equation (6.13) in which the element shape functions are prominent. The evaluation of these integrals is complicated by the fact that the element shape functions are defined in the local element coordinate system while the governing equation refers to the global x, y, z system. The transformation of coordinate systems is accomplished by use of the Jacobian matrix, [J], defined as

$$[J] = \begin{bmatrix} \frac{\partial x}{\partial \xi} & \frac{\partial y}{\partial \xi} & \frac{\partial z}{\partial \xi} \\ \frac{\partial x}{\partial \eta} & \frac{\partial y}{\partial \eta} & \frac{\partial z}{\partial \eta} \\ \frac{\partial x}{\partial \zeta} & \frac{\partial y}{\partial \zeta} & \frac{\partial z}{\partial \zeta} \end{bmatrix} \tag{6.16}$$

The terms in this matrix depend on the geometry of the element in such a way that

$$\frac{\partial x}{\partial \xi} = \sum_{i=1}^{20} \frac{\partial N_i}{\partial \xi} X_i \tag{6.17}$$

so that the Jacobian matrix for an element becomes

$$[J] = \begin{bmatrix} \sum_{i=1}^{20} \frac{\partial N_i}{\partial \xi} X_i & \sum_{i=1}^{20} \frac{\partial N_i}{\partial \xi} Y_i & \sum_{i=1}^{20} \frac{\partial N_i}{\partial \xi} Z_i \\ \sum_{i=1}^{20} \frac{\partial N_i}{\partial \eta} X_i & \sum_{i=1}^{20} \frac{\partial N_i}{\partial \eta} Y_i & \sum_{i=1}^{20} \frac{\partial N_i}{\partial \eta} Z_i \\ \sum_{i=1}^{20} \frac{\partial N_i}{\partial \zeta} X_i & \sum_{i=1}^{20} \frac{\partial N_i}{\partial \zeta} Y_i & \sum_{i=1}^{20} \frac{\partial N_i}{\partial \zeta} Z_i \end{bmatrix} \tag{6.18}$$

It should be remarked here that the representation of the relationship between the two coordinate systems given by equation (6.17) is not the only possible one. If the boundaries of the element were restricted to planar surfaces only, there would be no need to use the coordinates of all twenty nodes in the description of element shape. Only the corner nodes would be essential because they give enough information for the location of planar boundaries. In such a case the element would be called subparametric because the degree of the equations defining the element shape is less than the degree of the interpolation polynomials. The relationship given by equation (6.17) permits the element boundaries to be curved surfaces described by quadratic equations. Since these equations are of the same degree as the interpolation polynomials this is called an isoparametric element.

The Jacobian matrix is used in two ways in the evaluation of the first integral of equation (6.13). First, the integrand calls for the evaluation of partial derivatives of the shape functions with respect to the x, y, z coordinate system. This can be accomplished by noting from the chain rule for derivatives that

$$\frac{\partial N_i}{\partial \xi} = \frac{\partial N_i}{\partial x}\frac{\partial x}{\partial \xi} + \frac{\partial N_i}{\partial y}\frac{\partial y}{\partial \xi} + \frac{\partial N_i}{\partial z}\frac{\partial z}{\partial \xi} \tag{6.19}$$

and that $\partial x/\partial \xi$, $\partial y/\partial \xi$, and $\partial z/\partial \xi$ are terms of the Jacobian matrix. Consequently, we have

$$\begin{bmatrix} \frac{\partial N_i}{\partial \xi} \\ \frac{\partial N_i}{\partial \eta} \\ \frac{\partial N_i}{\partial \zeta} \end{bmatrix} = [J] \begin{bmatrix} \frac{\partial N_i}{\partial x} \\ \frac{\partial N_i}{\partial y} \\ \frac{\partial N_i}{\partial z} \end{bmatrix} \tag{6.20}$$

and

$$\begin{bmatrix} \frac{\partial N_i}{\partial x} \\ \frac{\partial N_i}{\partial y} \\ \frac{\partial N_i}{\partial z} \end{bmatrix} = [J]^{-1} \begin{bmatrix} \frac{\partial N_i}{\partial \xi} \\ \frac{\partial N_i}{\partial \eta} \\ \frac{\partial N_i}{\partial \zeta} \end{bmatrix} \tag{6.21}$$

The expression for the partial derivatives with respect to the local coordinate system are given in Table 6.2.

The second use of the Jacobian concerns the evaluation of the volume integral itself. The integral will be evaluated in terms of the element's local coordinate system, in which the values of each coordinate vary between + 1 and - 1. In order to give the integral the correct volume the change of scale included in the coordinate transformation must be accounted for. This is done by multiplying the integrand by the absolute value of the determinant of the Jacobian matrix, $|\det J|$.

TABLE 6.2

PARTIAL DERIVATIVES OF THE SHAPE FUNCTIONS

$$\partial N_1/\partial\xi = 1/8\ (1 - \eta)\ (1 - \zeta)\ (2\xi + \eta + \zeta + 1)$$

$$\partial N_2/\partial\xi = 1/8\ (1 - \eta)\ (1 - \zeta)\ (2\xi - \eta - \zeta - 1)$$

$$\partial N_3/\partial\xi = 1/8\ (1 + \eta)\ (1 - \zeta)\ (2\xi + \eta - \zeta - 1)$$

$$\partial N_4/\partial\xi = 1/8\ (1 + \eta)\ (1 - \zeta)\ (2\xi - \eta + \zeta + 1)$$

$$\partial N_5/\partial\xi = 1/8\ (1 - \eta)\ (1 + \zeta)\ (2\xi + \eta - \zeta + 1)$$

$$\partial N_6/\partial\xi = 1/8\ (1 - \eta)\ (1 + \zeta)\ (2\xi - \eta + \zeta - 1)$$

$$\partial N_7/\partial\xi = 1/8\ (1 + \eta)\ (1 + \zeta)\ (2\xi + \eta + \zeta - 1)$$

$$\partial N_8/\partial\xi = 1/8\ (1 + \eta)\ (1 + \zeta)\ (2\xi - \eta - \zeta + 1)$$

$$\partial N_9/\partial\xi = -\ 1/2\xi\ (1 - \eta)\ (1 - \zeta)$$

$$\partial N_{10}/\partial\xi = 1/4\ (1 - \eta^2)\ (1 - \zeta)$$

$$\partial N_{11}/\partial\xi = -\ 1/2\xi\ (1 + \zeta)\ (1 - \zeta)$$

$$\partial N_{12}/\partial\xi = -\ \partial N_{10}/\partial\xi$$

$$\partial N_{13}/\partial\xi = -\ 1/4\ (1 - \zeta^2)\ (1 - \eta)$$

$$\partial N_{14}/\partial\xi = \partial N_{13}/\partial\xi$$

$$\partial N_{15}/\partial\xi = 1/4\ (1 - \zeta^2)\ (1 + \eta)$$

$$\partial N_{16}/\partial\xi = \partial N_{15}/\partial\xi$$

$$\partial N_{17}/\partial\xi = -\ 1/2\xi\ (1 - \eta)\ (1 + \eta)$$

$$\partial N_{18}/\partial\xi = 1/4\ (1 - \eta^2)\ (1 + \zeta)$$

$$\partial N_{19}/\partial\xi = -\ 1/2\xi\ (1 + \eta)\ (1 + \zeta)$$

$$\partial N_{20}/\partial\xi = -\ \partial N_{18}/\partial\xi$$

TABLE 6.2 - continued

$$\partial N_1/\partial \eta = 1/8\ (1 - \xi)\ (1 - \zeta)\ (2\eta + \xi + \zeta + 1)$$

$$\partial N_2/\partial \eta = 1/8\ (1 + \xi)\ (1 - \zeta)\ (2\eta - \xi + \zeta + 1)$$

$$\partial N_3/\partial \eta = 1/8\ (1 + \xi)\ (1 - \zeta)\ (2\eta + \xi - \zeta - 1)$$

$$\partial N_4/\partial \eta = 1/8\ (1 - \xi)\ (1 - \zeta)\ (2\eta - \xi - \zeta - 1)$$

$$\partial N_5/\partial \eta = 1/8\ (1 - \xi)\ (1 + \zeta)\ (2\eta + \xi - \zeta + 1)$$

$$\partial N_6/\partial \eta = 1/8\ (1 + \xi)\ (1 + \zeta)\ (2\eta - \xi - \zeta + 1)$$

$$\partial N_7/\partial \eta = 1/8\ (1 + \xi)\ (1 + \zeta)\ (2\eta + \xi + \zeta - 1)$$

$$\partial N_8/\partial \eta = 1/8\ (1 - \zeta)\ (1 + \zeta)\ (2\eta - \xi + \zeta - 1)$$

$$\partial N_9/\partial \eta = -\ 1/4\ (1 - \xi^2)\ (1 - \zeta)$$

$$\partial N_{10}/\partial \eta = -\ 1/2\eta\ (1 + \xi)\ (1 - \zeta)$$

$$\partial N_{11}/\partial \eta = -\ \partial N_9/\partial \eta$$

$$\partial N_{12}/\partial \eta = -\ 1/2\eta\ (1 - \xi)\ (1 - \zeta)$$

$$\partial N_{13}/\partial \xi = -\ 1/4\ (1 - \zeta^2)\ (1 - \xi)$$

$$\partial N_{14}/\partial \eta = -\ 1/4\ (1 - \zeta^2)\ (1 + \xi)$$

$$\partial N_{15}/\partial \eta = -\ \partial N_{14}/\partial \eta$$

$$\partial N_{16}/\partial \eta = -\ \partial N_{13}/\partial \eta$$

$$\partial N_{17}/\partial \eta = -\ 1/4\ (1 - \xi^2)\ (1 + \zeta)$$

$$\partial N_{18}/\partial \eta = -\ 1/2\eta\ (1 + \xi)\ (1 + \zeta)$$

$$\partial N_{19}/\partial \eta = -\ \partial N_{17}/\partial \eta$$

$$\partial N_{20}/\partial \eta = -\ 1/2\eta\ (1 - \xi)\ (1 + \zeta)$$

TABLE 6.2 - continued

$$\partial N_1/\partial\zeta = 1/8\ (1 - \xi)\ (1 - \eta)\ (2\zeta + \xi + \eta + 1)$$

$$\partial N_2/\partial\zeta = 1/8\ (1 + \xi)\ (1 - \eta)\ (2\zeta - \xi + \eta + 1)$$

$$\partial N_3/\partial\zeta = 1/8\ (1 + \xi)\ (1 + \eta)\ (2\zeta - \xi - \eta + 1)$$

$$\partial N_4/\partial\zeta = 1/8\ (1 - \xi)\ (1 + \eta)\ (2\zeta + \xi - \eta + 1)$$

$$\partial N_5/\partial\zeta = 1/8\ (1 - \xi)\ (1 - \eta)\ (2\zeta - \xi - \eta - 1)$$

$$\partial N_6/\partial\zeta = 1/8\ (1 + \xi)\ (1 - \eta)\ (2\zeta + \xi - \eta - 1)$$

$$\partial N_7/\partial\zeta = 1/8\ (1 + \xi)\ (1 + \eta)\ (2\zeta + \xi + \eta - 1)$$

$$\partial N_8/\partial\zeta = 1/8\ (1 - \xi)\ (1 + \eta)\ (2\zeta - \xi + \eta - 1)$$

$$\partial N_9/\partial\zeta = -\ 1/4\ (1 - \eta^2)\ (1 - \xi)$$

$$\partial N_{10}/\partial\zeta = -\ 1/4\ (1 - \eta^2)\ (1 + \xi)$$

$$\partial N_{11}/\partial\zeta = -\ 1/4\ (1 - \xi^2)\ (1 + \eta)$$

$$\partial N_{12}/\partial\zeta = -\ 1/4\ (1 - \eta^2)\ (1 - \xi)$$

$$\partial N_{13}/\partial\zeta = -\ 1/2\ (1 - \xi)\ (1 - \eta)$$

$$\partial N_{14}/\partial\zeta = -\ 1/2\ (1 + \xi)\ (1 - \eta)$$

$$\partial N_{15}/\partial\zeta = -\ 1/2\ (1 + \xi)\ (1 + \eta)$$

$$\partial N_{16}/\partial\zeta = -\ 1/2\ (1 - \xi)\ (1 + \eta)$$

$$\partial N_{17}/\partial\zeta = -\ \partial N_9/\partial\zeta$$

$$\partial N_{18}/\partial\zeta = -\ \partial N_{10}/\partial\zeta$$

$$\partial N_{19}/\partial\zeta = -\ \partial N_{11}/\partial\zeta$$

$$\partial N_{20}/\partial\zeta = -\ \partial N_{12}/\partial\zeta$$

For those elements that do not have leaky boundaries the terms of the element stiffness matrix, k_{ij}, are given by

$$k_{ij} = \int_{-1}^{1}\int_{-1}^{1}\int_{-1}^{1} \left[K_{xx} \frac{\partial N_i}{\partial x} \frac{\partial N_j}{\partial x} + K_{yy} \frac{\partial N_i}{\partial y} \frac{\partial N_j}{\partial y} + k_{zz} \frac{\partial N_i}{\partial z} \frac{\partial N_j}{\partial z}\right] |\det J| \, d\zeta \, d\eta \, d\xi \qquad (6.22)$$

for

$$i = 1, 2, \ldots 20$$

$$j = 1, 2, \ldots 20$$

where the partial derivatives are obtained from equation (6.21) and Table 6.2.

Since the functions in the integrand of equation (6.22) depend on the geometry of the element, the integral must be evaluated numerically. Since the shape functions appearing in the integrand are quadratic in ξ, η, and ζ the integral can be evaluated exactly by Gaussian quadrature, using the eight sample points shown in Figure 6.4 with a weighting factor of 1.0 for each point. Equation (6.22) then becomes

$$k_{ij} = \sum_{n=1}^{8} g(\xi_n, \eta_n, \zeta_n) \qquad (6.23)$$

where

g = the integrand of equation (6.22)

ξ_n, η_n, ζ_n = the coordinates of the n^{th} sample point

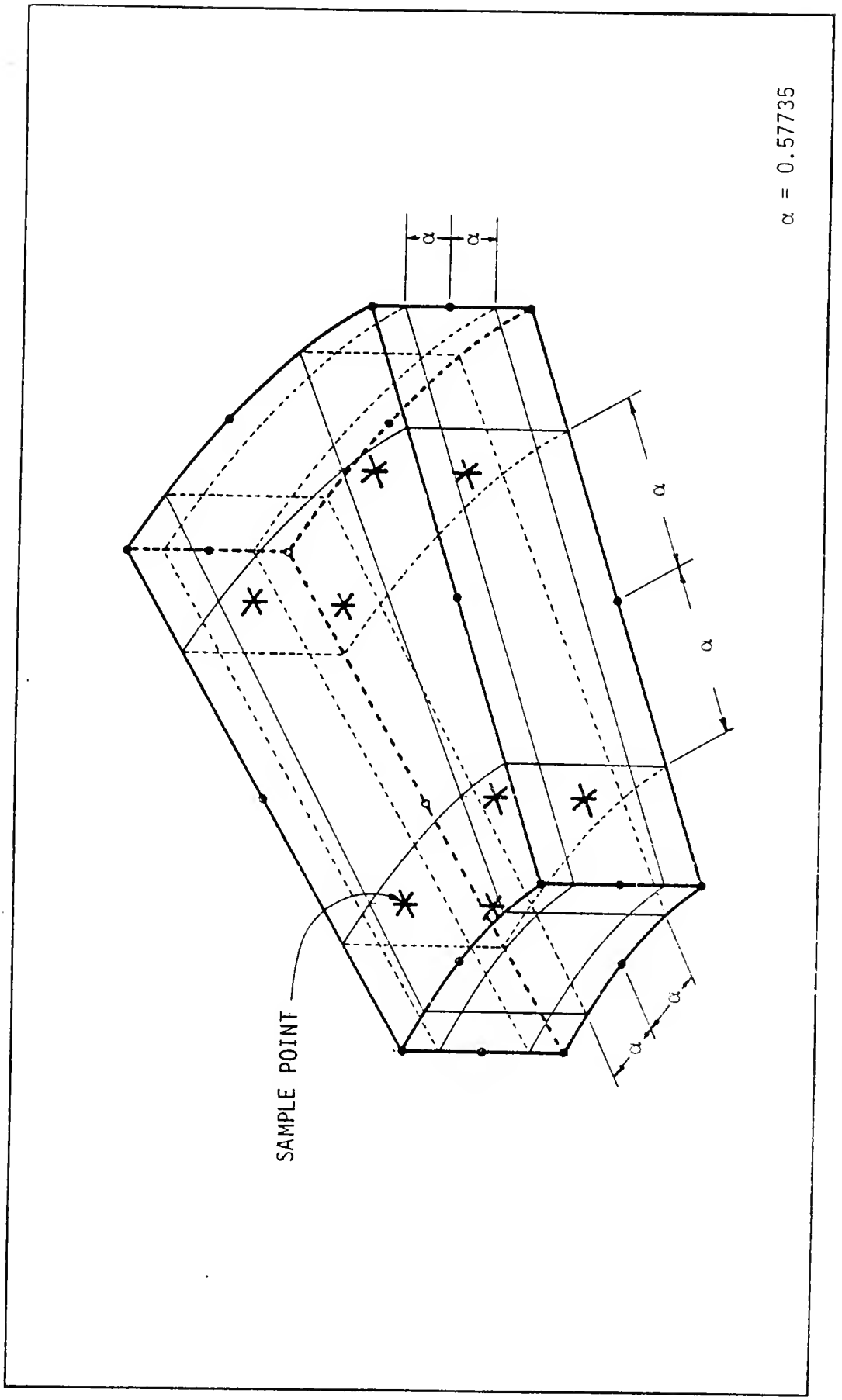

FIGURE 6.4. SAMPLE POINTS FOR GAUSSIAN QUADRATURE OF EQUATION (6.23)

If the element contains a leaky boundary the terms of the element stiffness matrix will also have contributions from the second integral in equation (6.13). This is a surface integral and, since leakage only occurs through surfaces in contact with the leaky layer, it is only integrated over the top side of the element. If the nodes of all elements are numbered consistantly as shown in Figure 6.1 then the only shape functions contributing to the surface integral are those associated with nodes 5, 6, 7, 8, 17, 18, 19, and 20. The others are all zero on this surface. The integral then becomes

$$\int_S N_i N_j/\beta^2 \, dA = \int_{-1}^{1} \int_{-1}^{1} N_i N_j/\beta^2 |\det J| \, d\eta \, d\xi \qquad (6.24)$$

for

$$i = 5, 6 \ldots 8, 17, 18 \ldots 20$$
$$j = 5, 6 \ldots 8, 17, 18 \ldots 20$$

Gaussian quatrature for this surface integral requires the nine sample points shown in Figure 6.5 and their respective weighting factors. The surface integral is evaluated numerically by

$$\int_{-1}^{1} \int_{-1}^{1} N_i N_j/\beta^2 |\det J| \, d\eta \, d\xi = \sum_{n=1}^{9} W_n \, g(\xi_n, \eta_n) \qquad (6.25)$$

where

g = the integrand of the integral on the left hand side

ξ_n, η_n = the coordinates of the n^{th} sample point

W_n = the weighting factor for the n^{th} sample point

The element stiffness matrix for a leaky element is obtained by adding

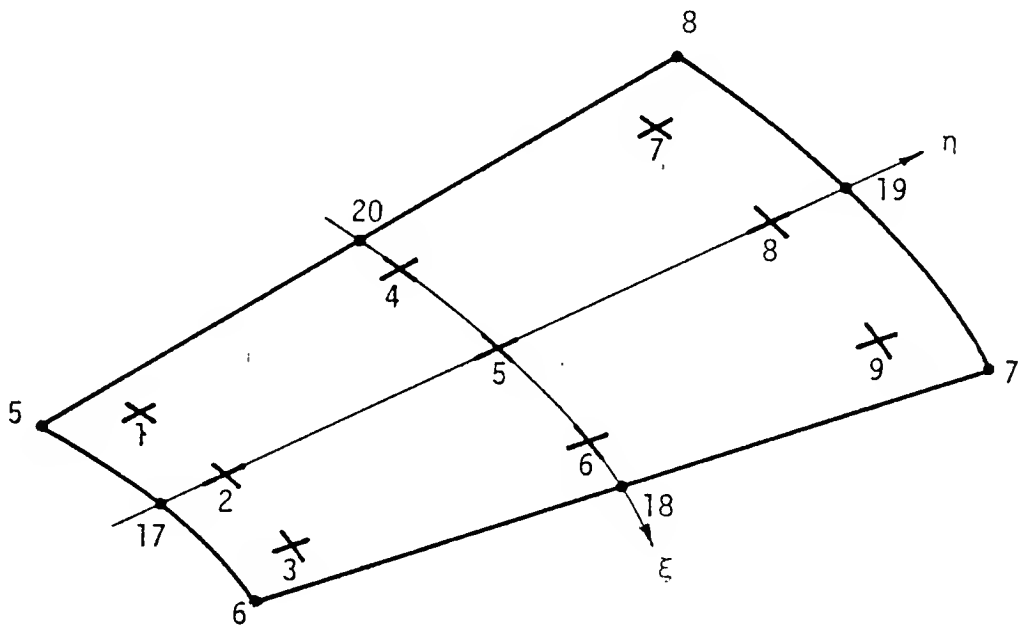

Sample Point	ξ	η	Weight Factor W_n
1	$-\alpha$	$-\alpha$	25/81
2	0	$-\alpha$	40/81
3	α	$-\alpha$	25/81
4	$-\alpha$	0	40/81
5	0	0	64/81
6	α	0	40/81
7	$-\alpha$	α	25/81
8	0	α	40/81
9	α	α	25/81

$\alpha = 0.7746$

FIGURE 6.5. SAMPLE POINTS AND WEIGHT FACTORS FOR GAUSSIAN QUADRATURE OF EQUATION (6.25)

the terms from equation (6.25) to those given by equation (6.23).

The terms of the element forcing matrix are given by the right hand side of equation (6.13). Since the first two terms in the surface integral deal with flow through the external boundaries of the flow domain they can be lumped together and treated as one. These, in effect, describe the boundary conditions of the problem. It will be assumed that the only impressed flow on the boundary of the flow domain will be due to the presence of a well. The domain can be subdivided in such a way that the only element surfaces in contact with the well are those which contain nodes 1, 2, 5, 6, 9, 13, 14, and 17. If the restriction is placed on this surface that it is always rectangular then the integral of the flow from the well over this surface can be evaluated once and for all to give the distribution of this flow among the nodes concerned. The terms of the element forcing matrix due to well flow, then, are given by

$$f_j = Q \int_{-1}^{1} \int_{-1}^{1} N_j \, |\det J| \, d\zeta \, d\xi \qquad (6.26)$$

where Q is the flow into the element and is assumed to be evenly distributed across the surface. This integral is evaluated numerically using the four sample points and the weighting functions shown in Figure 6.6. The results of this integration are that the inflow Q should be distributed among the eight nodes as follows

$$f_1 = f_2 = f_5 = f_6 = -Q/12 \qquad (6.27a)$$

$$f_9 = f_{13} = f_{14} = f_{17} = Q/3 \qquad (6.27b)$$

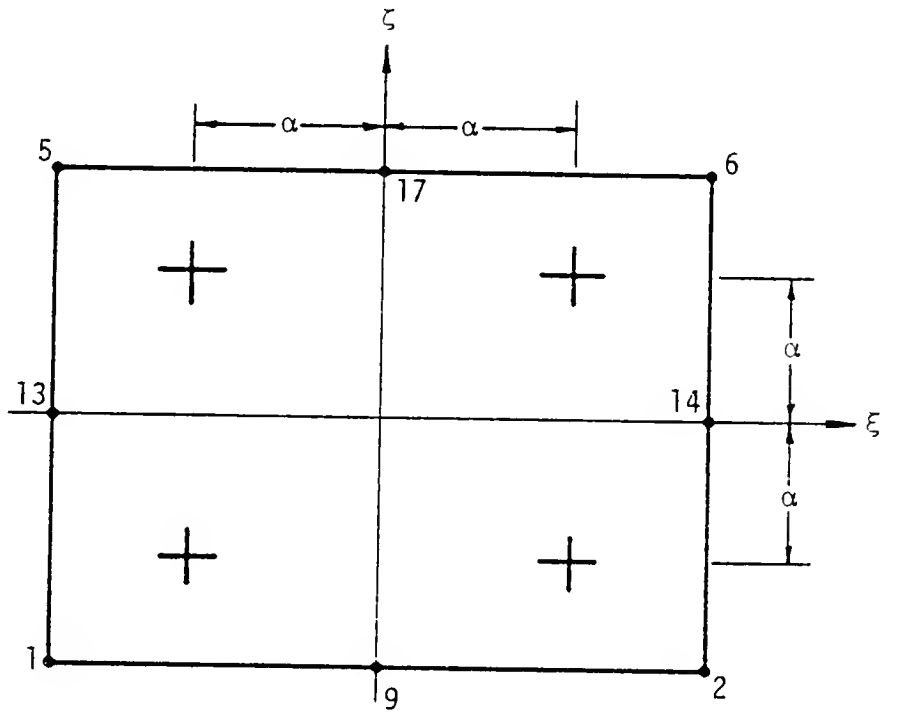

FIGURE 6.6. SAMPLE POINTS FOR GAUSSIAN QUADRATURE OF EQUATION (6.25)
α = 0.57735; WEIGHT FACTOR = 1

This somewhat surprising result is due to the fact that a non-linear interpolation function is being used.

The last term in the integral on the right hand side of equation (6.13) is part of the leakage term in the governing equation. It is integrated over the top surface of the leaky elements in much the same way as for the leakage terms in the element stiffness matrix except that only four sampling points are used.

Computer Implementation

The previous section showed how the individual terms of the element matrices are computed. For each element this results in a 20 x 20 element stiffness matrix, [k], and a 1 x 20 forcing matris, {f}. After these element matrices are obtained they must be inserted into the correct locations in the corresponding global matrices. If n is the number of nodal points which have been used to subdivide the flow domain, then the global matrices consist of an n x n stiffness matrix, [K], a 1 x n forcing matrix, {F}, and a 1 x n matrix of nodal unknowns, $\{\Phi\}$. These matrices, when arranged in the form of equation (6.15) represent a system of n algebraic equations in n unknowns which can be solved by any of several methods. In choosing a method of solution it is useful to observe that many of the terms the stiffness matrix, [K], are zero. In fact, if the flow domain has been subdivided into elements in a propitious manner, all of the non-zero terms will lie in a relatively narrow band centered on the diagonal of the matrix. If the method of Gaussian elimination is used to solve these equations the terms of the stiffness matrix which lie outside this band need not be dealt with at all. This makes the solution of the system of equations by Gaussian

elimination much more efficient than solution by inversion of the entire matrix. This advantage becomes even more pronounced when use is made of the symmetric nature of this matrix. This means that the actual bandwidth to be used consists only of the diagonal terms and the terms on one side of the diagonal within the non-zero strip. The bandwidth can be minimized by subdividing the region and numbering the nodes in such a way that the difference between the largest and smallest node numbers in any element is as small as possible. For elements with four nodes or less computer programs are available which automatically number the nodes to give minimum bandwidth (Collins, 1973). When the elements contain 20 nodes, however, bandwidth minimization is left to the ingenuity of the programmer.

Program Verification

In order to demonstrate the validity of the finite element model, a groundwater flow problem for which an analytical solution is available was chosen for comparison. This is the problem of axisymmetric flow from an injection well in a bounded leaky aquifer, which was described in Chapter 5. The solution is given in terms of modified Bessel functions by equation (5.38). If the position of the aquifer boundary is r_e and the push up, s, at that point is zero then equation (5.38) becomes

$$s = \frac{Q}{2\pi Kb}\left[K_0\,(r/B) - \frac{K_0(r_e/B)}{I_0(r_e/B)}\;I_0\,(r/B)\right] \qquad (6.28)$$

which is the solution given by Jacob (1946).

The analysis which led to equation (6.28) differs from the finite element model in that it is one dimensional in radial coordinates while

the model is three dimensional in Cartesian coordinates. However, when the value of the leakage coefficient, B, is large the flow is, in fact, nearly radial and the two solutions should coincide. As B gets smaller, the one dimensional solution becomes less valid and this comparison will show the limits of its accuracy.

The shape of the flow domain is shown in Figure 6.7. It is divided into seven elements with 92 nodes. Since the flow is axisymmetric, the sides and bottom of the wedge are boundaries across which there is no flow. Leakage is permitted across the top surface of the wedge and there is a specified flow rate into the narrow end from the well. There is an unspecified amount of flow through the outer end of the wedge where the drawdown is maintained at s = 0. The injection rate into the well is 0.1 m^3/s and since the flow is axisymmetric the wedge receives 1/12 of this, or 0.00833 m^3/s. Since the thickness of the aquifer is b = 10 m and the hydraulic conductivity is K = 0.001 m/s the one dimensional and three dimensional leakage coefficients are related by

$$B = \sqrt{Kb}\ \beta = 0.1\beta \tag{6.29}$$

The solutions for push up, s, given by the two methods for several values of the leakage coefficient, B, are shown in Figure 6.8. For B values of 60 m and greater the two solutions are indistinguishable at this scale. For the smaller values of B, the leakage rate is higher and the one dimensional solution gives lower values than the computer model. In these cases of high leakage rate, the vertical flow components are large enough to make the pressure distribution deviate noticeably from the hydrostatic. The solutions plotted for these cases are based on the piezometric head at mid depth in the aquifer.

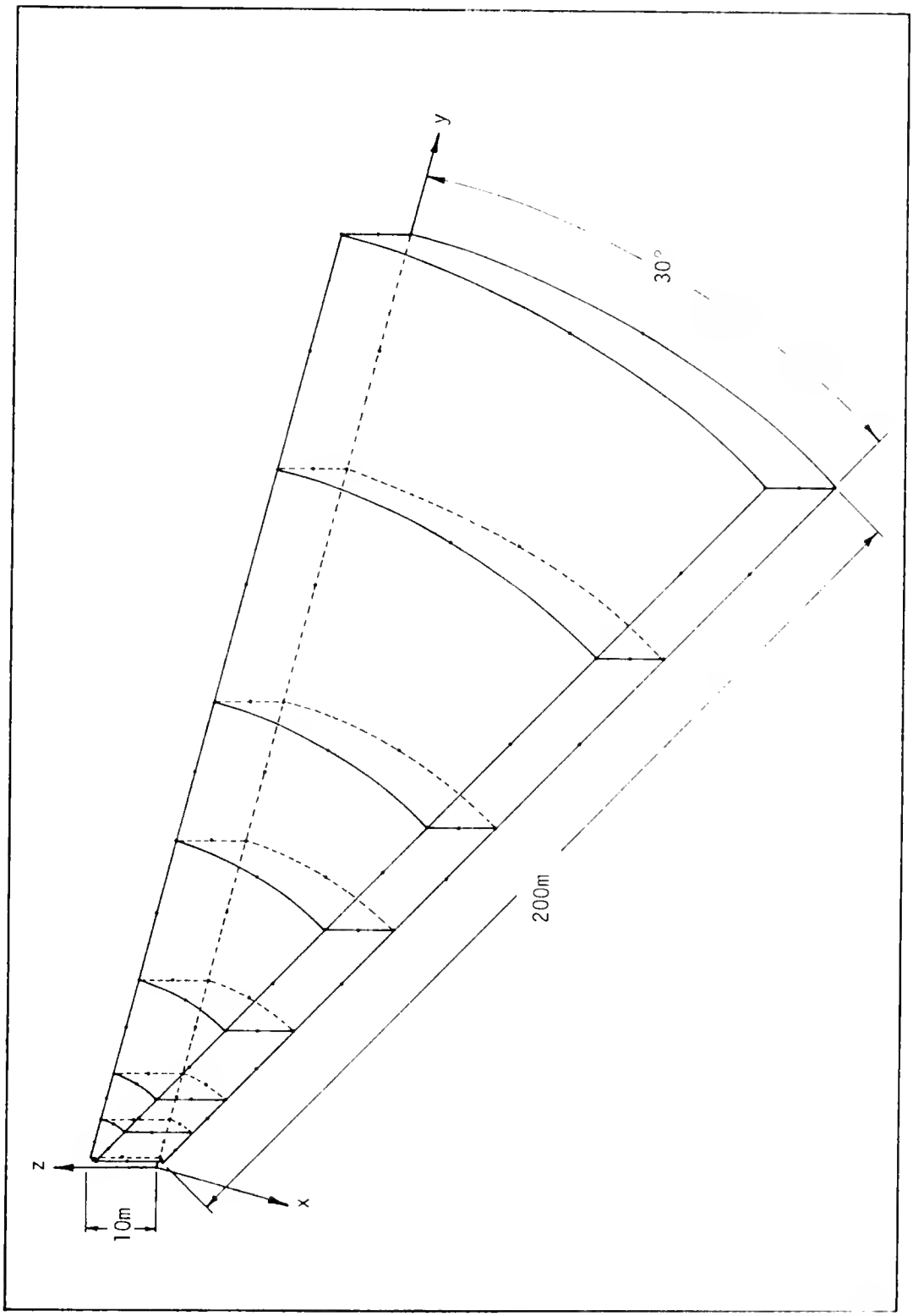

FIGURE 6.7. DIVISION OF FLOW DOMAIN INTO FINITE ELEMENTS

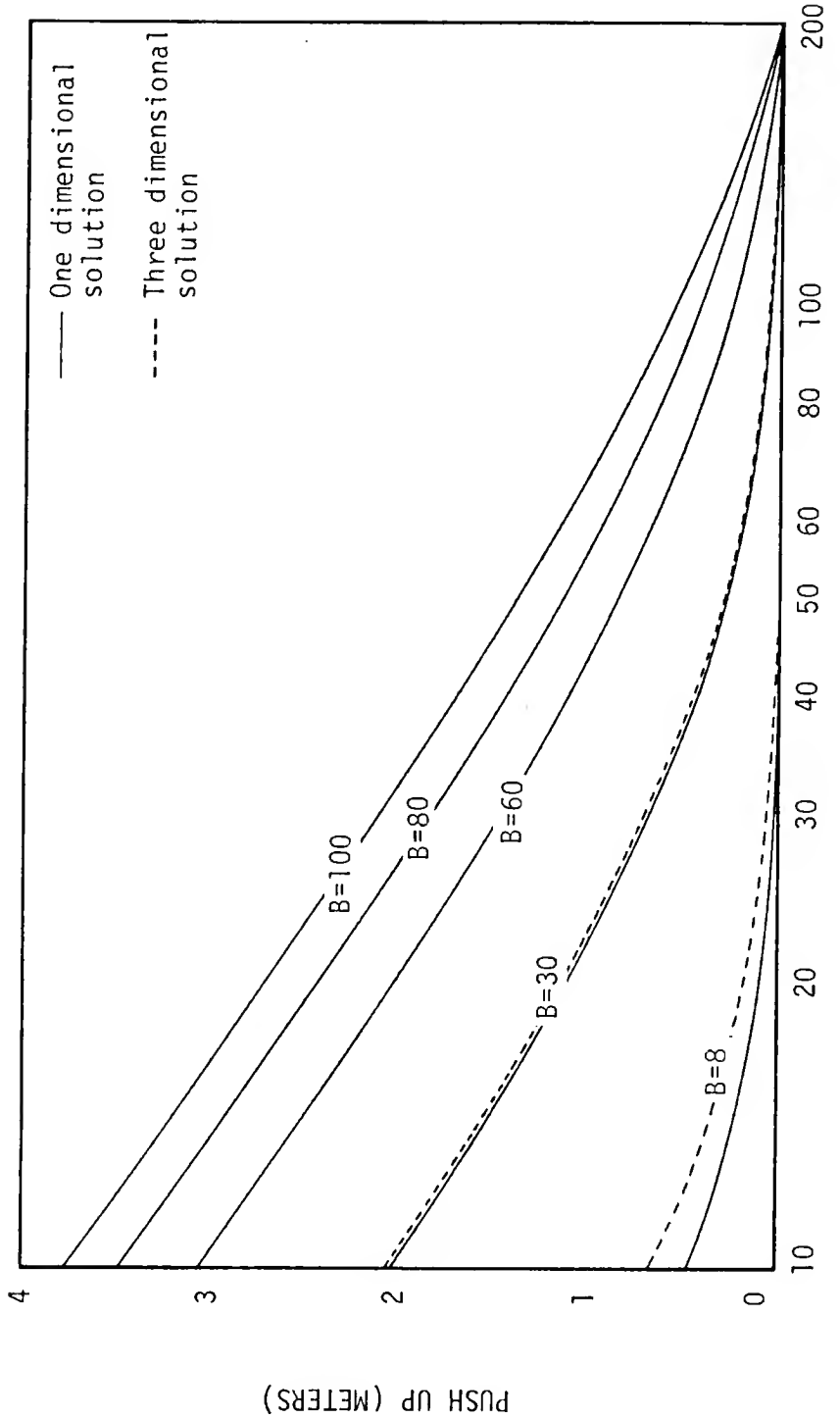

FIGURE 6.8. COMPARISON OF SOLUTIONS FOR FLOW FROM AN INJECTION WELL IN A BOUNDED LEAKY AQUIFER (CONSTANT HEAD BOUNDARY, s=0 AT r=200m)

Freshwater Lens in a Leaky Saline Aquifer

The logical extension of the injection well problem in a bounded aquifer is to check the solution given in Chapter 5 for an axisymmetric freshwater lens in a leaky aquifer. This can be done with the finite element model by successive repositioning of the interface and resolving of the boundary value problem until the interface boundary condition is satisfied.

As before, a 30° segment of the flow domain was modeled. The shape of this segment is shown in Figure 6.9. Repositioning of the interface is accomplished in two ways. First, the nodes are moved radially to increase or decrease the size of the lens. This is done by comparing pressure computed for the node at the toe of the interface with the pressure that would be required to satisfy the interface boundary condition. If the computed pressure is too high, then the distance to the toe, r_t, is increased. Since the radii of all of the other nodes are computed in proportion to r_t this increases the size of the entire lens. If the computed pressure is too low, r_t is reduced.

The second adjustment of the interface position is done by changing the elevation of all of the interfacial nodes except for the nodes on the interface toe. The revised elevation of each of these nodes is obtained from equation (3.17) based on the head computed for the node during the previous trial.

It was found that the application of both of these adjustments for each trial resulted in instability unless the initial guess of interface position was very good. However, when the two methods of adjustment were alternated, the scheme converged to the correct position in a fairly regular manner. This is not to say that convergence was always rapid.

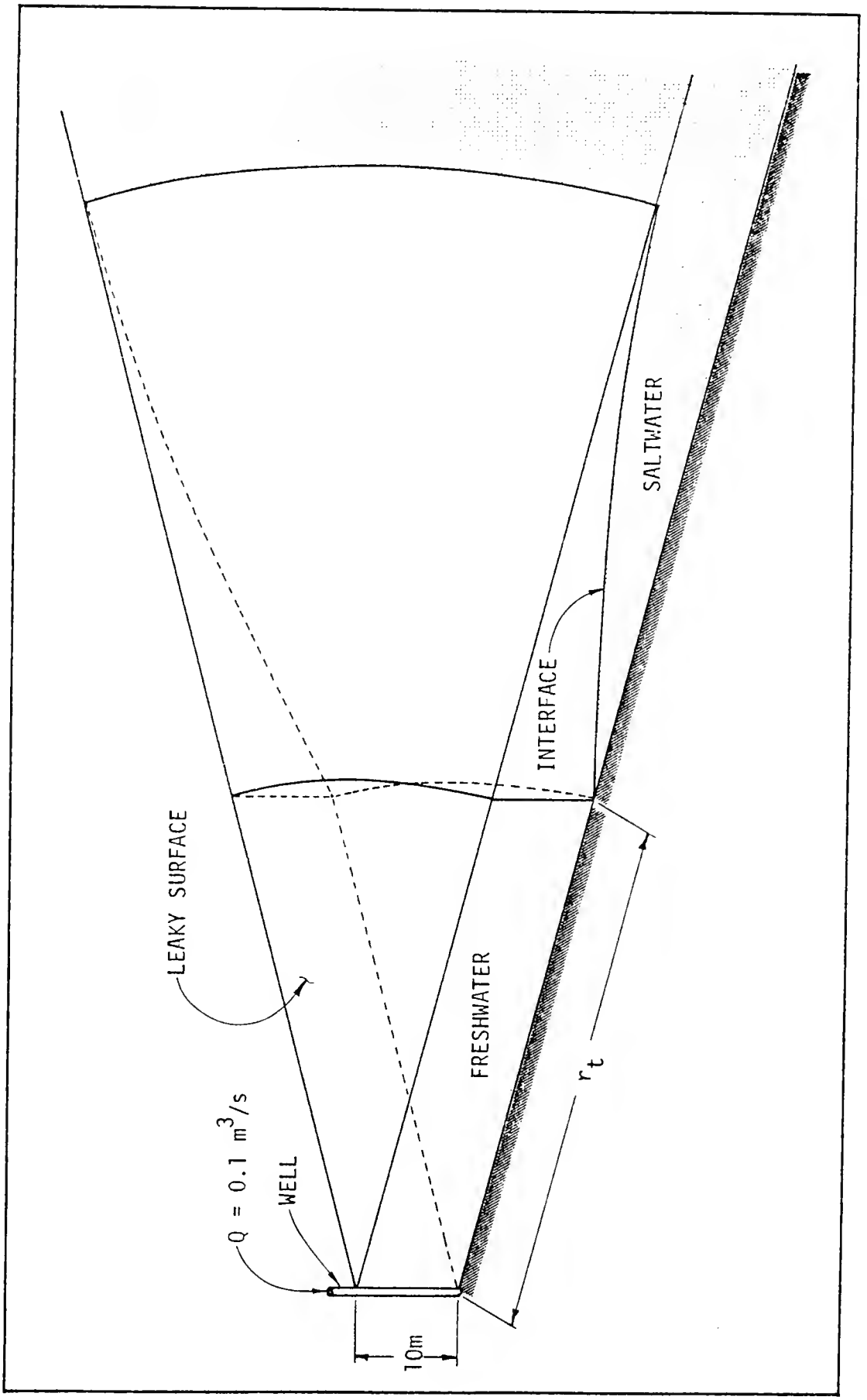

FIGURE 6.9. FLOW DOMAIN FOR NUMERICAL LOCATION OF THE INTERFACE IN A LEAKY AQUIFER

Often 15 to 20 iterations were required before a stable interface position could be reached. Actually, a very good initial guess of interface position could have been made using the method of Chapter 5. However, since the purpose of this analysis was to verify the accuracy of the two methods it was thought more advisable to arrive at the answer by totally independent means.

Figures 6.10 and 6.11 show the comparison of interface locations arrived at by the two methods under two different cases of injection rate and leakage coefficient.

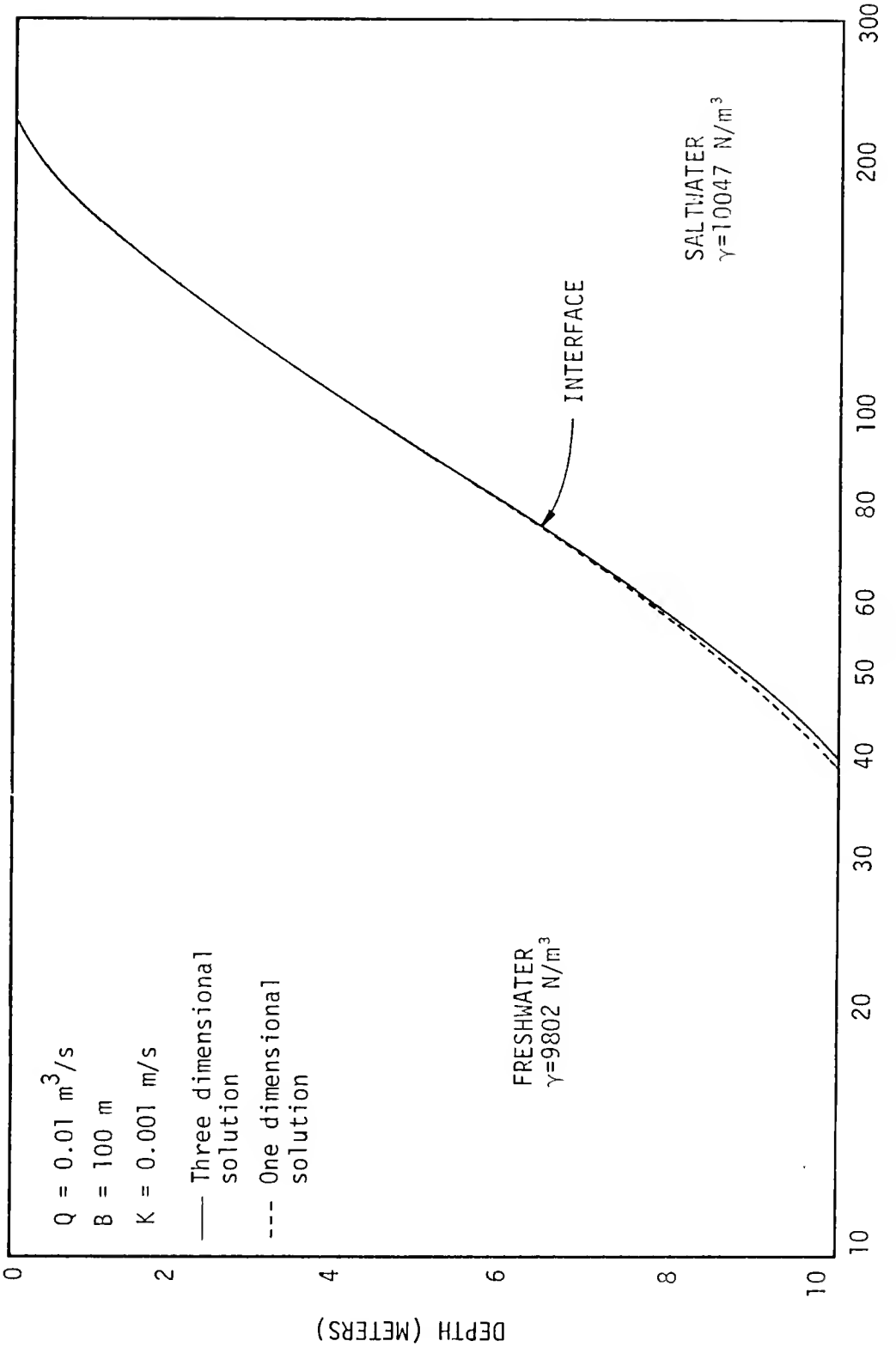

FIGURE 6.10. COMPARISON OF SOLUTIONS FOR A STEADY LENS IN A LEAKY AQUIFER

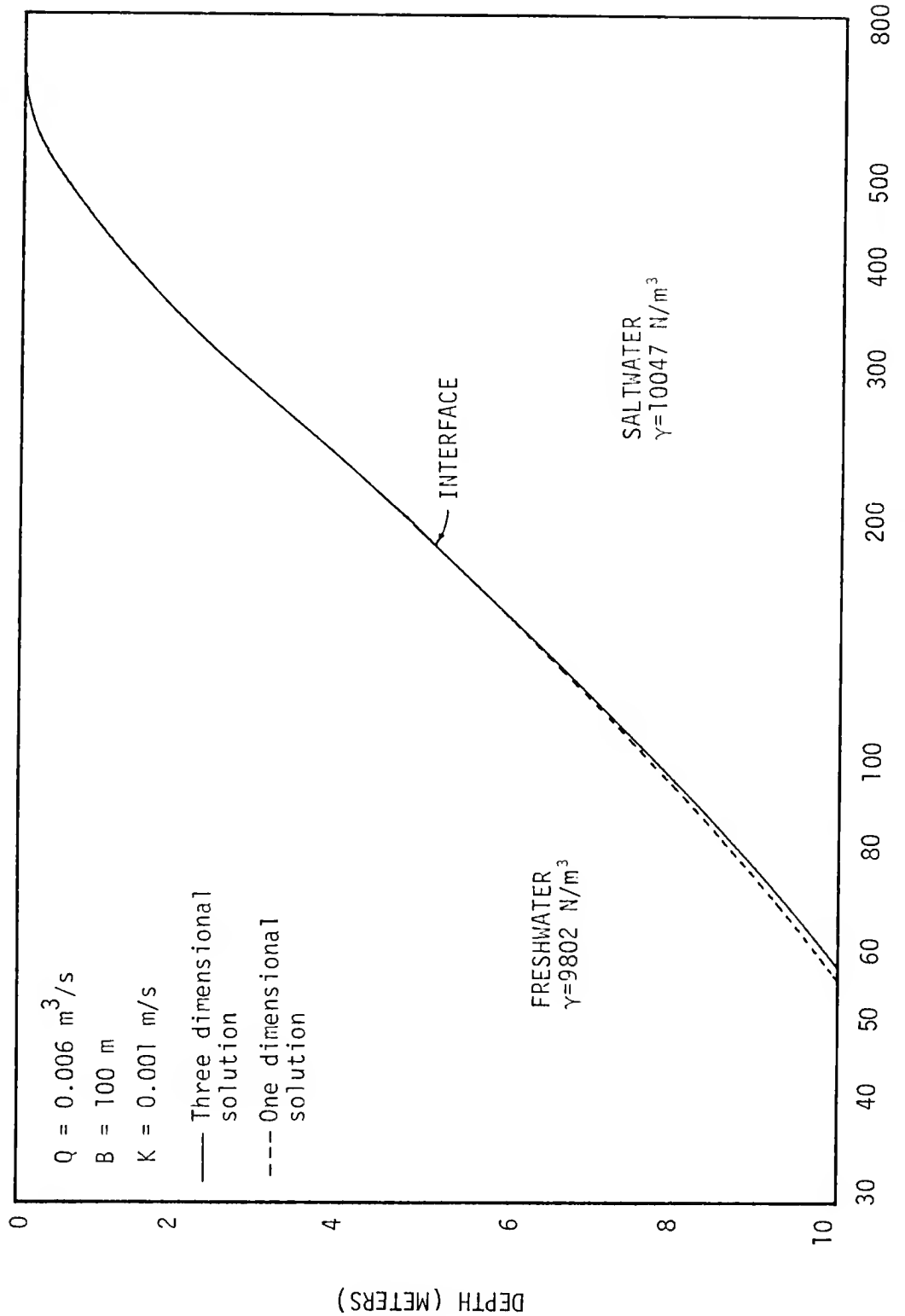

FIGURE 6.11. COMPARISON OF SOLUTIONS FOR A STEADY LENS IN A LEAKY AQUIFER

CHAPTER 7

NUMERICAL SIMULATION OF LENS GROWTH

General

Chapters 5 and 6 of this report have been concerned with locating the boundaries of freshwater lenses under steady flow conditions. The boundary between freshwater and saltwater was easily definable in such cases because there was no flow component normal to it and, consequently, no longitudinal dispersion. The plan of attack, then, was to treat the freshwater lens as a distinct flow domain separated from the resident saltwater by an interface. In the present chapter the problem of unsteady flow will be considered. Here there is a large component of flow normal to the outer boundary of the lens and longitudinal dispersion becomes significant. Since no interface can be distinguished to separate the injected fluid from the resident fluid, it is necessary to treat this as a single flow domain containing a non-homogeneous fluid.

The two equations which describe the movement of the freshwater lens are the governing equation for groundwater flow, given in Chapter 3 as equation (3.8), and the convective dispersion equation, given as equation (3.13). If the injected freshwater behaved as a tracer-like substance, the application of these equations would be relatively straightforward. Problems involving the dispersion of tracers have been solved both analytically and numerically by Hoopes and Harleman (1967), Ogata and Banks (1961) and others. The injected freshwater, however, differs from the resident saltwater in density and, to a lesser

degree, in viscosity. Consequently, the changes in fluid composition predicted by the dispersion equation have a direct influence on the parameters in the flow equation. In order to make these influences explicit, it is convenient to write the flow equation in terms of density, viscosity and pressure as

$$\nabla \cdot \frac{\rho k}{\mu} (\nabla P - \rho g \nabla z) = \frac{\partial (n\rho)}{\partial t} \tag{7.1}$$

This differs from equation (3.8) in that hydraulic conductivity is expressed in terms of intrinsic permeability and the fluid properties, piezometric head is expressed in terms of pressure and elevation, and the change in the mass of stored fluid is expressed directly.

The convective dispersion equation is expanded in a similar fashion as

$$\frac{\partial}{\partial t} (n\rho c) - \nabla \cdot \left[\rho c \frac{k}{\mu} (\nabla P - \rho g \nabla z)\right] = \nabla \cdot (\rho D) \cdot \nabla c \tag{7.2}$$

These two equations are coupled through the dependence of density and viscosity on the saltwater concentration as illustrated in the section on fluid properties in Chapter 3. This set of coupled equations, together with the constituative relations for fluid properties, must be solved numerically. It happens that a computer program is already available (INTERCOMP, 1976) which can applied to this problem. The three dimensional solutions for transient lens flow obtained with this numerical model are valuable in themselves as well as in providing a check on existing two dimensional solutions.

Description of the INTERCOMP Model

The INTERCOMP model was developed for the U.S. Geological Survey by INTERCOMP Resource Development and Engineering, Inc., of Houston,

Texas. It is a three-dimensional finite difference model which was designed to predict the effects of liquid waste disposal by deep well injection into saline aquifers. It is a model of very general applicability to flow in confined aquifers under a wide variety of boundary conditions. Basically, it consists of a numerical solution to equations (7.1) and (7.2) together with the equation of energy transport by convection and conduction. Since the influence of temperature is being neglected in this report, only that part of the computer program which deals with equations (7.1) and (7.2) will be used.

The difficulties involved in applying finite difference approximations to equation (7.2) have been well documented (von Neumann and Richtmyer, 1950; Stone and Brian, 1963). Basically, the problem is that if the finite difference approximation to either the time derivative or the convective spatial derivative is correct only to the first order, then the resulting second order truncation error has the same form as the dispersive term of the equation. This error is called numerical dispersion and its magnitude can be such that it masks the actual physical dispersion being modeled. If a second order correct differencing scheme is used, the truncation error no longer has the same form as the dispersive term but a restriction must be imposed on the time and distance steps used in order to ensure the stability of the solution. The actual form of this restriction depends on the differencing scheme being used.

The INTERCOMP model provides users with a choice of differencing schemes. For the computational runs mentioned in this report, the time derivatives were represented by the Crank-Nicholson approximation and

the spatial derivatives by the central difference approximation. Since both of these differencing methods are correct to the second order, their application results in no numerical dispersion. However, to ensure stability, the time and distance steps should be chosen to satisfy the following requirement:

$$\frac{q_x \, \Delta t}{2n \, \Delta x} \leq 1.0 \qquad (7.3)$$

Good results can often be obtained even if this criterion is exceeded, but they are not ensured.

The Crank-Nicholson differencing method is an implicit one because it makes use of unknown values of the dependent variable. This results in large system of simultaneous algebraic equations which must be solved at each time step. The model can solve these equations either by reduced bandwidth Gaussian elimination or by successive overrelaxation. In this report, the latter method was used.

The INTERCOMP model has the capability to solve either three dimensional problems in cartesian coordinates or axisymmetric problems in cylindrical coordinates. Since the problems to be solved here deal with flow from a single well, the cylindrical coordinate system is used.

For axisymmetric flow in a confined aquifer the boundary conditions consist of no-flow boundaries at the top and bottom of the aquifer, a prescribed rate of inflow at the well, and a constant head boundary at infinity. The boundary condition at infinity is simulated by calculating the rate of efflux from the peripheral grid blocks based on the rate of change of pressure, the compressibility of the fluid and porous medium, and the total pore volume of the modeled portion of the aquifer.

More sophisticated methods for simulating infinite aquifers are available (Carter and Tracy, 1960), but since pressure distribution is of more interest than absolute pressure in the analysis of freshwater lenses, this was considered sufficient.

Input data for this model includes specification of the grid size, time step, and method of solution as well as the properties of the porous medium, resident fluid, and injected fluid. The finite difference grid used in the various computer runs is shown in Figure 7.1. The grid points shown in this figure are computational nodes which represent the center of the grid blocks into which the flow region is divided. The pressure and concentration at each of these points is computed at every time step. The modeled region is subdivided into 10 horizontal strips of equal Δz and 25 vertical strips grouped in three zones of equal $\Delta ln(r)$. The time step used with this grid was $t = 0.1$ day.

A series of simulations using different injection rates and aquifer configurations was run in order to show the effects of the different flow parameters on the shape of the freshwater lens. Those properties of the aquifer and the resident and injected fluids which were not varied are listed in Table 7.1.

Application of the numerical model results in a list of the pressures and concentrations for all of the grid points at selected time steps. In these results pure freshwater is assigned a concentration of one, and undiluted saltwater a concentration of zero. From the model's viewpoint, the only difference between these two fluids is their density.

Model Verification

The accuracy of the INTERCOMP model, when used for its intended purpose, was verified for several test cases by its developers

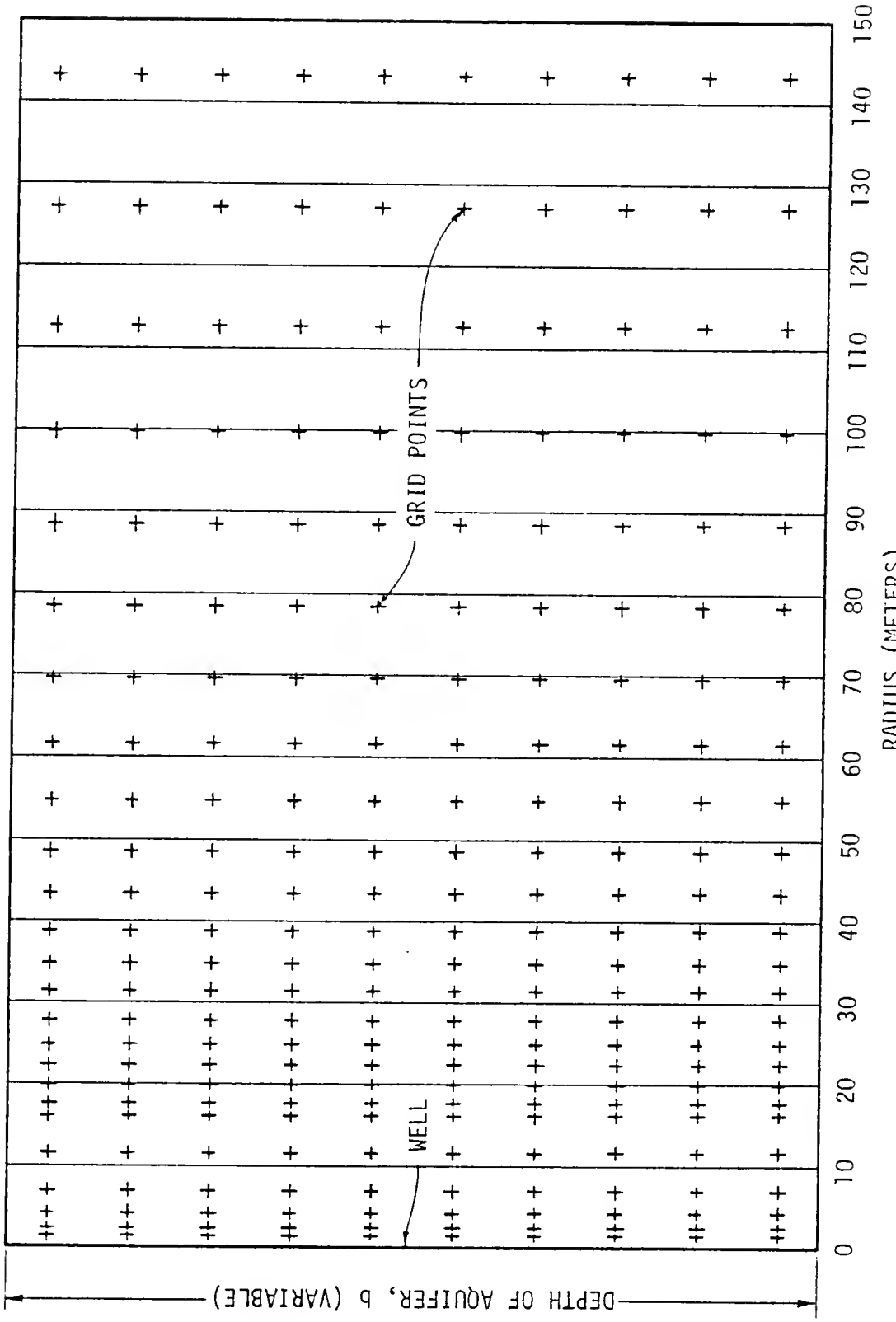

FIGURE 7.1. FINITE DIFFERENCE GRID USED WITH THE INTERCOMP MODEL

TABLE 7.1

FLUID AND AQUIFER PROPERTIES USED WITH THE INTERCOMP MODEL

Property	Value in English Units	Value in SI Units
Water Compressibility, α	3.3×10^{-6}/psi	4.725×10^{-10}/Pa
Aquifer Compressibility, β	1.0×10^{-7}/psi	1.45×10^{-11}/Pa
Porosity, n	0.2	0.2
Specific Storage, S_s	1.439×10^{-6}/ft	4.72×10^{-6}/m
Freshwater Unit Weight, γ_f	62.31 lb/ft^3	9788 N/m^3
Saltwater Unit Weight, γ_s	63.87 lb/ft^3	10033 N/m^3
Freshwater viscosity, μ_f	2.25×10^{-5} lb·s/ft^2	1.0773 cp
Saltwater viscosity, μ_s	2.25×10^{-5} lb·s/ft^2	1.0773 cp
Molecular Diffusivity, D_m	1.0×10^{-3} ft^2/day	1.075×10^{-9} m^2/s
Longitudinal Dispersivity, α_ℓ	20.0 ft	6.1 m
Transverse Dispersivity, α_t	4.0 ft	1.22 m

(INTERCOMP, 1976). It was also tested by Papadopulos and Larson (1978) against field data for a heated water storage well (Molz et al.) which it matched satisfactorily. In order to verify the model with the grid shown in Figure 7.1 and the input data of Table 7.1, a test case was used in which the density of the injected water was the same as that of the resident saltwater. Thus the problem was reduced to the case of constant injection of a tracer-like substance for which approximate analytical solutions are available. The approximate solution given by Hoopes and Harleman (1965) for injection of a tracer with concentration c = 1 into an aquifer with initial concentration c = 0 everywhere is

$$c = 1/2 \text{ erfc } \left[\frac{r'/2 - t'}{\sqrt{4/3\ r'^3}}\right] \tag{7.4}$$

where

$$r' = r/\alpha_\ell$$

$$t' = \frac{tQ}{2\pi bn\alpha_\ell^2}$$

α_ℓ = longitudinal dispersivity

erfc = the complimentary error function

t = time since the start of injection

A comparison of the concentration profile predicted by equation (7.4) with that predicted by the INTERCOMP model for the same flow conditions is shown in Figure 7.2. It should be mentioned that equation (7.4) is only an approximate solution because it was obtained by setting the initial rate of change of concentration, $\partial c/\partial t$, equal to zero at the

well, which was represented as a line source. Because of this, it predicts the presence of a finite amount of tracer in the aquifer at time t = 0. This initial error remains constant in the approximate solution as time progresses and results in the predicted edge of the tracer cloud being farther from the well than it should be. The exact solution to the problem was given by Ogata (1958) but, unfortunately, it contains an integral which cannot be explicitly evaluated. Hoopes and Harleman evaluated Ogata's solution numerically for a few specific cases and compared it to their approximate solution. The results they obtained in this way look identical to the comparison shown in Figure 7.2.

Lens Formation in Aquifers With Weak Vertical Flow

The experimental results presented in Chapter 4 indicated that the thickness of the saline aquifer may have a significant influence on the shape of the freshwater lens. Consequently, the initial simulations were done with a relatively thin aquifer in which vertical flow components would have little chance to develop. It was expected that under these conditions the formation of the freshwater lens would proceed as predicted by previous investigators who neglected vertical flow components entirely (Kimbler, Kazman and Whitehead, 1975). Figure 7.3 shows the results of numerical simulation of a freshwater lens in a 10-meter thick aquifer after 40 days of injection. The left border of the figure can be taken as the location of the well. The mixing zone is represented as that part of the flow region between the 90% and 10% concentration lines, although the selection of these concentrations was arbitrary. The 50% concentration line can be considered to represent the position of an imaginary interface which would exist if there were no dispersion. Note that the lines of equal concentration are straight

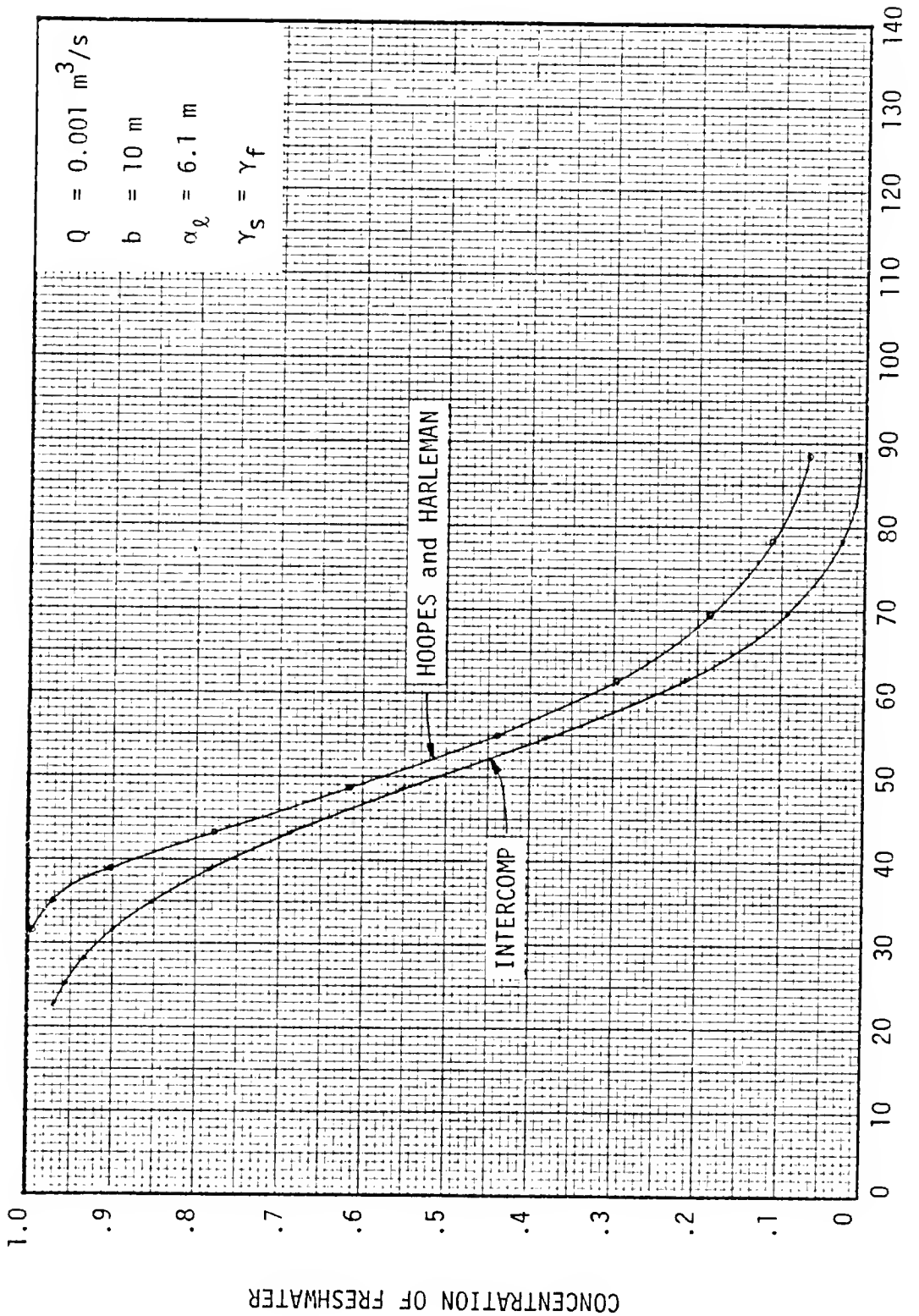

FIGURE 7.2. COMPARISON OF THE CONCENTRATION DISTRIBUTIONS PREDICTED BY THE INTERCOMP MODEL AND THE APPROXIMATE SOLUTION OF HOOPES AND HARLEMAN

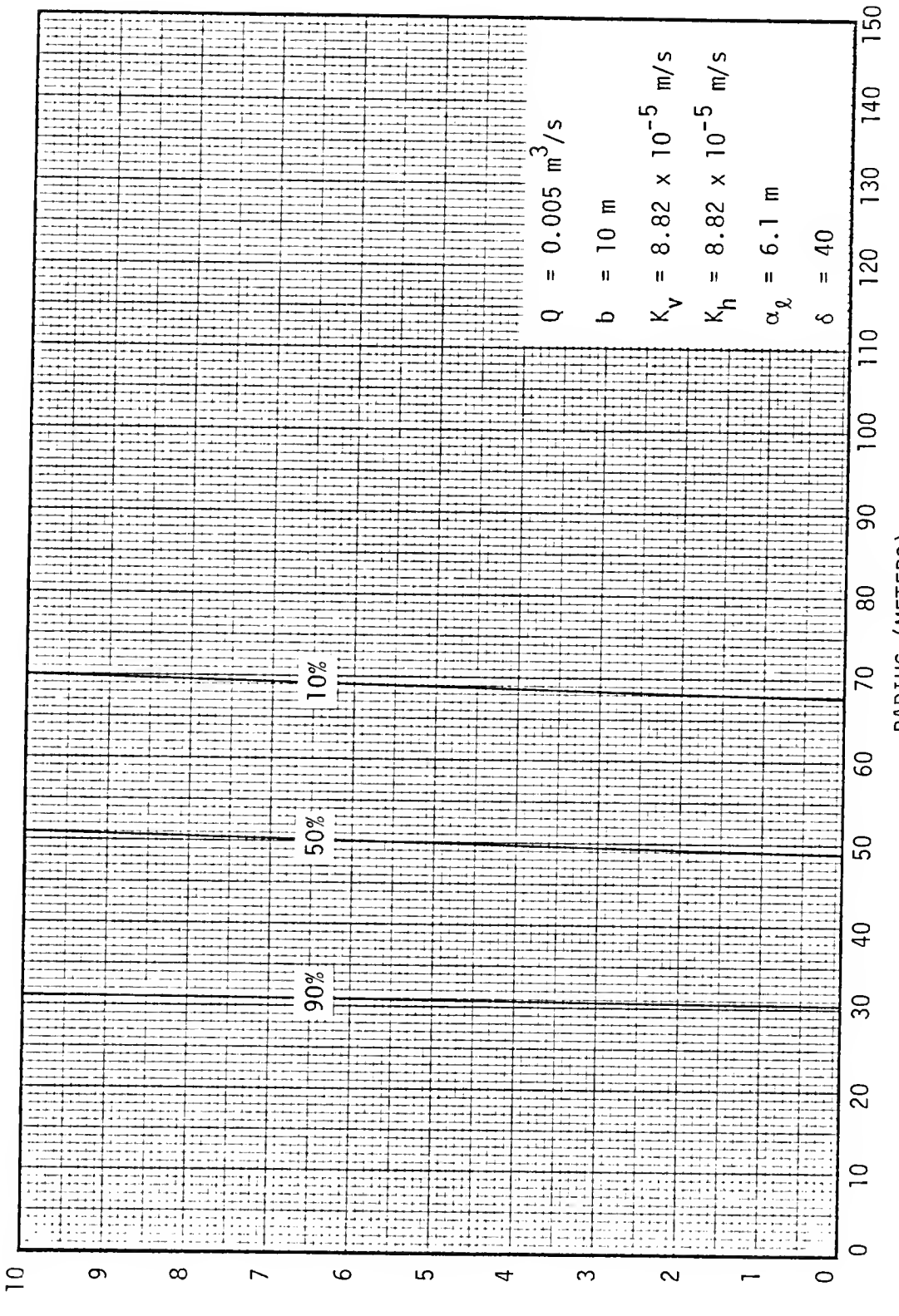

FIGURE 7.3. LINES OF CONSTANT CONCENTRATION AFTER 40 DAYS OF INJECTION

and that after 40 days of injection their departure from the vertical is still very slight. In this case, the amount of freshwater which could be recovered from the lens is limited primarily by dispersion.

The thinness of the saline aquifer suppresses gravity segregation of the fluids in two ways. First, the pressure differential caused by the difference in fluid density is very small in a thin aquifer compared to the pressure gradients created by the injection well. Second, the opportunity for vertical flow components to develop is limited by the small vertical dimensions of the aquifer. If the aquifer were to be made thicker and the vertical hydraulic conductivity were reduced, then only the second of these suppressing influences would be in effect. This was done in the numerical simulation illustrated by Figure 7.4. The aquifer in this case was 50 meters thick but the vertical hydraulic conductivity was reduced by an order of magnitude. The injection rate was also increased so that the horizontal velocities would be similar to those in the previous run. In this case, the lines of equal concentration are slightly curved but their rate of rotation toward the horizontal is not significantly greater.

Lens Formation in Aquifers With Strong Vertical Flow

It would be interesting, now, to see the effect of the vertical flow components on the formation of a lens in a thick aquifer in which they are not suppressed. Figure 7.5 shows the results of a simulation which was identical to the previous one in every way except that the vertical hydraulic conductivity was made equal to the horizontal. The difference between this figure and Figure 7.4 indicates that the vertical flow components in a thick aquifer can be quite strong. Their effect is to increase the rate of gravitational segregation and to make the

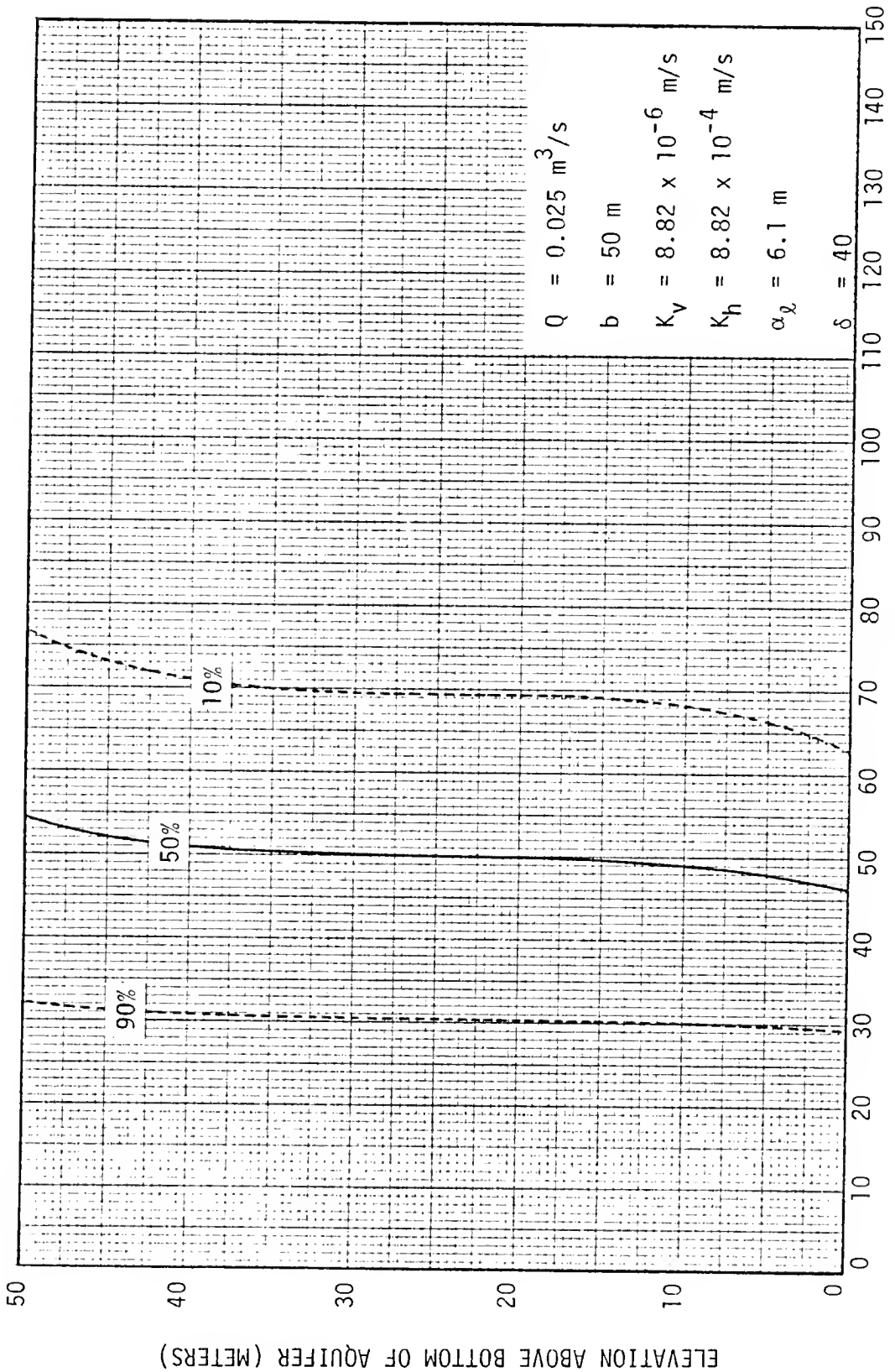

FIGURE 7.4. LINES OF CONSTANT CONCENTRATION AFTER 40 DAYS OF INJECTION

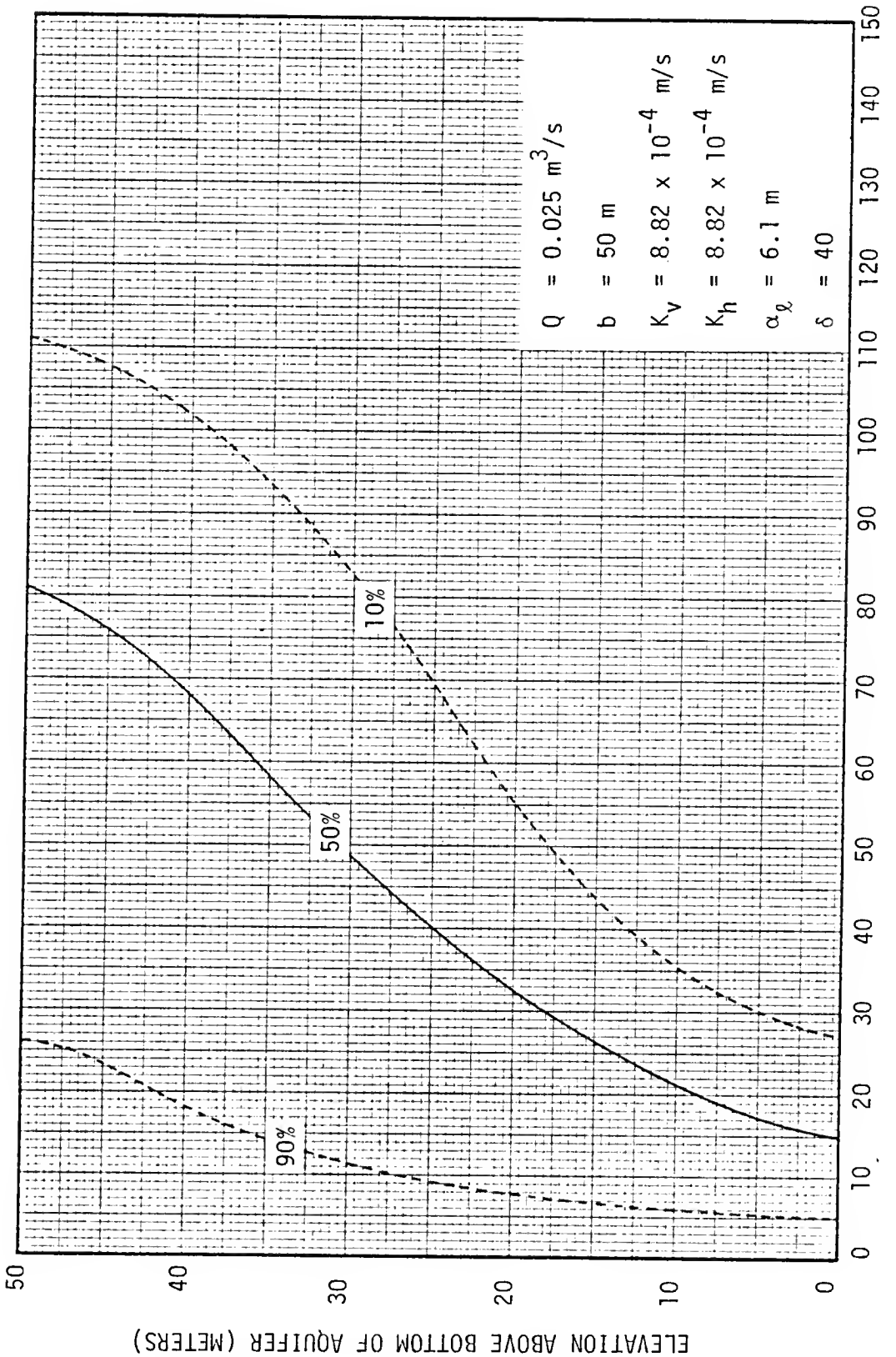

FIGURE 7.5. LINES OF CONSTANT CONCENTRATION AFTER 40 DAYS OF INJECTION

mixing zone much wider at the top than at the bottom. The reason for this latter phenomenon is revealed in Figure 7.6 which illustrates the movement of the 50% concentration line during the 40 days of injection. The lower part of this lens remained almost stationary after the 10th day. Evidently, the flow in this region was primarily tangential to the equal concentration lines so that only lateral dispersion was active. The longitudinal dispersion associated with the growth of the lens was limited to its upper part. From the viewpoint of freshwater storage, the conditions illustrated in Figure 7.6 are even worse than they appear. Because of the cylindrical geometry of the lens, the volume of water stored is proportional to the square of the lens radius. The greater part of the injected freshwater is stored beyond the toe of the lens and cannot be recovered undiluted by pumping from the well.

Dimensionless Representation of Lens Growth

It is evident from the numerical simulations that storage of freshwater in lenses is much more effective in thin saline aquifers than in thick ones. Since the concept of thickness is relative, it is convenient to present the numerical results in a dimensionless form which provides a basis for comparing one aquifer to another. This is done by defining a dimensionless time, t', an average radius $\bar{r}$, and an aquifer coefficient, λ, as

$$t' = Qt/b^3 \tag{7.5a}$$

$$\bar{r} = \left[\frac{Qt}{\pi bn}\right]^{1/2} \tag{7.5b}$$

$$\lambda = b^2K/Q \tag{7.5c}$$

The results of a series of numerical simulations are presented in terms

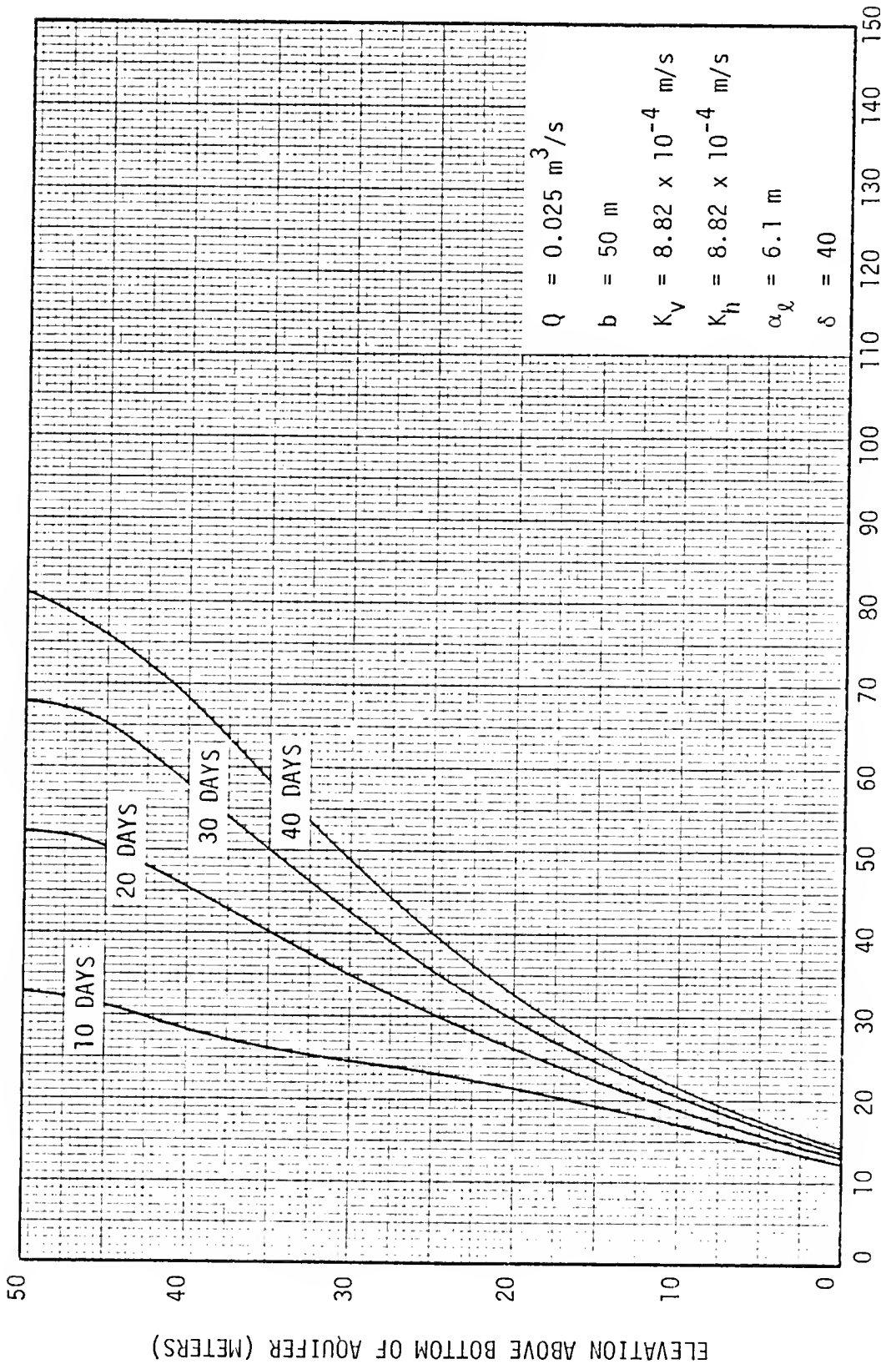

FIGURE 7.6. MOVEMENT OF THE 50% CONCENTRATION LINE WITH CONTINUOUS INJECTION

of these variables in Figure 7.7. The absissa of this chart gives values of $r_t/\bar{r}$, where r_t is the radius of the toe of the 50% concentration line and $\bar{r}$, as given by equation (7.5b), would be the radius of this line if there were no gravitational segregation.

Figure 7.7 indicates that aquifers with small values of λ are more favorable to the storage of freshwater. The applicability of this figure for predictive purposes, however, is limited to homogeneous and isotropic aquifers with a longitudinal dispersivity of 6.1 meters and a Ghyben-Herzberg ratio of $\delta = 40$.

The Influence of Dispersion on Lens Shape

Previous investigators have found that the rate of gravitational segregation of fluids of different density is retarded by dispersion across the interface between them (Gardner, Downie and Wyllie, 1962; Esmail and Kimbler, 1967). This effect was included in Whitehead's analysis of freshwater lenses in thin aquifers (Whitehead, 1974). Figure 7.8 shows a comparison of two freshwater lenses after 30 days of injection under conditions that were identical except for the dispersivity of the porous medium. The difference in the amount of dispersion has an obvious effect on the shape of the lens. The rate of rotation of the equal concentration lines toward the horizontal is reduced by doubling the dispersivity. For very extensive and thin lenses and long term storage this could have a significant effect on the recovery efficiency. For the case shown, however, the reduction in gravity segregation was balanced by an increase in the width of the mixing zone so that the amount of freshwater which could be recovered was not greatly changed.

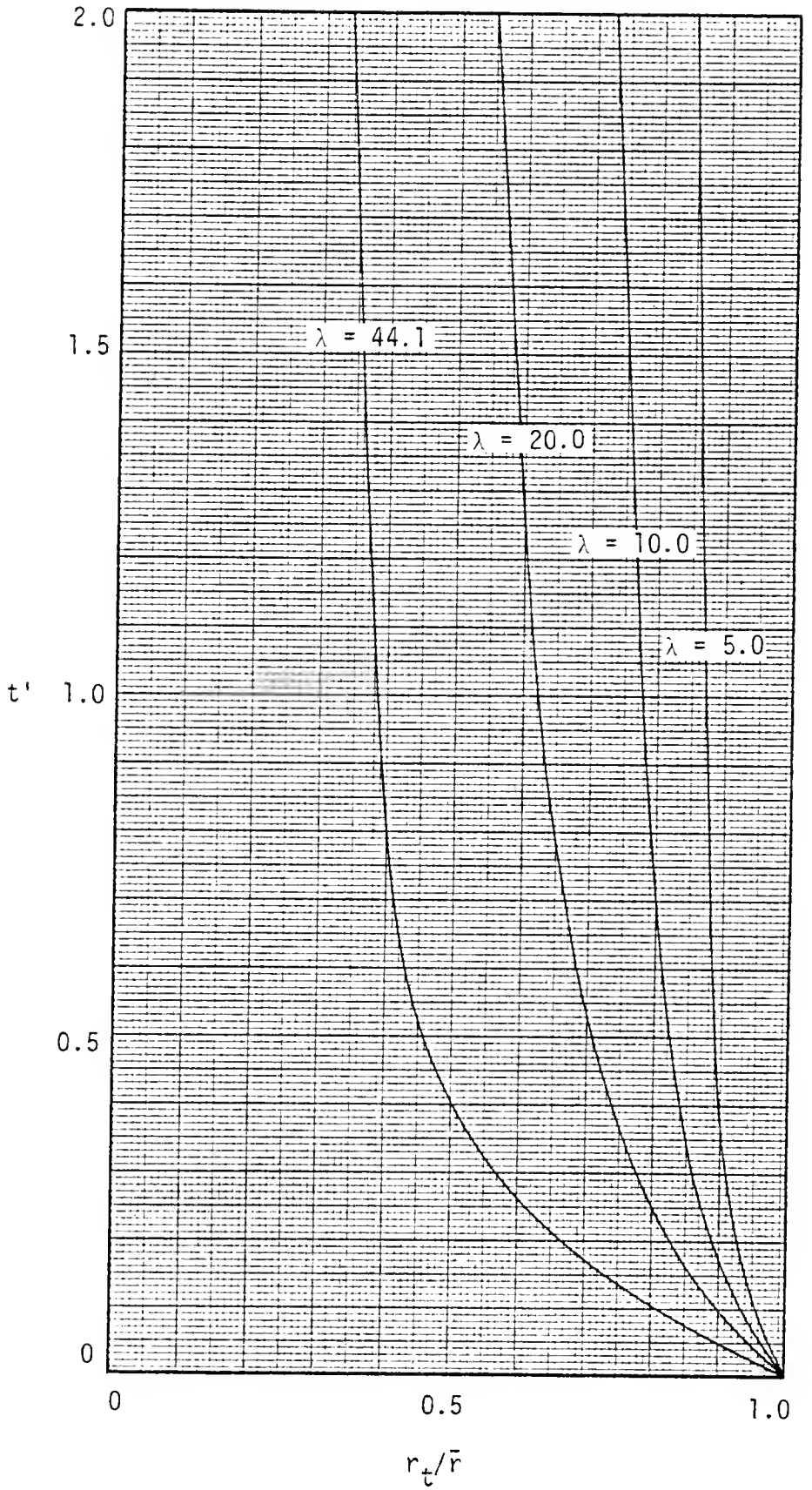

FIGURE 7.7. A DIMENSIONLESS REPRESENTATION OF GRAVITATIONAL SEGREGATION DURING LENS GROWTH

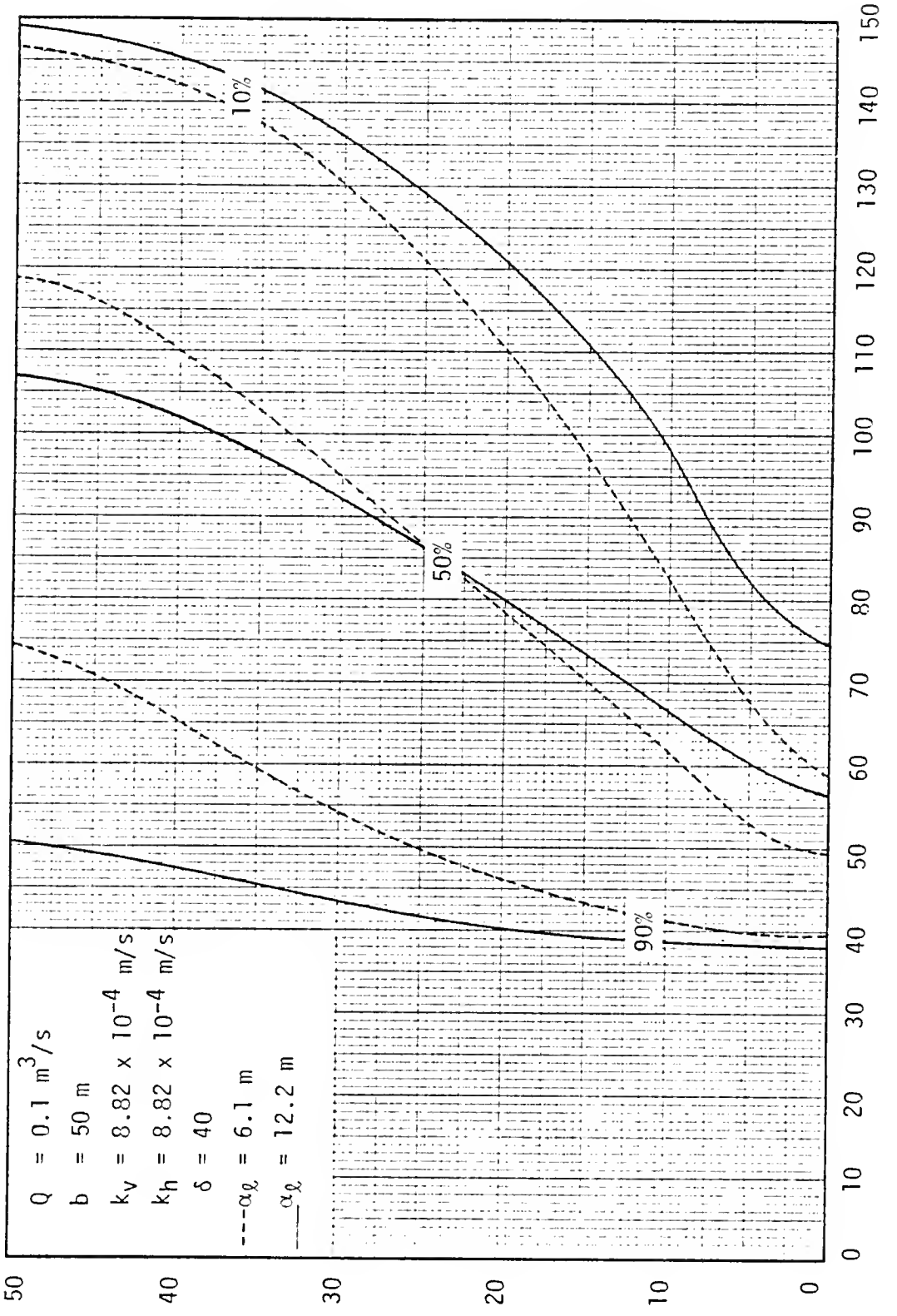

FIGURE 7.8. COMPARISON OF LENS BOUNDARIES AFTER 30 DAYS OF INJECTION WITH DIFFERENT DISPERSIVITIES

Changes in Lens Shape During Recovery

The production of freshwater from a lens is accompanied by the same irreversible processes of dispersion and gravity segregation that were present during its injection. The only difference is that during production the lens boundaries are flowing in the direction of increasing pressure gradient so that the rate of movement of the boundaries increases rapidly as the well is approached. Figures 7.9 and 7.10 illustrate the collapse of freshwater lenses during production. The aquifer of Figure 7.9 has a λ value of 2.5 so conditions are relatively favorable for the storage of freshwater. The lens in this figure was formed by injection of freshwater at a rate of 0.1 m^3/s for 30 days. Removal of freshwater from the lens was begun on the 31st day at the same pumping rate. By the 54th day, the 50% concentration line had broken through to the well. The amount of water produced at that time was 74% of the amount that had been injected although the produced water was not 100% fresh.

Figure 7.10 illustrates the same sequence of events in an aquifer having a λ value of 22.05. In this case the 50% line reached the well by the 38th day and the recovery efficiency at this time was 27%.

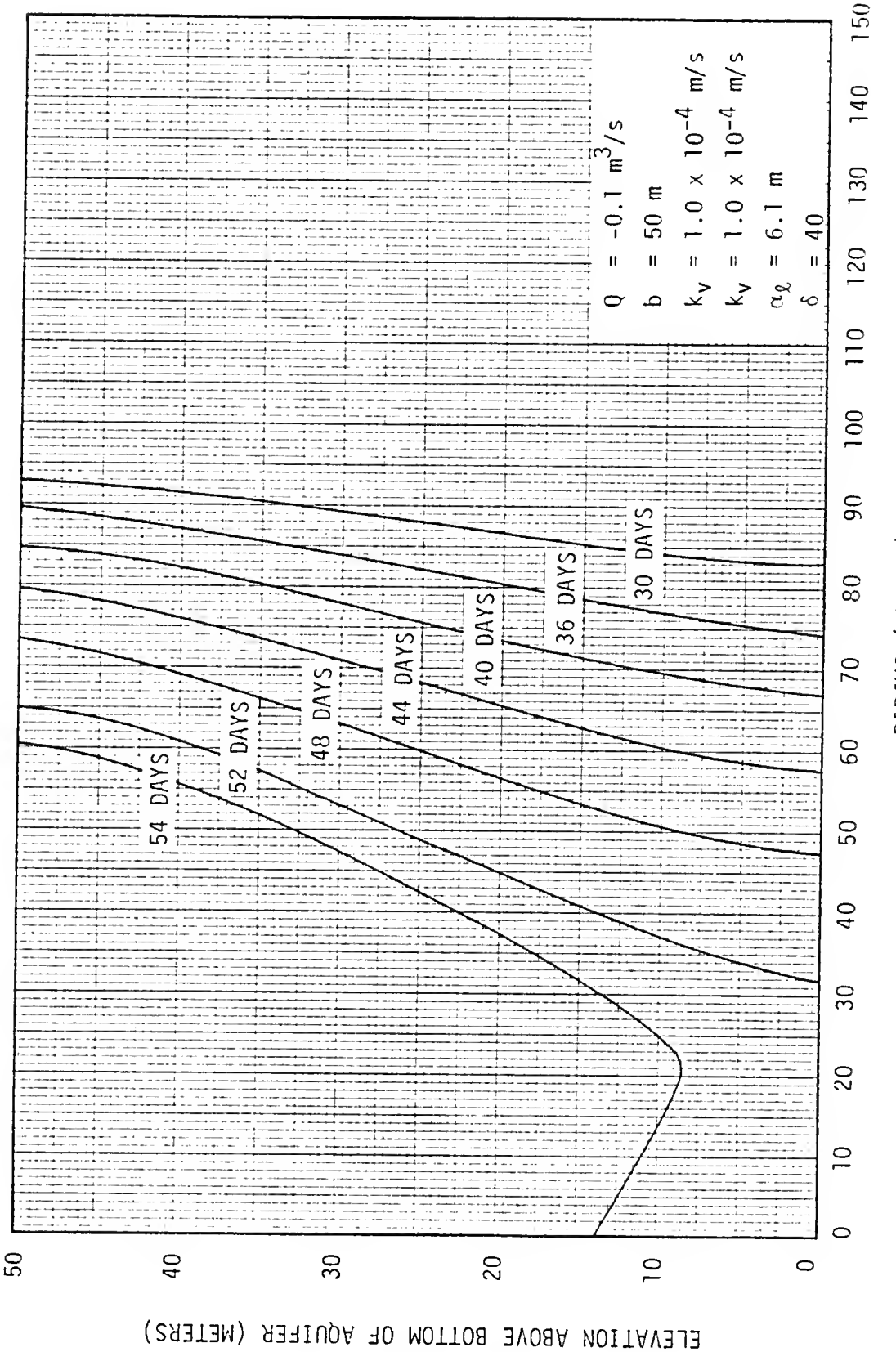

FIGURE 7.9. MOVEMENT OF 50% CONCENTRATION LINES DURING PRODUCTION OF FRESHWATER FROM A LENS

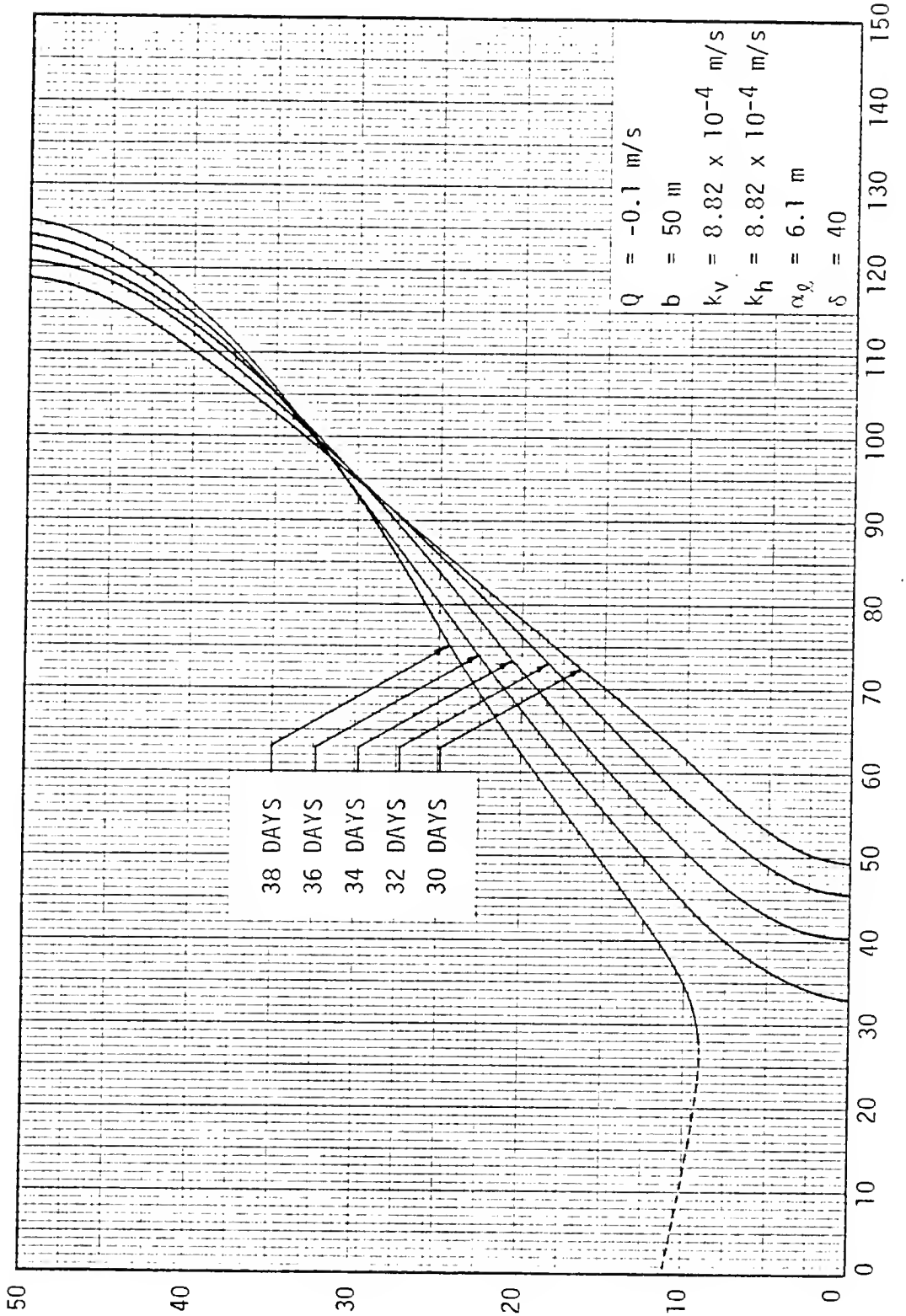

FIGURE 7.10. MOVEMENT OF 50% CONCENTRATION LINE DURING PRODUCTION OF FRESHWATER FROM A LENS

CHAPTER 8

CONCLUSIONS

1. The equation for predicting the rate of rotation of an initially vertical interface between two fluids of different density given by Gardner, Downie and Kendall (1962) matches the experimental data from the narrow Hele-Shaw model quite well. The shape of this interface as it rotates toward the horizontal is nearly straight as assumed in the derivation of the equation. When the depth of the flow region is doubled, however, the moving interface becomes more curved and the rotation rate is greater than predicted. This is probably caused by the increased opportunity for vertical flow in the thicker model aquifer.

2. Saltwater intrusion in coastal aquifers can be alleviated on a local scale by the creation of a freshwater lens or a series of such lenses. Such measures could be especially useful in highly developed coastal zones where the natural recharge of the coastal aquifer is reduced by land drainage practices and the construction of impermeable land surfaces. An injection well scheme of this type could be evaluated and designed using the Girinskii potential method presented in Chapter 5.

3. It seldom happens in nature that an aquifer is confined by completely impervious layers. Many aquifers that might be considered as possible sites for freshwater lens storage projects are actually more or less leaky. The amount of leakage that would be caused by

the injection of freshwater has an important influence on the size of freshwater lens that can be formed. The limiting size of lens that can be formed under a given set of flow conditions in a leaky aquifer can be determined using the design chart developed in Chapter 5.

4. The classical one-dimensional solution for flow in leaky aquifers which was developed by Jacob (1946) gives essentially the same results as the three-dimensional numerical solution as long as the ratio of B/b is greater than 10.

5. The three-dimensional finite element model developed in Chapter 6 gives very stable and reliable solutions to the groundwater flow equation within the curved boundaries typical of a freshwater lens. The extra programming effort required by the use of quadratic interpolation functions and the 20 node elements is rewarded by the larger element size and more flexible element shape it makes possible.

6. The location of a stationary interface can be found by iterative solution of the boundary value problem within the freshwater lens using the three-dimensional finite element model. If the resident saltwater is also in motion, the same technique can be used but two boundary value problems must be solved at each iteration. Unless the initial guess of the location of the interface is very good, a large number of iterations may be needed.

7. The INTERCOMP finite difference model is very useful in tracing the movement of a transient freshwater lens. This model is capable of handling non-homogeneous and non-isotropic aquifers. If the temperature variations within the aquifer are substantial, it would be desirable to include their effects also. This can be done with the INTERCOMP model. It would certainly be worthwhile for anyone

planning a large scale lens storage project to check its feasibility with this model first.

8. The vertical components of flow within a freshwater lens can have a very powerful influence on the shape of the lens. Previous analyses have assumed that vertical flow components are negligible. This must be true if the lens is to be useful for freshwater storage, but, in general, it is not true. In thick aquifers with good vertical hydraulic conductivity, the vertical components of flow have a predominant influence and under these conditions the feasibility of storage in freshwater lenses is highly questionable.

9. The concept of storing water in freshwater lenses for future use is based on an idealization of groundwater flow. When the natural conditions conform closely to these idealized conditions, reasonably high recovery efficiency can be achieved. With each new departure from the ideal conditions, however, the recovery efficiency is reduced and the scheme rapidly becomes unfeasible.

APPENDIX

FINITE ELEMENT PROGRAM DOCUMENTATION

Input Data

The required input data for this program consists of an initial data list and a repeated data list. The initial data list is read by the main program and consists of the following variables:

IBWTH = Bandwith of the discretization scheme

B2 = β^2, the modified leakage coefficient

HO = Piezometric head in the aquifer above the leaky layer

NUNODS = Number of nodes

NUMELS = Number of elements

XKX = K_{xx}

YKY = K_{yy}

ZKZ = K_{zz}

RT = Radius of the interface toe

DEPTH = Thickness of the saline aquifer

QQ = Rate of injection

M = Number of the first element with an adjustable boundary

The repeated data list is read in subroutine LDCAT and consists of the following variables:

R = Ratio of node radius to RT

TH(1) = Elevation of the top tier of nodes

TH(2) = Elevation of the middle tier of nodes

TH(3) = Elevation of the bottom tier of nodes

Flow Chart

The finite element model consists of a main program and seven subroutines. The primary function of the main program is to control the subroutines in which most of the actual computations are accomplished.

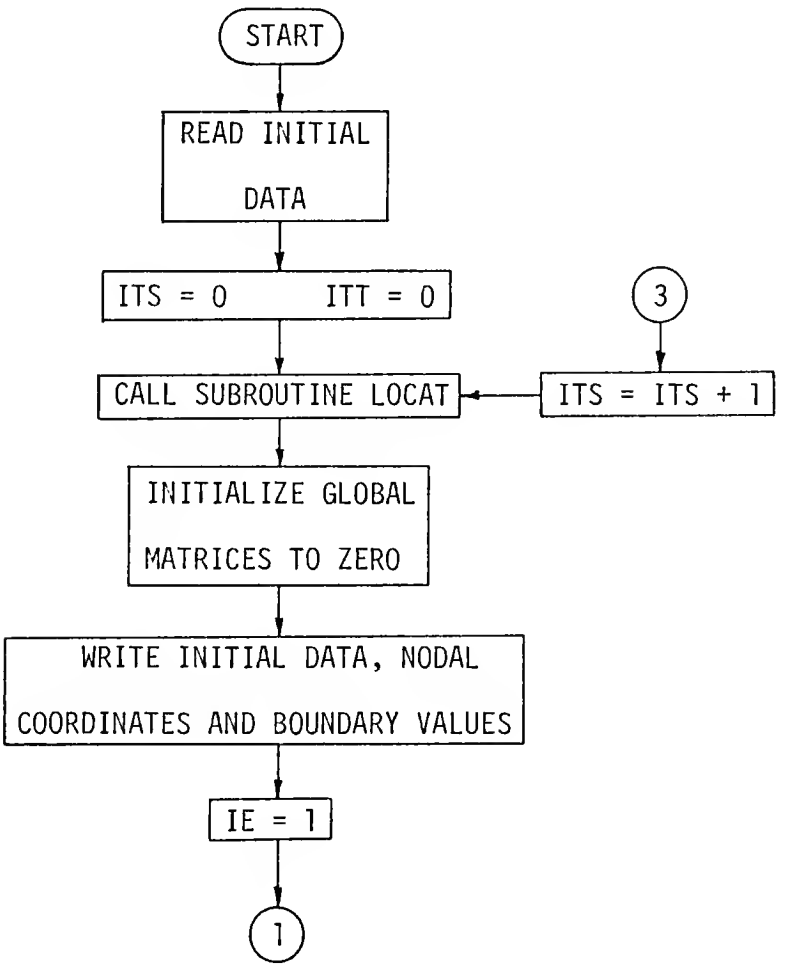

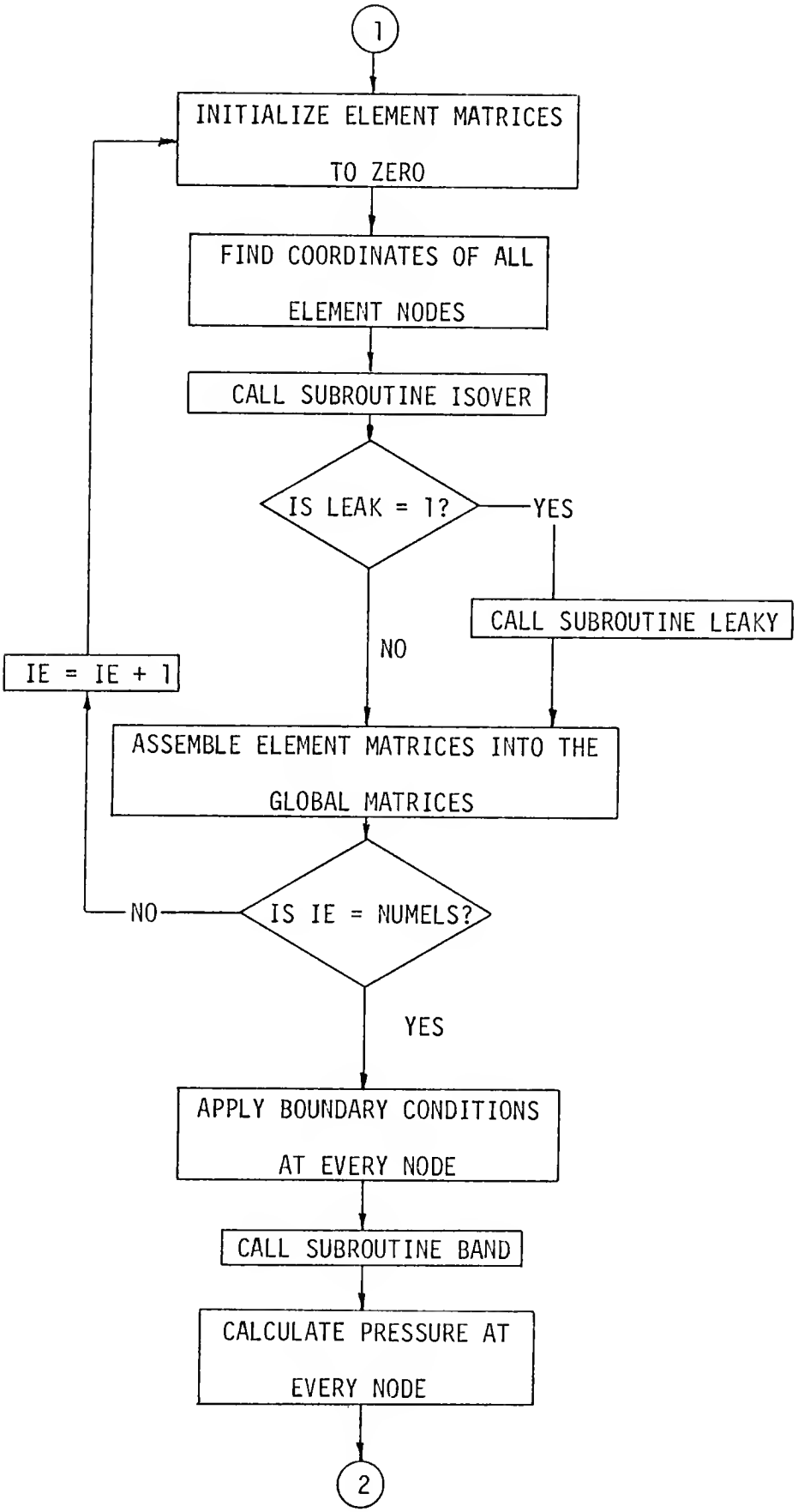
1
INITIALIZE ELEMENT MATRICES TO ZERO
FIND COORDINATES OF ALL ELEMENT NODES
CALL SUBROUTINE ISOVER
IS LEAK = 1?
YES
NO
CALL SUBROUTINE LEAKY
IE = IE + 1
ASSEMBLE ELEMENT MATRICES INTO THE GLOBAL MATRICES
IS IE = NUMELS?
NO
YES
APPLY BOUNDARY CONDITIONS AT EVERY NODE
CALL SUBROUTINE BAND
CALCULATE PRESSURE AT EVERY NODE
2

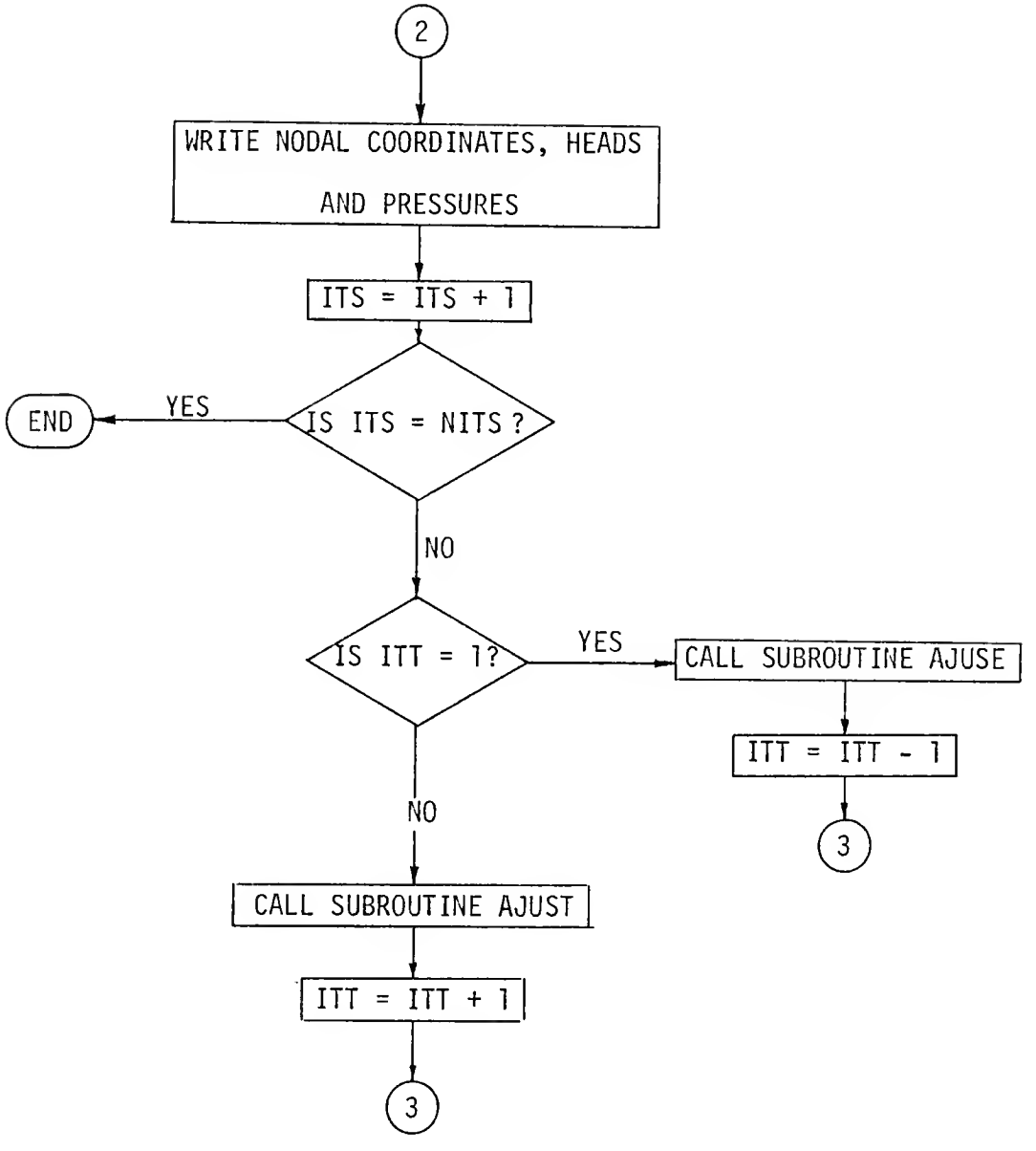
2
WRITE NODAL COORDINATES, HEADS AND PRESSURES
ITS = ITS + 1
IS ITS = NITS ?
YES
END
NO
IS ITT = 1?
YES
CALL SUBROUTINE AJUSE
ITT = ITT - 1
3
NO
CALL SUBROUTINE AJUST
ITT = ITT + 1
3

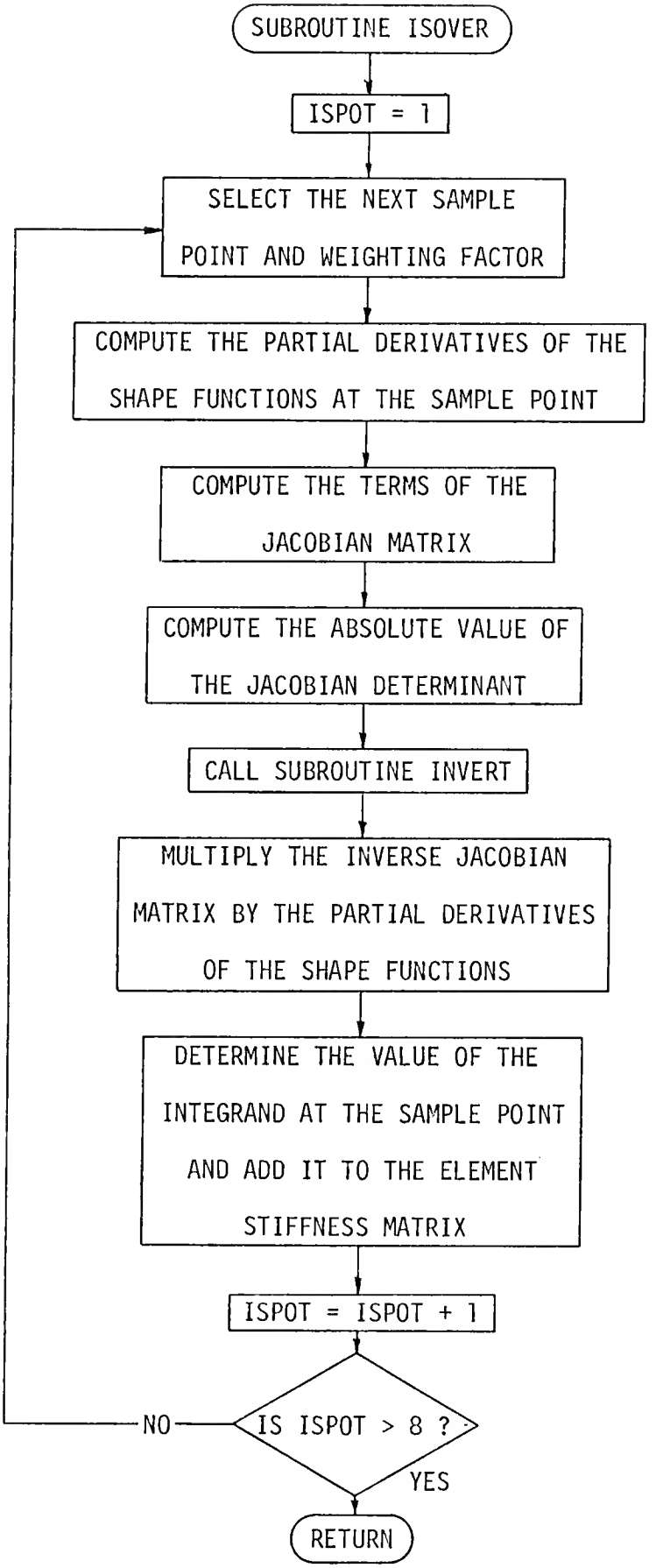
SUBROUTINE ISOVER
ISPOT = 1
SELECT THE NEXT SAMPLE POINT AND WEIGHTING FACTOR
COMPUTE THE PARTIAL DERIVATIVES OF THE SHAPE FUNCTIONS AT THE SAMPLE POINT
COMPUTE THE TERMS OF THE JACOBIAN MATRIX
COMPUTE THE ABSOLUTE VALUE OF THE JACOBIAN DETERMINANT
CALL SUBROUTINE INVERT
MULTIPLY THE INVERSE JACOBIAN MATRIX BY THE PARTIAL DERIVATIVES OF THE SHAPE FUNCTIONS
DETERMINE THE VALUE OF THE INTEGRAND AT THE SAMPLE POINT AND ADD IT TO THE ELEMENT STIFFNESS MATRIX
ISPOT = ISPOT + 1
IS ISPOT > 8 ?
NO
YES
RETURN

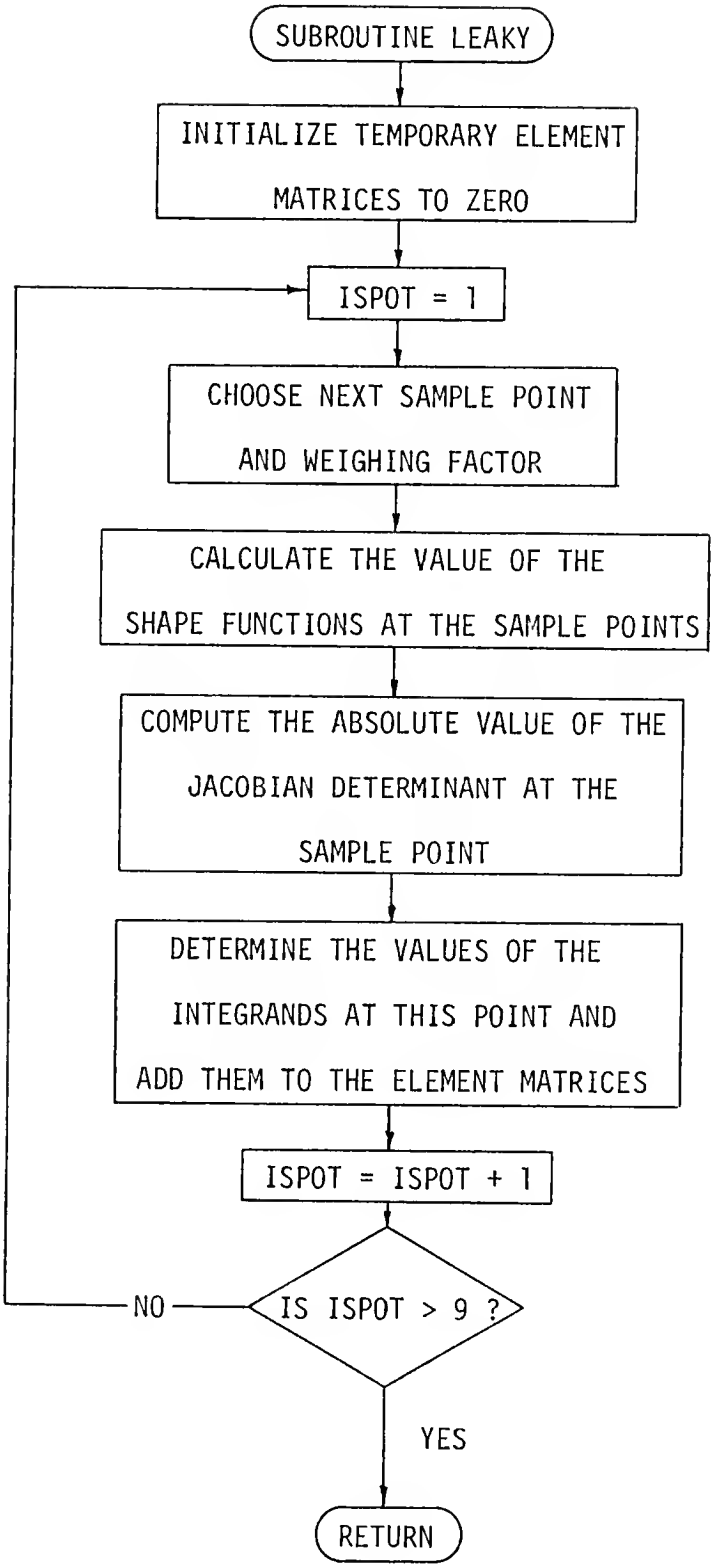
SUBROUTINE LEAKY
INITIALIZE TEMPORARY ELEMENT MATRICES TO ZERO
ISPOT = 1
CHOOSE NEXT SAMPLE POINT AND WEIGHING FACTOR
CALCULATE THE VALUE OF THE SHAPE FUNCTIONS AT THE SAMPLE POINTS
COMPUTE THE ABSOLUTE VALUE OF THE JACOBIAN DETERMINANT AT THE SAMPLE POINT
DETERMINE THE VALUES OF THE INTEGRANDS AT THIS POINT AND ADD THEM TO THE ELEMENT MATRICES
ISPOT = ISPOT + 1
IS ISPOT > 9 ?
NO
YES
RETURN

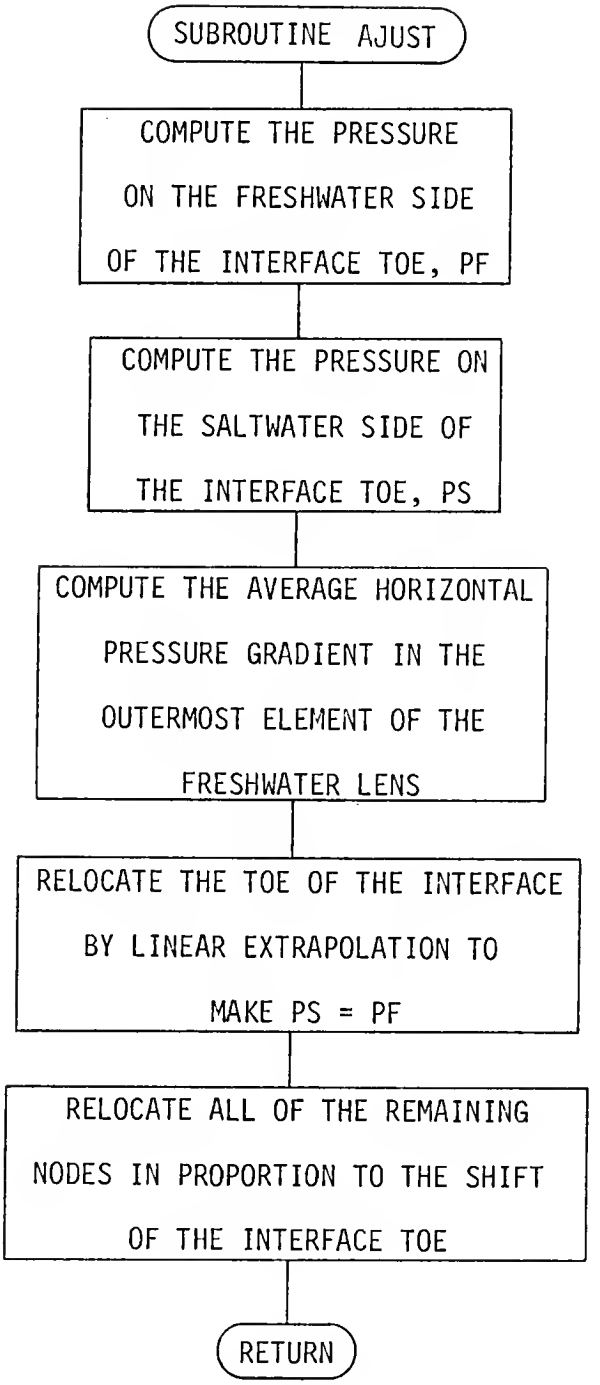
SUBROUTINE AJUST
COMPUTE THE PRESSURE ON THE FRESHWATER SIDE OF THE INTERFACE TOE, PF
COMPUTE THE PRESSURE ON THE SALTWATER SIDE OF THE INTERFACE TOE, PS
COMPUTE THE AVERAGE HORIZONTAL PRESSURE GRADIENT IN THE OUTERMOST ELEMENT OF THE FRESHWATER LENS
RELOCATE THE TOE OF THE INTERFACE BY LINEAR EXTRAPOLATION TO MAKE PS = PF
RELOCATE ALL OF THE REMAINING NODES IN PROPORTION TO THE SHIFT OF THE INTERFACE TOE
RETURN

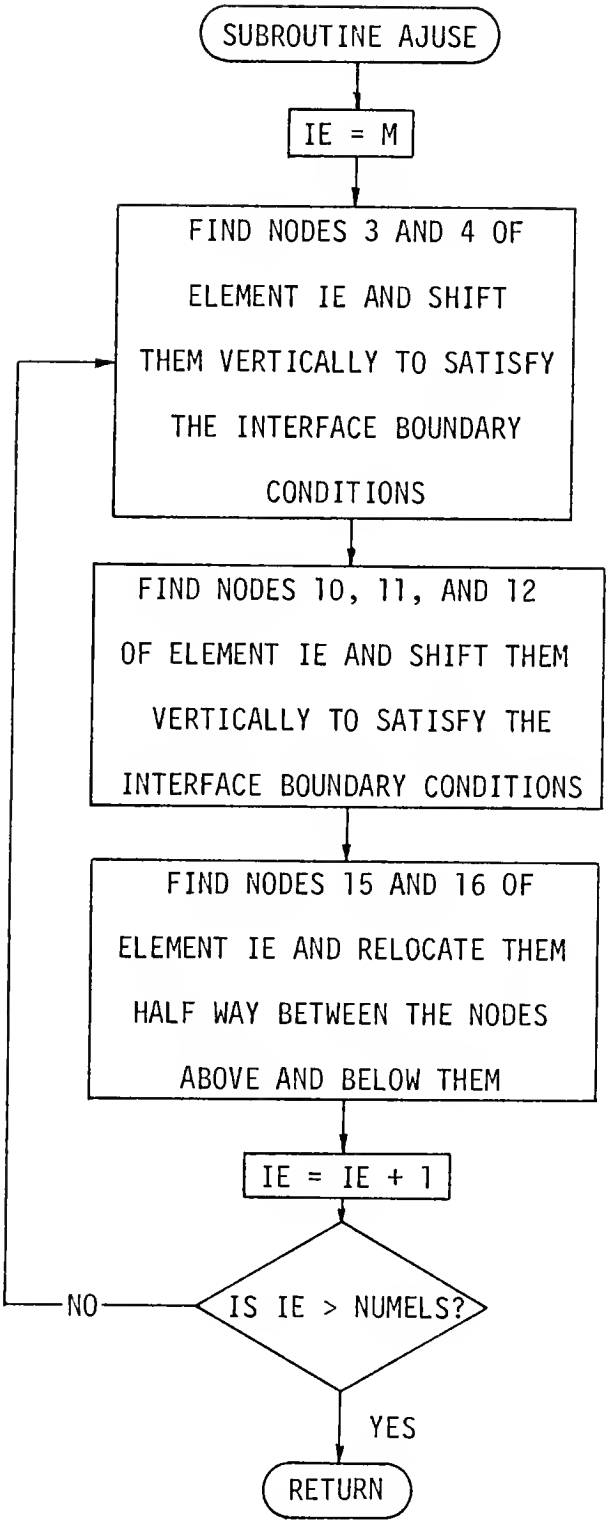
SUBROUTINE AJUSE
IE = M
FIND NODES 3 AND 4 OF ELEMENT IE AND SHIFT THEM VERTICALLY TO SATISFY THE INTERFACE BOUNDARY CONDITIONS
FIND NODES 10, 11, AND 12 OF ELEMENT IE AND SHIFT THEM VERTICALLY TO SATISFY THE INTERFACE BOUNDARY CONDITIONS
FIND NODES 15 AND 16 OF ELEMENT IE AND RELOCATE THEM HALF WAY BETWEEN THE NODES ABOVE AND BELOW THEM
IE = IE + 1
IS IE > NUMELS?
NO
YES
RETURN

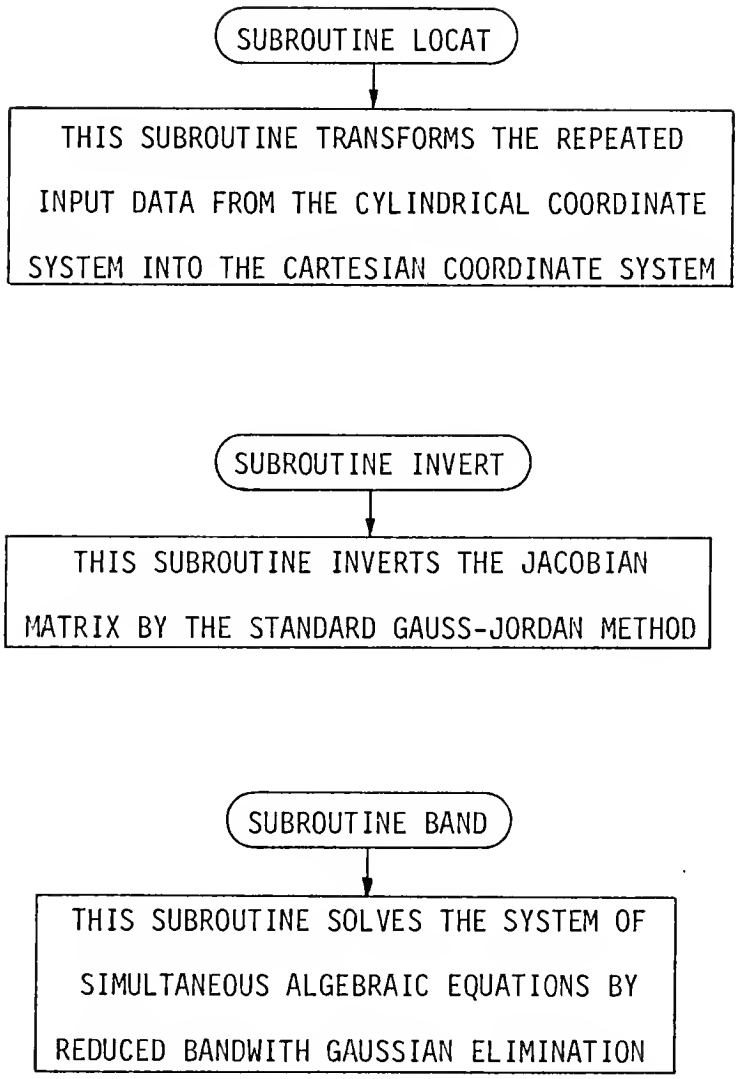
SUBROUTINE LOCAT
THIS SUBROUTINE TRANSFORMS THE REPEATED INPUT DATA FROM THE CYLINDRICAL COORDINATE SYSTEM INTO THE CARTESIAN COORDINATE SYSTEM
SUBROUTINE INVERT
THIS SUBROUTINE INVERTS THE JACOBIAN MATRIX BY THE STANDARD GAUSS-JORDAN METHOD
SUBROUTINE BAND
THIS SUBROUTINE SOLVES THE SYSTEM OF SIMULTANEOUS ALGEBRAIC EQUATIONS BY REDUCED BANDWITH GAUSSIAN ELIMINATION

```
$JOB
      DIMENSION A(200,[illegible]),BNV(200),F(200),N(50,20),X(200),Y(200)
     1,Z(200),[illegible],ITYPE(50),LEAK(50),RN(200),THN(200)
      DIMENSION EA(20,20),EF(20),EX(20),EY(20),EZ(20)
      COMMON EA,EF,EX,EY,EZ
      READ(5,1000) IBWTH,NUNODS,NUMELS,NITS
      READ(5,1010) [illegible],XKX,YKY,ZKI
      READ(5,1011) RT,DEPTH,QQ,M
      ITS=0
      [illegible]=0
      CALL [illegible](NUNODS,NUMELS,RT,QQ,X,Y,Z,ITYPE,LEAK,[illegible],BNV,N,RN,THN)
    3 DO 4 I=1,NUNODS
      F(I)=0.0
      DO 4 J=1,[illegible]
    4 A(I,J)=0.0
      VOLUME=0.0
      TLA=0.0
      IF (ITS .GT. 0) GO TO 10
      WRITE(6,2000)
      WRITE(6,2010) IBWTH,NUNODS,NUMELS
      WRITE(6,2020) [illegible],XKX,YKY,ZKI
      WRITE(6,2025) QQ,M
      WRITE(6,2030)
      WRITE(6,2035)
      DO 5 I=1,NUMELS
    5 WRITE(6,2040) I,ITYPE(I),LEAK(I),(N(I,J),J=1,20)
      WRITE(6,2050)
      WRITE(6,2055)
      DO 8 I=1,NUNODS
    8 WRITE(6,2060) I,X(I),Y(I),Z(I),BNV(I),G(I)
   10 DO 70 IE=1,NUMELS
      DO 35 I=1,20
      EF(I)=0.0
      DO 35 J=1,20
   35 EA(I,J)=0.0
      DO 40 I=1,20
      IT=N(IE,I)
      EX(I)=X(IT)
      EY(I)=Y(IT)
   40 EZ(I)=Z(IT)
   50 CALL [illegible](XKX,YKY,ZKI,VOLUME)
   55 LEA=LEAK(IE)
      IF (LEA .NE. 1) GO TO 65
      CALL LEAKY([illegible],TLA)
   65 DO 69 I=1,20
      IR=N(IE,I)
      F(IR)=F(IR)+EF(I)
      DO 69 J=1,20
      IC=N(IE,J)-IR+1
      IF (IC .LE. 0) GO TO 69
      A(IR,IC)=A(IR,IC)+EA(I,J)
   69 CONTINUE
   70 CONTINUE
      DO 80 I=1,NUNODS
      F(I)=F(I)+G(I)
      IF (BNV(I) .EQ. -1.0) GO TO 80
      A(I,1)=1.0E15
      F(I)=BNV(I)*1.0E15
   80 CONTINUE
      WRITE(6,2070) VOLUME
      WRITE(6,2080) TLA
      WRITE(6,2100) (F(I),I=1,NUNODS)
      CALL BAND(NUNODS,IBWTH,A,F)
      WRITE(6,2085)
      DO 90 I=1,NUNODS
      P=[illegible]*(F(I)+DEPTH-Z(I))
   90 WRITE(6,2090) I,X(I),Y(I),Z(I),F(I),P
      ITS=ITS+1
      IF (ITS .GE. NITS) GO TO 999
      IF (IT[illegible] .EQ. 1) GO TO 95
      CALL ADJST(NUNODS,RT,X,Y,DEPTH,F,N,RN,THN,M)
      ITT=ITT+1
      GO TO 3
   95 CALL ADJSE(N,M,NUMELS,Z,DEPTH,F)
      ITT=ITT+1
      GO TO 3
 1000 FORMAT(4I5)
 1010 FORMAT(E10.[illegible],3F10.5)
 1011 FORMAT(2F10.[illegible],[illegible])
 2000 FORMAT(1H0,[illegible],[illegible] JOB PARAMETERS)
 2010 FORMAT(1X,7HIBWTH =,I4,5X,8HNUNODS =,I4,5X,8HNUMELS =
     1,I4
 2020 FORMAT(1X,4HEE = E10.4,5X,4H[illegible] =,F10.5,5X,5HXKX = F10.5,
     15X,5HYKY = F10.5,5X,5HZKI = F10.5
```

```
      2025 FORMAT(1( 3H00=,E10.4,5X,2HM=,I4)
      2030 FORMAT(1HO,'ELEMENT',5X,4HTYPE,5X,4HLEAK,5X,15H   1   2   3
     1 15H4    5    6    7    8    9   10   11   12   13   14   15   16
     2 21H 17   18   19   20)
      2035 FORMAT(1X,80H
     1 1H )
      2040 FORMAT(4X,I5,7X,I4,2X,I4,5X,20I4)
      2050 FORMAT(1HO,4HNODE,5X,5H   X   ,5X,5H   Y   ,5X,5H   Z   ,5X,
     1 11H        3NV,,5X,10H        Q
      2055 FORMAT(1X,40H
     1 1H )
      2060 FORMAT(1X,I4,3F10.4,3X,F10.7,5X,F10.7)
      2070 FORMAT(1HO,15H TOTAL VOLUME =,E15.5,/,40X,
     1 10H*********  STIFFNESS MATRIX  *********)
      2080 FORMAT(1X,E13.3)
      2085 FORMAT(1H1,19H TOTAL LEAKY AREA =,E13.5,/,40X,
     1 10H*********  FORCE MATRIX  *********  )
      2086 FORMAT(1HO,5H NODE NO.,10X,1HX,19X,1HY,19X,1HZ,17X,4HHEAD,15X,
     1 15HPRESSURE/RY,9H---------,6X,10H----------,10X,10H----------,
     2 10X,10H----------,9X,11H----------,9X,11H----------,
      2090 FORMAT(4X,I4,8X,F10.5,10X,F10.5,10X,F10.5,9X,E11.4,9X,E13.5)
     1 END
           END

           SUBROUTINE LEAKY(B2,HO,TLA)
           DIMENSION EA(20,20),BU(20,2),EP(20),EX(20),EY(20),EZ(20),SN(20)
           COMMON EA,EP,EX,EY,EZ
           DO 1 I=1,20
           EP(I)=0.0
         1 SN(I)=0.0
           IBOT=1
           ALPHA=0.7745967
           DD=25.0/81.0
           DM=40.0/81.0
           W=DD
           XI=-ALPHA
           YI=-ALPHA
           GO TO 10
         2 XI=0.0
           W=DM
           GO TO 10
         3 XI=ALPHA
           W=DD
           GO TO 10
         4 XI=0.0
           W=DM
           GO TO 10
         5 XI=0.0
           W=64.0/81.0
           GO TO 10
         6 XI=-ALPHA
           W=DM
           GO TO 10
         7 YI=ALPHA
           W=DD
           GO TO 10
         8 XI=0.0
           W=DM
           GO TO 10
         9 XI=ALPHA
           W=DD
        10 YM=1.0-YI
           YP=1.0+YI
           XIM=1.0-XI
           XIP=1.0+XI
           YB=2.0*YI
           R5=(XI+YI)*YIM/4.0
           R6=(XI-YI)*YIM/4.0
           R7=(XI+YI)*YIP/4.0
           R8=(XI-YI)*YIP/4.0
           R17=-XI*YIM
           R18=(1.0-YI*YI)/2.0
           R19=-XI*YIP
           R20=-R18
           EA(I,1)=R5*E(15)-R6*E(16)+R7*E(17)+R8*E(18)
          1+R17*EX(17)+R18*EX(18)+R19*EX(19)+R20*EX(20)
           BU(I,2)=R5*E(15)+R6*E(16)+R7*E(17)+R8*E(18)
          1+R17*EY(17)+R18*EY(18)+R19*EY(19)+R20*EY(20)
           YB=2.0*YI
           R5=(YB+XI)*XIM/4.0
           R6=(YB-XI)*XIP/4.0
           R7=(YB+XI)*XIP/4.0
           R8=(YB-XI)*XIM/4.0
           R19=(1.0-XI*XI)/2.0
```

```
      SUBROUTINE INVERT (A,N,T,DET)
C     INVERT THE JACOBIAN MATRIX
      DIMENSION A(3,3),T(3,3)
      DO 5 I=1,3
      DO 5 J=1,3
      T(I,J)=0.0
      A(I,J+3)=0.0
      IF (I .EQ. J) T(I,J)=1.0
      IF (I .EQ. J) A(I,I+3)=1.0
    6 CONTINUE
      DO 10 K=1,3
      IF(A(K,K) .NE. 0.0) GO TO 10
      KK=K+1
      DO 8 I=KK,3
      IF(A(I,K) .EQ. 0.0) GO TO 8
      DO 7 J=K,6
      B1=A(K,J)
      A(K,J)=A(I,J)
      A(I,J)=B1
    7 CONTINUE
      GO TO 10
    8 CONTINUE
      GO TO 12
   10 B1=A(K,K)
      DO 11 IP=K,6
   11 A(K,IP)=A(K,IP)/B1
      DO 15 I=1,3
      IF(I .EQ. K) GO TO 15
      B1=A(I,K)
      DO 14 J=K,6
   14 A(I,J)=A(I,J)-B1*A(K,J)
   15 CONTINUE
   16 CONTINUE
      DO 17 I=1,3
      DO 17 J=1,3
   17 T(I,J)=A(I,J+3)
      GO TO 20
   12 WRITE(6,1000) IE
 1000 FORMAT (1H0,29HJACOBIAN INVERSE DOES NOT EXIST
     1 ,10HAT ELEMENT NO ,I4)
   20 RETURN
      END

      SUBROUTINE BAND(NNODS,IBWTH,A,B)
      DIMENSION A(200,99),B(200),D(99)
      DO 10 N=1,NNODS
      PIVOT=A(N,1)
```

```
      IF(K .EQ. NUNODS) GO TO 100
      DO 20 J=2,IBWTH
      C(J)=A(K,J)
      A(K,J)=A(K,J)/A(K,1)
   20 CONTINUE
      DO 30 L=2,IBWTH
      I=K+L-1
      IF(NUNODS .LT. I) GO TO 30
      J=0
      DO 40 LL=L,IBWTH
      J=J+1
      A(I,J)=A(I,J) -C(L)*A(K,LL)
   40 CONTINUE
      F(I)=F(I)-C(L)*F(K)
   30 CONTINUE
  100 CONTINUE
      K=K-1
      IF(K .EQ. 0) GO TO 200
      DO 50 J=2,IBWTH
      L=K+J-1
      IF(NUNODS .LT. L) GO TO 50
      F(K)=F(K)-A(K,J)*F(L)
   50 CONTINUE
      GO TO 100
  200 CONTINUE
  300 CONTINUE
  201 RETURN
      END

      SUBROUTINE ISOVER(KX,KY,KZ,VOLUME)
      DIMENSION EA(20,20),AU(3,3),T(3,3),
     1IDNY(20),DNY(20),DNZ(20),EX(20),EY(20),EZ(20),EF(20),
     2DNX(20),DNY(20),DNZ(20)
      COMMON EA,EF,EX,EY,EZ
      ISPOT=1
      ALPHA=0.57735027
      XI=-ALPHA
      YI=-ALPHA
      ZI=-ALPHA
      GO TO 10
    2 XI=ALPHA
      GO TO 10
    3 YI=ALPHA
      GO TO 10
    4 XI=-ALPHA
      GO TO 10
    5 YI=-ALPHA
      ZI=ALPHA
      GO TO 10
    6 XI=ALPHA
      GO TO 10
    7 YI=ALPHA
      GO TO 10
  100 XI=-ALPHA
   10 XIP=1.0+XI
      XIM=1.0-XI
      YIP=1.0+YI
      YIM=1.0-YI
      ZIP=1.0+ZI
      ZIM=1.0-ZI
      DNX(1)=YIM*ZIM*(0.0+XI+YI+ZI+1.0)/8.0
      DNX(2)=YIM*ZIM*(0.0+XI-YI-ZI-1.0)/8.0
      DNX(3)=YIP*ZIM*(0.0+XI+YI-ZI-1.0)/8.0
      DNX(4)=YIP*ZIM*(0.0+XI-YI+ZI+1.0)/8.0
      DNX(5)=YIM*ZIP*(0.0+XI+YI-ZI+1.0)/8.0
      DNX(6)=YIM*ZIP*(0.0+XI-YI+ZI-1.0)/8.0
      DNX(7)=YIP*ZIP*(0.0+XI+YI+ZI+1.0)/8.0
      DNX(8)=YIP*ZIP*(0.0+XI-YI-ZI+1.0)/8.0
      DNX(9)=-XIM*ZIM/4.0
      DNX(10)=-YIP*ZIM/4.0
      DNX(11)=-XIP*ZIM/4.0
      DNX(12)=-DNX(10)
      DNX(13)=-XIM*ZIP/4.0
      DNX(14)=-DNX(11)
      DNX(15)=-YIM*ZIP/4.0
      DNX(16)=-DNX(9)
      DNX(17)=-XIM*YIP/2.0
      DNX(18)=-YIP*XIP/4.0
      DNX(19)=-XIP*ZIP/2.0
      DNX(20)=-DNX(17)
      DNY(1)=XIM*ZIM*(0.0+XI+YI+ZI+1.0)/8.0
      DNY(2)=XIM*ZIM*(0.0+XI+YI-ZI-1.0)/8.0
      DNY(3)=XIP*ZIM*(0.0+XI+YI-ZI-1.0)/8.0
      DNY(4)=XIM*ZIM*(0.0+XI+YI-ZI-1.0)/8.0
```

```
      DNYI(5)=-(1.0+ZIP+YI)*XIP/4.0
      DNYI(6)=XIP*YIP*(2.0*ZI-XI-YI+1.0)/8.0
      DNYI(7)=XIP*YIP*(2.0*ZI+XI+YI+1.0)/8.0
      DNYI(8)=XIM*YIP*(2.0*ZI-XI+YI-1.0)/8.0
      DNYI(9)=-(1.0-XI*XI)*YIM/4.0
      DNYI(10)=-(1.0+ZIP+XI)*YIM/2.0
      DNYI(11)=-DNYI(9)
      DNYI(12)=-(1.0+ZIM+XI)*YIM/2.0
      DNYI(13)=-(1.0-ZI*ZI)*XIM/4.0
      DNYI(14)=-(1.0-ZI*ZI)*XIP/4.0
      DNYI(15)=-(1.0-ZI*ZI)*XIP/4.0
      DNYI(16)=-DNYI(13)
      DNYI(17)=-(1.0-YI+XI)*ZIP/4.0
      DNYI(18)=-(1.0+ZIP+YI)/2.0
      DNYI(19)=-DNYI(17)
      DNYI(20)=-(1.0+ZIM+YI)/2.0
      DNZI(1)=XIM*YIM*(2.0*ZI+XI+YI+1.0)/8.0
      DNZI(2)=XIP*YIM*(2.0*ZI-XI+YI+1.0)/8.0
      DNZI(3)=XIP*YIP*(2.0*ZI-XI-YI-1.0)/8.0000000
      DNZI(4)=XIM*YIP*(2.0*ZI+XI-YI+1.0)/8.0000000
      DNZI(5)=XIM*YIM*(2.0*ZI-XI-YI-1.0)/8.0
      DNZI(6)=XIP*YIM*(2.0*ZI+XI-YI-1.0)/8.0000000
      DNZI(7)=XIP*YIP*(2.0*ZI+XI+YI-1.0)/8.0000000
      DNZI(8)=XIM*YIP*(2.0*ZI-XI+YI-1.0)/8.0000000
      DNZI(9)=-(1.0-XI*XI)*YIM/4.0
      DNZI(10)=-(1.0-YI+YI)*XIP/4.0
      DNZI(11)=-(1.0-XI+XI)*YIP/4.0
      DNZI(12)=-(1.0-YI+YI)*XIM/4.0
      DNZI(13)=-XIM*YIM*ZI/2.0
      DNZI(14)=-XIP*YIM*ZI/2.0
      DNZI(15)=-XIP*YIP*ZI/2.0
      DNZI(16)=-XIM*YIP*ZI/2.0
      DNZI(17)=-DNZI(9)
      DNZI(18)=-DNZI(10)
      DNZI(19)=-DNZI(11)
      DNZI(20)=-DNZI(12)
      TAJ=0.0
      DO 15 I=1,20
   15 TAJ=TAJ+DNXI(I)*EX(I)
      AJ(1,1)=TAJ
      TAJ=0.0
      DO 16 I=1,20
   16 TAJ=TAJ+DNXI(I)*EY(I)
      AJ(1,2)=TAJ
      TAJ=0.0
      DO 17 I=1,20
   17 TAJ=TAJ+DNXI(I)*EZ(I)
      AJ(1,3)=TAJ
      TAJ=0.0
      DO 18 I=1,20
   18 TAJ=TAJ+DNYI(I)*EX(I)
      AJ(2,1)=TAJ
      TAJ=0.0
      DO 19 I=1,20
   19 TAJ=TAJ+DNYI(I)*EY(I)
      AJ(2,2)=TAJ
      TAJ=0.0
      DO 20 I=1,20
   20 TAJ=TAJ+DNYI(I)*EZ(I)
      AJ(2,3)=TAJ
      TAJ=0.0
      DO 21 I=1,20
   21 TAJ=TAJ+DNZI(I)*EX(I)
      AJ(3,1)=TAJ
      TAJ=0.0
      DO 22 I=1,20
   22 TAJ=TAJ+DNZI(I)*EY(I)
      AJ(3,2)=TAJ
      TAJ=0.0
      DO 23 I=1,20
   23 TAJ=TAJ+DNZI(I)*EZ(I)
      AJ(3,3)=TAJ
      DJ=AJ(1,1)*AJ(2,2)*AJ(3,3)-AJ(1,1)*AJ(2,3)*AJ(3,2)
     1+AJ(1,2)*AJ(2,3)*AJ(3,1)-AJ(1,2)*AJ(2,1)*AJ(3,3)
     2+AJ(1,3)*AJ(2,1)*AJ(3,2)-AJ(1,3)*AJ(2,2)*AJ(3,1)
      DJAX=ABS(DJ)
      CALL INVERT(AJ,T,IE)
      DO 30 I=1,20
      DNXI(I)=T(1,1)*DNXI(I)+T(1,2)*DNYI(I)+T(1,3)*DNZI(I)
      DNYI(I)=T(2,1)*DNXI(I)+T(2,2)*DNYI(I)+T(2,3)*DNZI(I)
   30 DNZI(I)=T(3,1)*DNXI(I)+T(3,2)*DNYI(I)+T(3,3)*DNZI(I)
      DO 35 I=1,20
      DO 35 J=1,20
   35 EA(I,J)=EA(I,J)+WX*DNXI(I)*DNXI(J)+WY*DNYI(I)*DNYI(J)
```

```
     1+ZKZ+ENZ(I)*BNZ(J))*DJA/
      VOLUME=VOLUME+DJA(
      ISPOT=ISPOT+1
      IF(ISPOT .EQ. 2) GO TO 2
      IF(ISPOT .EQ. 3)GO TO 3
      IF(ISPOT .EQ. 4) GO TO 4
      IF(ISPOT .EQ. 5) GO TO 5
      IF(ISPOT .EQ. 6) GO TO 6
      IF(ISPOT .EQ. 7) GO TO 7
      IF(ISPOT .EQ. 8) GO TO 8
      RETURN
      END

      SUBROUTINE LOCAT(NUNODS,NUMELS,RT,QQ,X,Y,Z,ITYPE,LEAK,Q,BNV,N,
     1RN,THN)
      DIMENSION X(200),Y(200),Z(200),TH(3),N(50,20),BNV(200),Q(200)
     1,ITYPE(50),LEAK(50),RN(200),THN(200)
      THA=0.5235988
      QQP=QQ/3.0
      Q12M=-QQ/12.0
      ST=SIN(THA)
      ST2=SIN(THA/2.0)
      CT=COS(THA)
      CT2=COS(THA/2.0)
      JJ=0.0
      READ (5,1010) R,TH(1),TH(2),TH(3)
      RR=R
      GO TO 9
    5 READ (5,1010) RR,TH(1),TH(2),TH(3)
      R=RR*RT
    9 DO 10 I=1,3
      JJ=JJ+1
      RN(JJ)=RR
      THN(JJ)=0.0
      X(JJ)=0.0
      Y(JJ)=R
      Z(JJ)=TH(I)
   10 CONTINUE
      JJ=JJ+1
      RN(JJ)=RR
      THN(JJ)=THA/2.0
      X(JJ)=R*ST2
      Y(JJ)=R*CT2
      Z(JJ)=TH(1)
      JJ=JJ+1
      RN(JJ)=RR
      THN(JJ)=THA/2.0
      X(JJ)=R*ST2
      Y(JJ)=R*CT2
      Z(JJ)=TH(3)
      DO 20 I=1,3
      JJ=JJ+1
      RN(JJ)=RR
      THN(JJ)=THA
      X(JJ)=R*ST
      Y(JJ)=R*CT
      Z(JJ)=TH(I)
   20 CONTINUE
      IF(JJ .GE. NUNODS) GO TO 100
      READ(5,1020)RR,TH(1),TH(2)
      R=RR*RT
      DO 30 I=1,2
      JJ=JJ+1
      RN(JJ)=RR
      THN(JJ)=0.0
      X(JJ)=0.0
      Y(JJ)=R
   30 Z(JJ)=TH(I)
      DO 40 I=1,2
      JJ=JJ+1
      RN(JJ)=RR
      THN(JJ)=THA
      X(JJ)=R*ST
      Y(JJ)=R*CT
   40 Z(JJ)=TH(I)
      GO TO 5
  100 NU1=NUNODS-8
      DO 101 I=1,NU1
  101 BNV(I)=-1.0
      NU1=NUNODS-7
      DO 102 I=NU1,NUNODS
  102 BNV(I)=0.0
      G(1)=Q12M
      G(2)=QQP
```

```
      Q(3)=Q12M
      Q(4)=QDP
      Q(5)=QDP
      Q(6)=Q12M
      Q(7)=QDP
      Q(8)=Q12M
      DO 105 I=9,NUNODS
  105 Q(I)=0.0
  110 N(1,1)=3
      N(1,2)=8
      N(1,3)=20
      N(1,4)=13
      N(1,5)=1
      N(1,6)=6
      N(1,7)=18
      N(1,8)=13
      N(1,9)=5
      N(1,10)=12
      N(1,11)=17
      N(1,12)=10
      N(1,13)=2
      N(1,14)=7
      N(1,15)=19
      N(1,16)=14
      N(1,17)=4
      N(1,18)=11
      N(1,19)=16
      N(1,20)=9
      ITYPE(1)=1
      LEAK(1)=1
      DO 130 IE=2,NUMELS
      DO 120 J=1,20
  120 N(IE,J)=N(IE-1,J)+12
      ITYPE(IE)=1
      LEAK(IE)=1
  130 CONTINUE
 1010 FORMAT(4F10.5)
 1020 FORMAT(3F10.5)
      RETURN
      END

      SUBROUTINE AJUST(NUNODS,RT,X,Y,DEPTH,F,N,RN,THN,M)
      DIMENSION N(30,20),F(200),RN(200),THN(200),X(200),Y(200)
      J=N(M,1)
      PT=(F(J)+DEPTH)*9802.0
      PS=DEPTH*10047.0
      J1=N(M-1,1)
      P1=(F(J1)+DEPTH)*9802.0
      SLOP=(PT-P1)/(RT*(1.0-RN(J1)))
      RT=RT+0.5*(PS-PT)/SLOP
      DO 10 I=9,NUNODS
      TH=THN(I)
      X(I)=RN(I)*RT*SIN(TH)
      Y(I)=RN(I)*RT*COS(TH)
   10 CONTINUE
      RETURN
      END

      SUBROUTINE AJUSE(N,M,NUMELS,Z,DEPTH,F)
      DIMENSION N(30,20),Z(200),F(200)
      DO 40 I=M,NUMELS
      DO 10 II=3,4
      J=N(I,II)
      ZZ=41.00816*DEPTH-40.0*(F(J)+DEPTH)
      IF(ZZ .LT. 0.0) ZZ=Z(J)/2.0
      IF(ZZ .GE. DEPTH) ZZ=(DEPTH-Z(J))/2.0+Z(J)
   10 Z(J)=ZZ
      DO 15 II=10,12
      J=N(I,II)
      ZZ=41.00816*DEPTH-40.0*(F(J)+DEPTH)
      IF(ZZ .LT. 0.0) ZZ=Z(J)/2.0
      IF(ZZ .GE. DEPTH) ZZ=(DEPTH-Z(J))/2.0+Z(J)
   15 Z(J)=ZZ
      DO 20 II=15,16
      J=N(I,II)
      JU=N(I,II-12)
   20 Z(J)=(DEPTH+Z(JU))/2.0
   40 CONTINUE
      RETURN
      END
$ENTRY

      JOB PARAMETERS
```

REFERENCES

Agrawal, B. K. 1975. Effect of Viscosity Ratio on the Recovery of Fresh Water Stored in Saline Aquifers, M.S. Thesis, Louisiana State University, Baton Rouge, LA.

Bear, J. 1972. Dynamics of Fluids in Porous Media. American Elsevier. New York.

Bear, J. and G. Dagan. 1964. Some Exact Solutions of Interface Problems by Means of the Hodograph Method. Journal of Geophysical Research 69(8):1563-1572.

Carter, R. D. and G. W. Tracy. 1960. An Improved Method for Calculating Water Influx. Transactions, Society of Petroleum Engineers of AIME 216:415-417.

Collins, R. J. 1973. Bandwidth Reduction by Automatic Renumbering. International Journal for Numerical Methods in Engineering 6: 345-356.

Childley, T. R. E. and J. W. Lloyd. 1977. A Mathematical Model Study of Fresh-Water Lenses. Ground Water 15(3):215-222.

Dagan, G. and J. Bear. 1967. Solving the Problem of Local Interface Upcoming in a Coastal Aquifer by the Method of Small Perturbations. Journal of Hydraulic Research 6(1):15-44.

D'Amico, J. A. 1975. Effect of Dip on the Subsurface Storage or Disposal of Fluids in Saline Aquifers, M.S. Thesis, Louisiana State University, Baton Rouge, LA.

De Weist, R. J. M. 1965. Geohydrology. John Wiley & Sons, New York.

Esmail, O. J., and O. K. Kimbler. 1967. Investigation of the Technical Feasibility of Storing Fresh Water in Saline Aquifers. Water Resources Research 3(3):683-695.

Gardner, G. H. F., J. Downie and H. A. Kendall. 1962. Gravity Segregation of Miscible Fluids in Linear Models. Trans Society of Petroleum Engineers of AIME, 225(pt. II):95-104.

Gardner, G. H. F., J. Downie and M. R. J. Wyllie. 1962. Problems in the Recovery of Gas From Aquifers Used for Natural Gas Storage. Journal of the Institute of Petroleum 48(457):1-6.

Glazunov, I. S. 1967. Artificial Formation of Fresh Ground Water Lenses by Means of Wells. Symposium of Haifa; Artificial Recharge and Management of Aquifers, I.A.S.H., p. 237-242.

Gloves, R. E. 1959. The Pattern of Fresh-Water Flow in a Coastal Aquifer. Journal of Geophysical Research 64(4):457-459.

Harleman, D. R. F. and R. R. Rumer. 1962. The Dynamics of Salt-Water Intrusion in Porous Media, MIT Hydrodynamics Laboratory Report No. 55.

Henry, H. R. 1959. Salt Intrusion Into Fresh-Water Aquifers. Journal of Geophysical Research 64(11):1911-1919.

Hoopes, J. A. and D. R. F. Harleman. 1965. Waste Water Recharge and Dispersion in Porous Media. MIT Hydrodynamics Laboratory Report No. 75.

Hoopes, J. A. and D. R. F. Harleman. 1967. Waste Water Recharge and Dispersion in Porous Media. Journal of the Hydraulics Division ASCE 93(HY5):51-72.

INTERCOMP. 1976. A Model for Calculating Effects of Liquid Waste Disposal in Deep Saline Aquifer Part I - Development, Part II - Documentation. U.S. Geological Survey, Water Resources Investigations 76-61.

Jacob, C. E. 1946. Radial Flow in a Leaky Artesian Aquifer Transactions. American Geophysical Union 27(2):198-205.

Kaufman, D. W. 1960. Sodium Chloride. Reinhold Publishing Corporation, New York.

Kimbler, O. K., R. G. Kazmann and W. R. Whitehead. 1975. Cyclic Storage of Fresh Water in Saline Aquifers. Bulletin No. 10, Louisiana Water Resources Institute, Louisiana State University, Baton Rouge, LA.

Kimbler, O. K. and W. R. Whitehead. 1977. Effect of Viscosity Ratio on the Recovery of Fresh Water Stored in Saline Aquifers. Completion Report Louisiana Water Resources Research Institute, Louisiana State University, Baton Rouge, LA.

Kishi, Y. and Y. Fukno. 1977. Studies on Salinization of Groundwater. I. Theoretical Consideration on the Three-Dimensional Movement of the Salt Water Interface Caused by the Pumpage of Confined Groundwater in Fan-Shaped Alluvium. Journal of Hydrology 35:1-29.

Kumar, A. and O. K. Kimbler. 1970. Effect of Dispersion, Gravitational Segregation, and Formation Stratification on the Recovery of Fresh Water Stored in Saline Aquifers. Water Resources Research 6(6): 1689-1700.

Langhtee, E. J. 1974. The Use of Bounding Wells to Control Flux in Underground Water Storage Projects. M.S. Thesis, Louisiana State University, Baton Rouge, LA.

Molz, F. J. and L. C. Bell. 1977. Head Gradient Control in Aquifers Used for Fluid Storage. Water Resources Research 13(4):795-798.

Molz, F. J., J. C. Warman and T. E. Jones. 1978. Aquifer Storage of Heated Water: Part I - A Field Experiment. Ground Water 16(4): 234-241.

Muskat, M. 1946. The Flow of Homogeneous Fluids Through Porous Media. McGraw-Hill, New York.

Ogata, A. 1958. Dispersion in Porous Media. Ph.D. Dissertation, Northwestern University, Evanston, Illinois.

Ogata, A. and R. B. Banks. 1961. A Solution of the Differential Equation of Longitudinal Dispersion in Porous Media. Professional Paper 411-A, U.S. Geological Survey.

Papadopulos, S. S. and S. P. Larson. 1978. Aquifer Storage of Heated Water: Part II - Numerical Simulation of Field Results. Ground Water 16(4):242-248.

Segerlind, L. J. 1976. Applied Finite Element Analysis. John Wiley & Sons, New York.

Shamir, V. and D. R. F. Harleman. 1966. Numerical and Analytical Solutions of the Dispersion Problems in Homogeneous Aquifers. MIT Hydrodynamics Laboratory Report No. 89.

Shamir, V. and G. Dagan. 1971. Motion of the Seawater Interface in Coastal Aquifers: A Numerical Solution. Water Resources Research 7(3):644-657.

Smith, C. G., Jr. and J. S. Hanor. 1975. Underground Storage of Treated Water: A Field Test. Ground Water 13(5):410-417.

Stone, H. L. and P. L. T. Brian. 1963. Numerical Solution of Convective Transport Problems. Journal of American Institute of Chemical Engineers 9(5):681-688.

Strack, O. D. L. 1976. A Single-Potential Solution for Regional Interface Problems in Coastal Aquifers. Water Resources Research 12(6):1165-1174.

Tate, P. T. 1976. Effect of Dip on the Storage of Fresh Water (or the Disposal of Waste) in a Saline Aquifer, M.S. Thesis, Louisiana State University, Baton Rouge, LA.

Van Der Veer, P. 1977. Analytical Solution for Steady Interface Flow in Coastal Aquifer Involving a Phreatic Surface with Precipitation. Journal of Hydrology 34:1-11.

von Neumann, J. and R. D. Richtmyer. 1950. A Method for the Numerical Calculation of Hydrodynamic Shocks. Journal of Applied Physics 21:232-237.

Werner, D. and W. Kley. 1977. Problems of Heat Storage in Aquifers. Journal of Hydrology 34:35-43.

Whitehead, W. R. 1974. Storage of Fresh Water in Saline Aquifers Using a Well Field, Ph.D. Dissertation, Louisiana State University, Baton Rouge, LA.

Wooding, R. A. 1963. Mixing-Layer Flows in a Saturated Porous Medium. Journal of Fluid Mechanics 19(1):103-112.

Zienkiewicz, O. C. 1971. The Finite Element Method in Engineering Science. McGraw-Hill, London.

BIOGRAPHICAL SKETCH

John Patrick Glass was born August 18, 1946, in Wolf Lake, Indiana. He received the degree of Bachelor of Science in civil engineering at the University of Florida in August, 1971.

He worked as rural development volunteer with International Voluntary Services, Inc. in Vietnam from 1967 to 1970. From 1971 to 1974 he was a designer and project engineer with Palmer and Mallard and Associates, Inc., consulting engineers of Sumter, South Carolina.

In 1973 he married the former Miss Claudette T. Chenu.

In September of 1974 he returned to the University of Florida to attend graduate school. In March, 1976, he received the Master of Engineering degree and since that time has been working toward his doctorate.

I certify that I have read this study and that in my opinion it conforms to acceptable standards of scholarly presentation and is fully adequate, in scope and quality, as a dissertation for the degree of Doctor of Philosophy.

B. A. Christensen, Chairman
Professor of Civil Engineering

I certify that I have read this study and that in my opinion it conforms to acceptable standards of scholarly presentation and is fully adequate, in scope and quality, as a dissertation for the degree of Doctor of Philosophy.

B. E. Ruth
Professor of Civil Engineering

I certify that I have read this study and that in my opinion it conforms to acceptable standards of scholarly presentation and is fully adequate, in scope and quality, as a dissertation for the degree of Doctor of Philosophy.

D. P. Spangler
Associate Professor of Geology

This dissertation was submitted to the Graduate Faculty of the College of Engineering and to the Graduate Council, and was accepted as partial fulfillment of the requirements for the degree of Doctor of Philosophy.

June 1979

Dean, College of Engineering

Dean, Graduate School